EFFECTS OF HEAT TREATMENT AFTER HOT ROLLING ON THE CORROSION AND MECHANICAL PROPERTIES OF Mg- Zn- Ca- Mn BIOMATERIALS

2024
MASTER THESIS
METALLURGICAL AND MATERIALS ENGINEERING

Laith Mohammed Abdullah AL MASHHADANI

Thesis Advisor
Prof.Dr. Ali GÜNGÖR

EFFECTS OF HEAT TREATMENT AFTER HOT ROLLING ON THE CORROSION AND MECHANICAL PROPERTIES OF Mg- Zn- Ca- Mn BIOMATERIALS

Laith Mohammed Abdullah AL MASHHADANI

Thesis Advisor
Prof. Dr. Ali GÜNGÖR

T.C.
Karabuk University
Institute of Graduate Programs
Department of Metallurgical and Materials Engineering
Prepared as
Master Thesis

KARABUK
April 2024

I certify that, in my opinion, the thesis submitted by Laith Mohammed Abdullah AL MASHHADANI titled "EFFECTS OF HEAT TREATMENT AFTER HOT ROLLING ON THE CORROSION AND MECHANICAL PROPERTIES OF Mg- Zn- Ca- Mn BIOMATERIALS" is fully adequate in scope and quality as a thesis for the degree of Master of Science.

Prof. Dr. Ali GÜNGÖR .....

Thesis Advisor, Department of Metallurgical And Materials Engineering

This thesis is accepted by the examining committee with a unanimous vote in the Department of Metallurgical and Materials Engineering as a Master of Science thesis. 03/04/2024

Examining Committee Members (Institutions)	Signature
Chairman: Prof. Dr. H. Özkan GÜLSOY (MÜ)	online
Member : Prof. Dr. Ali GÜNGÖR (KBU)	.....
Member : Assoc. Prof. Dr. Alper İNCESU (KBU)	.....

The degree of Master of Science by the thesis submitted is approved by the Administrative Board of the Institute of Graduate Programs, Karabuk University.

Assoc. Prof. Dr. Zeynep ÖZCAN .....

Director of the Institute of Graduate Programs

"I declare that all the information within this thesis has been gathered and presented under academic regulations and ethical principles, and I have, according to the requirements of these regulations and principles, cited all those which do not originate in this work as well."

Laith Mohammed Abdullah Al MASHHADANI

ABSTRACT

M. Sc. Thesis

EFFECTS OF HEAT TREATMENT AFTER HOT ROLLING ON THE CORROSION AND MECHANICAL PROPERTIES OF Mg- Zn- Ca- Mn BIOMATERIALS

Laith Mohammed Abdullah AL MASHHADANİ

Karabük University
Institute of Graduate Programs
Department of Metallurgical and Materials Engineering

Thesis Advisor
Prof. Dr. Ali GÜNGÖR
April 2024, 105 pages

The effects of Zn ratio, thermomechanical processing and heat treatment on the microstructure, mechanical properties, and corrosion resistance of Mg-1Zn-0.2Ca-0.3Mn and Mg-3Zn-0.2Ca-0.3Mn (wt.%) magnesium alloys were investigated in this thesis. Alloys were produces using gravity die casting. Cast alloys were homogenized at 400 °C for 12 h. After that, two sets of samples from each alloy were sliced using wire erosion. Both sets of the alloys were hot rolled at 250 °C. Then, post heat treatment at 325 °C for 10, 20, 30, 60, and 120 minutes was applied to the hot rolled alloys to compare the effect of post heat treatment on the properties of the hot rolled alloys.

All of the samples were characterized using optic microscope, field emission scanning electron microscope with EDS attachment (SEM-EDS), X-ray diffraction (XRD), tensile tests, micro hardness measurements, and immersion corrosion tests.
The results showed that homogenized alloys have large and uniform grain distributions, and the microstructure of the alloys consist of α-Mg matrix and $Ca_2Mg_6Zn_3$ intermetallic phases. Hot rolling results in finer and elongated grain formation. Hot rolling increased the mechanical properties and hardness of the investigated alloys. After post heat treatment at 120 min, both alloys showed lower hardness and yield strength but higher elongation. In addition, heat treatments applied after hot rolling greatly improved the corrosion properties of the alloys. Immersion corrosion tests showed that corrosion rate of the alloys decreased with increasing immersion time due to the formation of protective layer on the surface of the alloys. Immersion corrosion tests also showed that hot rolling has negative effect on the corrosion resistance of the alloys. However, subsequent heat treatment reduces the negative effect of the hot rolling on the corrosion resistance of the alloys. Among the alloys, Alloy-2 heat treated at 325 °C for 120 min after hot rolling exhibited better mechanical properties (modulus of elasticity, yield and tensile strength, and hardness) and lower corrosion rate than Alloy-1. Therefore, the properties of Alloy-2 can be further improved, and its biocompatibility can be investigated for biodegradable orthopedic implant applications.

Key Words : Hot Rolling, Heat Treatment, Corrosion, Mechanical Properties.
Science Code : 91513

ÖZET

Yüksek Lisans Tezi

SICAK HADDELEME SONRASI ISIL İŞLEMİN Mg-Zn-Ca-Mn BİYOMATERYALLERİN KOROZYON VE MEKANİK ÖZELLİKLERİ ÜZERİNDEKİ ETKİLERİ

Laith Mohammed Abdullah AL MASHHADANI

Karabük Üniversitesi
Lisansüstü Eğitim Enstitüsü
Metalurji ve Malzeme Mühendisliği Anabilim Dalı

Tez Danışmanı
Prof. Dr. Ali GÜNGÖR
Nisan 2024, 105 sayfa

Bu tezde Mg-1Zn-0.2Ca-0.3Mn ve Mg-3Zn-0.2Ca-0.3Mn (% ağırlıkça) magnezyum alaşımlarının mikroyapısı, mekanik özellikleri ve korozyon direncine Zn oranının, termomekanik işlemin ve ısıl işlemin etkileri araştırılmıştır. Alaşımlar metal kalıba döküm yöntemiy üretildi. Dökme alaşımlar 400 °C'de 12 saat homojenleştirildi. Daha sonra her alaşımdan iki set numune tel erozyon kullanılarak dilimlendi. Alaşımların her iki seti de 250 °C'de sıcak haddelendi. Daha sonra, son ısıl işlemin sıcak haddelenmiş alaşımların özellikleri üzerindeki etkisini belirlemek için 325 °C'de 10, 20, 30, 60 ve 120 dakika son ısıl işlem uygulandı.

Bütün numuneler optik mikroskop, EDS eklentili alan emisyon taramalı elektron mikroskobu (SEM-EDS), X-ışını kırınımı (XRD), çekme testleri, mikro sertlik ölçümleri ve daldırma korozyon testleri kullanılarak karakterize edildi.

Sonuçlar, homojenleştirilmiş alaşımların iri ve üniform tane dağılımlarına sahip olduğunu ve alaşımların mikro yapısının α-Mg matrisi ve $Ca_2Mg_6Zn_3$ intermetalik fazlardan oluştuğunu gösterdi. Sıcak haddeleme daha ince ve uzun taneli yapı oluşumuna neden olmuştur. Sıcak haddeleme incelenen alaşımların mekanik özelliklerini ve sertliğini arttırmıştır. Her iki alaşım da 120 dakikadaki ısıl işlemden sonra daha düşük sertlik ve akma dayanımı, fakat daha yüksek uzama göstermiştir. Ayrıca sıcak haddeleme sonrasında uygulanan ısıl işlemler alaşımların korozyon özelliklerini büyük ölçüde iyileştirmiştir. Daldırma korozyon testleri, alaşımların yüzeyinde koruyucu tabaka oluşması nedeniyle daldırma süresinin artmasıyla alaşımların korozyon hızının azaldığını göstermiştir. Daldırma korozyon testleri ayrıca sıcak haddelemenin alaşımların korozyon direncini olumsuz etkilediğini göstermiştir. Ancak haddelemeden sonra uygulanan ısıl işlemin sıcak haddelemenin alaşımların korozyon direnci üzerindeki olumsuz etkisini azalttığını göstermiştir. Alaşımlar arasında, sıcak haddelemeden sonra 325 °C'de 120 dakika boyunca ısıl işleme tabi tutulan Alaşım-2, Alaşım-1'e göre daha iyi mekanik özellikler (elastikiyet modülü, akma ve çekme mukavemeti ve sertlik) ve daha düşük korozyon hızı sergilemiştir. Bu nedenle, biyobozunur ortopedik implant uygulamaları için Alloy-2'nin özellikleri daha da geliştirilebilir ve biyouyumluluğu araştırılabilir.

Anahtar Kelimeler: Sıcak Haddeleme, Isıl Işlem, Korozyon, Mekanik Özellikler

Bilim Kodu **:** 91513

ACKNOWLEDGMENT

In the beginning, I want to thank God for all the blessings He has given me. First and foremost, I offer my sincerest gratitude to my supervisor, Prof. Dr. Ali GÜNGÖR, who has supported me throughout my thesis with his patience and knowledge and allowed me to work on such a fascinating project. I could feel his idealistic drive and personal generosity toward the better in all our meetings. It was a pleasure and a great honor for me to work with him. I would also like to acknowledge the financial support provided by the Scientific Research Projects Coordination Unit of Karabuk University with KBÜBAP-22-YL-119 project number, and I also thank them. I am also deeply grateful to Prof. Dr. Hayrettin AHLATCI in Karabuk University for scientific support and the use of the Department of Metallurgical and Materials Engineering laboratory facilities. All thanks and appreciation to Ph.D. Ameer Al-Humairi for helping me prepare the simulated body fluid. I would like to express my gratitude to my teacher, Dr. Ali J. Addie, for his interest and assistance. I thank my friend and colleague Mohammed Sultan, colleagues at the university, and the work for supporting me. I also truly enjoyed working in their friendly and supportive research group.

Last but not least, I wish to extend my heartfelt gratitude to my parents and siblings for their unceasing assistance and consistent encouragement, which always motivated me to strive for something better. I appreciate the unwavering encouragement and positive presence of my wife, sons, and daughters, whose continual optimism provided invaluable support while completing this thesis.

CONTENTS

Page

Page

Page

LIST OF FIGURES

Page

Page

LIST OF TABLES

Page

SYMBOLS AND ABBREVITIONS INDEX

SYMBOLS

Mg : Magnesium

Zn : Zinc

Ca : Calcium

Mn : Manganese

YS : Yielding Strength

UTS : Ultimate Tensile Strength

HV : Hardness of Vickers

MPa : Megapascal

ABBREVIATIONS

FCC	: Face Centered Cubic
HCP	: Hexagonal Close-Packed.
EDS	: Energy Dispersive X-ray Spectroscopy
SEM	: Scanning Electron Microscopy
XRD	: X-Ray Diffraction
SBF	: Simulated Body Fluid
SFE	: The stacking fault energy
LAGBs	: The low-angle grain boundaries
DRX	: The dynamic recrystallization
SRV	: The static recovery
SRX	: The static recrystallization
T_m	: The melting point of material
CRSS	: critical resolved shear stress

PART 1

INTRODUCTION

1.1. INTRODUCTION

The study of biomaterials is crucial to human survival and longevity because it can help the elderly people, also those who need biomedical implants to extend their life [1]. Science and technological advances have allowed it possible to fabricate and reengineer biomaterials into useful medical implants and devices, which are utilized in medical implants or devices that come into contact with the human biological system [2].

Biomaterial is a broad term that refers to several that has been approved for use in human bodies. Biomaterials can be described as substances utilized to change or to return functionalities of biological tissues and work constantly in touch with bodily fluids [3]. In other words, any natural or artificial biomaterial that is utilized to replace or support a part of an organ or tissue while being in close proximity to it is referred to as a biomaterial [4]. In order for biomaterials to function within the human body, they must possess certain properties such as good biocompatibility, being non-toxic and non-carcinogenic, and having mechanical and physical properties to augment or replace bodily tissues [5].

The increase of traffic accidents over the last decades has led to a substantial surge in the demand for metallic plates as a healing modality for treating bone fractures. In addition, since the average implant service life is between (10-15) years, there is a strong likelihood that orthopedic surgery patients will require revision procedures at some point in their lives [6].

Recently, metal plates have been implanted to repair or replace organs that have failed or been lost, as well as organs with unsatisfactory functionality [6]. The implant materials can be categorized into non-degradable and degradable materials [7]. Although metals, ceramics, and polymers are all utilized to make implant materials, metals have an edge over the other two due to a greater balance of strength, toughness, and ductility. Metallic biomaterials with high corrosion resistance frequently used as permanent implant materials in orthopedic surgery include Ti alloys, stainless steel, and Co-Cr alloys, among others. However, these metallic alloys can't be used as temporary implant materials (screws, pins, bone plates, etc.) since doing so involves a second surgery procedure that carries a risk of infection [8]. Thus, increasing the risk of harm and cost to the patient. On the other hand, it is anticipated that biodegradable metals will erode gradually and without damage to the bodies living, also preserve their mechanical integrity during the crucial tissue mending phase, and then totally disintegrate after completing their task [9]. Therefore, temporary implants, in high demand because of their capacity to naturally dissolve in the body's environment, eliminate the need for the time-consuming subsequent surgery that would otherwise be required for implant removal following fracture healing. Also, lessens long-term consequences [10].

Magnesium and its alloys may be used as biodegradable substances for orthopedic purposes, particularly as temporary stents due to their degradable and biocompatible properties [11]. In addition, it has drawn a lot of interest as cardiology interventional devices. At the same time, Mg alloys have a lower risk of stress shielding than conventional metallic biomaterials like titanium and stainless steel. On the other hand, magnesium alloys often break down within a few weeks, and Mg^{2+} ions are frequently produced which are helpful for bone healing. However, if magnesium alloy corrosion is left uncontrolled, it might result in an unanticipated mechanical breakdown before tissue regeneration. For magnesium alloys utilized as therapeutic implants in physiological settings with high chloride levels and/or pH values of 7.4–7.6, this is a serious problem. Therefore, controlling corrosion rate of Mg alloys has become an important and urgent problem [12]. Furthermore, the principal challenges facing magnesium (Mg) and its alloys pertain to their relatively weak flexibility and strength, which pose fundamental obstacles to their widespread application across

various domains [13]. Therefore, it is crucial to improve both the corrosion resistance and mechanical properties including modulus of elasticity, ductility, toughness, tensile and yield strength of Mg and its alloys [12].

One of the best ways to increase corrosion resistance and the mechanical properties of magnesium alloys is to use alloying elements [12]. The addition of alloying elements generally affects the mechanical properties of Mg alloys through plastic and inherent elastic capabilities, structural stability, microstructural development, etc. [13]. Rare earth elements and aluminium (Al) are often employed to modify the degradation rate of magnesium alloys, but their potential adverse impact on biocompatibility with the human body must be thoroughly considered [12]. Moreover, the high cost of the RE components is a clear drawback although the Mg alloys' notable performance increases [14]. One of the most important components for maintaining healthy bodily processes is zinc (Zn). However, zinc may accelerate corrosion rate if it forms the Mg_xZn_y phase. Song et al. determined that increased volume fraction of the Mg_xZn_y phase that behaves as a micro cathode accelerates corrosion [12]. In addition, the addition of zinc can enhance the tensile strength in magnesium alloys through the solid-solution mechanism, enhancing age-hardening response, refining grain size, and minimizing the detrimental effects of the impurity elements on corrosion resistance. The Mg-Zn binary alloy's current use is restricted by its wide temperature range of crystallization and hot cracking [14]. As another alloying element is calcium (Ca). Ca weakens the basal texture, improves formability, and increases the strength and ductility of the alloy by solid solution and dispersion strengthening mechanisms. Also, Ca improves corrosion resistance by forming a more corrosion-resistant oxide layer and increases ductility to produce a desirable balance of strength and ductility. When Ca and Zn are used together in the Mg alloy, stable intermetallic phase, $Ca_2Mg_6Zn_3$, that is beneficial for applications involving high temperatures may form. On the other hand, $Ca_2Mg_6Zn_3$ phase can accelerate the corrosion rate of Mg matrix since it behaves as a cathode due to its greater standard electrode potential compared to magnesium. The mechanical properties of Mg-Zn-Ca alloys, however, deteriorate when zinc concentration rises over 4.0 wt.% because of coarsening of the grain. Casting that sticks or tears hotly and splits violently is likewise influenced by calcium levels of more than 1 wt.%

[14]. As another alloying element, manganese (Mn) can increase corrosion resistance and the strength of magnesium alloys. According to the studies, addition of Mn can cause MnO film formation on the surface of Mg alloys that prevents chloride ions from penetrating and enhancing corrosion resistance [12]. By adding Mn to the alloy, the formability, thermal conductivity, and microstructure may all be changed [14]. In addition, the mechanical properties of magnesium alloys can be substantially enhanced through thermomechanical processing techniques such as hot rolling, extrusion, and forging. These techniques involve inducing changes such as weak texture, refining the grain structure, and increasing work hardening. Nevertheless, it is imperative to emphasize that the utilization of these methodologies necessitates the availability of suitable equipment and adherence to specific process conditions [13].

As a result, there are inherent challenges of simultaneously attaining satisfactory corrosion resistance and essential mechanical strength in quaternary alloy systems through alloying alone. Consequently, the augmentation of both resistance of corrosion and mechanical properties require the application of thermomechanical and heat treatment processes.

In the present work, two Mg alloys, Mg-1Zn- 0.2Ca-0.3Mn and Mg-3Zn-0.2Ca-0.3Mn in wt.%, were investigated. Zn, Ca, and Mn were chosen as the alloying elements since they are advantageous, non-toxic, and safe for the human body. The thermomechanical process and heat treatment were applied to the alloys produced by utilizing the gravity die-casting method. Through these processes, the microstructure of the alloy is changed, and the mechanical and corrosion resistance of the alloy can be improved. After casting, homogenization heat treatment, hot rolling, and post heat treatment applied to the alloys. Details of the processes are given in Part Four of this thesis.

1.2 THE AIM OF THE WORK

The aim of this study is to enhance the mechanical properties and corrosion resistance of magnesium-based biomaterials by Zn content of the alloy,

thermomechanical process, and post heat treatment. The following procedures were used to reach the aim of this study:

- Designing two different Mg, Zn, Ca, and Mn elements by changing Zn ratio.
- Producing the alloys using gravity casting.
- Homogenization of cast alloys.
- Application of hot rolling to homogenized alloys.
- Application of post heat treatment at a constant temperature for different annealing times after hot rolling.
- Determination of microstructure, mechanical properties, and corrosion rate of the alloys experimentally.
- Compare and contrast the influences of zinc, hot-rolling, and post-heat treatment on the mechanical properties and corrosion rate of magnesium alloys.

Recently, several studies on Mg-Zn-Ca-Mn and related biomaterials have been studied. The differences of this study from the other studies are different Ca and Zn ratios, hot rolling temperature, and deformation ratio, post heat treatment temperature and durations after hot rolling that result in different microstructures because of the removal of stored energy in the material which in turn affects the mechanical properties and corrosion resistance of the alloys.

PART 2

LITERATURE REVIEW

Over the past few decades, a lot of research has been done on the properties of biodegradable magnesium alloys. This led to the development and manufacture of a variety of alloys that are excellent candidates for use in the medical industry. However, further work is needed to improve the mechanical properties and biocorrosion resistance of these alloys.

In this part, we reviewed the literature on enhancing the performance, corrosion behavior, and mechanical properties of biodegradable magnesium alloys.

Kavyani et al. (2022) studied the Mg-Zn-Ca-Mn alloy's microstructural development, mechanical properties, and biocorrosion performance under various heat treatment, extrusion, and half-equal channel angular pressing (HECAP) process conditions. The grain size of the Mg-Zn-Ca-Mn alloy was refined following extrusion and HECAP after a two-pass operation. After two passes through the HECAP process, the homogenized alloy's grains were significantly refined from 345 mμ to 2 mμ, according to their findings. However, after the HECAP procedure, the existence of finer $MgZ_6n_3Ca_2$ and α-Mn phases was observed using field emission scanning electron microscopy (FESEM). As for, the mechanical properties of the HECAPed samples including yield strength, ultimate tensile strength, and elongation, increased by 208%, 144%, and 100%, respectively, in comparison to the homogenized one. As well, the sample with two passes of HEACP showed the maximum biocorrosion resistance. According to immersion tests and electrochemical corrosion tests, the sample's ability to build a more durable protective film layer on the grain boundaries is related to its uniform grain refined microstructure [15].

Dae Hyun Cho et al. (2022) studied the effect of Mn in Mg-4Zn-0.5Ca-xMn (x = 0, 0.4, or 0.8 wt.%) alloys by squeeze casting method. They found the addition of Mn led to a positive effect on the microstructure, mechanical, and corrosion properties. On the other hand, the volume fraction of the $Ca_2Mg_6Zn_3$ phase concurrently

increases and the dendritic microstructure of squeeze-cast Mg-4Zn-0.5Ca-xMn becomes more consistent and refined as the Mn concentration rises. The improvement in the yield strength, ultimate strength, and ductility of the squeeze-cast Mg-4Zn-0.5Ca-xMn alloys increased with increasing Mn content due to grain refinement primarily. Also, the best yield strength, ultimate tensile strength, and elongation (201 ± 6, 280 ± 5, 22 ± 2) were obtained in Mg-4Zn-0.5Ca-0.8Mn. Higher Mn increased the corrosion resistance of squeeze-cast Mg-4Zn-0.5Ca-xMn alloys as shown by an electrochemical corrosion test in Hank's solution at 36.5 °C. Furthermore, squeeze-cast Mg-4Zn-0.5Ca alloy with Mn showed good biocompatibility [16].

Xia Chen et al. (2021) studied the effect of Sn content on the microstructure and mechanical properties of Mg-Zn-Mn-Ca alloy. The addition of Sn led to Mg-Zn-Mn-Ca alloy enhanced the mechanical properties. The addition of Sn prevented the formation of $Ca_2Mg_6Zn_3$ phase by promoting the formation of CaMgSn phase. In addition, the inclusion of Sn accelerated the recrystallization process. When Sn was added to the alloy Mg-6Zn-1Mn-0.5Ca, it led the formation of feather-like CaMgSn phase which seldomly dissolved into the matrix after solid solution treatment. Moreover, Sn containing alloy showed fully recrystallized microstructure, and its texture enhanced up to 3 wt.% Sn. After this concentration, Sn led to a decrease in these properties. The strength of as-extruded alloys continuously rose up to Sn concentration of 2 wt.% before drastically decreasing at 3 wt.%. The yield strength, ultimate tensile strength, and elongation of the as-extruded Mg-6Zn-1Mn-2Sn-0.5Ca alloy were 299 MPa, 366 MPa, and 9.2%, respectively. Precipitate strengthening was the primary factor in strengthening. During aging, Sn refines the precipitates, reduces precipitate size, and increases precipitate density (concentration) that result in a more concentrated and closely packed arrangement within the material structure. High density of precipitates that act as reinforcement create additional barriers to impede

dislocation movement, thereby enhance the material's mechanical properties. The yield strength, ultimate tensile strength, and elongation of the peak-aged Mg-6Zn-1Mn-2Sn-0.5Ca alloy were each 379 MPa, 407 MPa, and 7.5%, respectively [17].

M. Kaviani et al. (2019) carried out a study about how thermomechanical process variables affect the mechanical properties, microstructure, and biocorrosion behavior of a pre-extruded Mg-Zn-Ca-Mn alloy. Hot compression tests have been conducted at temperatures ranging from 300 to 450 °C and strain rates ranging from 0.001 to 1 s-1 in order to observe the impact of various parameters such as deformation temperature and strain rate, as well as the role of the restoration process namely dynamic recrystallization (DRX) on microstructural evolution and corrosion resistance of hot forged samples. The alloy underwent changes leading to the arrangement of additional phases within it (secondary phase distribution) and the formation of new grains through dynamic recrystallization (DRX). These changes in the material's structure and properties were directly caused by the thermomechanical process applied to it. The corrosion rate decreased by the microstructure improvement from 0.31 to 0.12 (mm/year). High corrosion resistance was achieved at 400 °C thanks to fine grain and recrystallized microstructure. Additionally, the presence of the secondary phase particles led to the establishment of a uniform distribution of grain sizes, thereby providing an additional enhancement to the corrosion resistance observed at 400 °C [18].

N. Pulido. González et al. (2022) studied the effect of the impact of heat treatment on the mechanical and biocorrosion properties of the alloys Mg-1wt% Zn-1wt% Ca (ZX11) and Mg-3wt% Zn-0.4wt% Ca (ZX30). When examining the microstructure of the as-cast ZX11 alloys, it was found to consist of α-Mg grains separated by large Mg_2Ca and $Ca_2Mg_6Zn_3$ particles. In contrast, the as-cast ZX30 alloys had a microstructure composed of α-Mg grains separated by $Ca_2Mg_6Zn_3$ particles. They found that the $Ca_2Mg_6Zn_3$ precipitates at the grain boundaries were completely dissolved in the ZX11 alloy after solution treatment. However, in the ZX30 alloy, they are mostly redistributed to create a more linked structure, which exhibits a poor age-hardening response. Galvanic corrosion and corrosion rate, as a result, decreased after solution treatment in the former but increased in the latter. For both alloys, the

peak-aged state exhibits the greatest rate of corrosion, possibly as a result of an excessive amount of fine $Ca_2Mg_6Zn_3$ particles functioning as cathodic sites. The ZX11 alloy exhibits better biocorrosion behavior than the ZX30 alloy due to its lower $Ca_2Mg_6Zn_3$ phase composition and thus lesser galvanic corrosion [19].

Junjian Fu et al. (2017) investigated the impact of alloying elements on the mechanical properties of magnesium. In order to do this, they carried out mixing magnesium with Zn, Ca, and Mn components to create novel Mg- Zn-Mn-Ca alloy to study the impact of alloying elements on the mechanical properties. They found that MgZnCa phase is the main secondary phase in the alloys. As well as, the increase of Zn reduced the as-cast magnesium alloys' grain size, which in turn enhanced the alloys' mechanical properties. Therefore, the mechanical properties of the Mg-4Zn-0.2Mn-0.2Ca alloy, including yield strength, elongation, and hardness increased by 69 MPa, 14.7 %, and 53.4 HV, in comparison to the alloy Mg-2Zn-0.2Mn-0.2Ca by 58.4 MPa, 13.1 %, and 49.3 HV, respectively. Concurrently, the secondary phase, which was mostly dispersed at the grain boundaries, was partially dissolved in the matrix during the solution treatment, which increased the plasticity of the Mg-Zn-Mn-Ca alloy in its as-cast state. In addition, increasing the Zn resulted in the higher volume percentage of the secondary phase. Therefore, the as-cast alloys' mechanical properties might be enhanced by the addition of Zn due to the significant influence it had on grain refinement [20].

Kaibo Nie et al. (2019) investigated the microstructure, texture, and mechanical properties of Mg-Zn-Ca-Mn alloys for three different Zn/Ca weight ratios (2.63, 1.22, and 0.53). They found the as-cast alloys' grain size was noticeably reduced as the Zn/Ca ratio fell, and an increase followed this in the volume percentage of the second phase. On the other hand, The Mg-1.4Zn-2.6Ca-0.5Mn alloy extruded at 270 °C at an extrusion speed of 0.01 mm/s exhibited superior mechanical properties with a yield strength of approximately 387.8 MPa and ultimate tensile strength of approximately 409.2 MPa [21].

Alper Incesu and Ali Gungor (2020) studied the behavior of Mg-Zn-Ca alloys. They produced six Mg-Zn-Ca alloys by using gravity casting and investigated the

microstructure, mechanical properties, and corrosion resistance of the alloys. They observed that the microstructure was made up of the matrix phase (α-Mg), $Ca_2Mg_6Zn_3$, and Mg_2Ca for the alloy with a Zn/Ca ratio of 0.37 (ZX12). Also, they noticed the reduction in grain size when the alloy's Zn content and Ca content were both increased. The hardness of magnesium increased with increasing the Zn and Ca of the alloy. According to the study, mechanical properties are favorably impacted by low Ca concentrations (0.2 wt%) and adversely impacted by high Ca concentrations (1.8 wt%). On the other hand, the corrosion resistance of alloys is directly influenced by the Zn/Ca atomic ratio. The Mg_2Ca phase corrodes preferentially by acting as anode. In other words, it sacrifices itself and prevents the corrosion of Mg matrix. On the other hand, $Ca_2Mg_6Zn_3$ phase acts as a cathode and cause the degradation of Mg matrix. After hot rolling, the immersion and electrochemical corrosion rates of the alloys significantly increased, except for the immersion corrosion rate of the ZX30 alloy. According to the study, Mg-0.94Zn-0.16Ca alloy may be used as a bone fixation plate material due to its 121 ± 2.1 yield strength, 226 ± 3.7 tensile strength, % 4.1 ± 0.2 elongations, and 0.062 mm/yr immersion corrosion rate [22].

Hamdy Ibrahim et al. (2017) studied the effect of Mn and heat treatment on the mechanical properties and in vitro corrosion properties of Mg-Zn-Ca alloy. The study showed that Mg-1.2Zn-0.5Ca alloy underwent substantial grain refinement as a result of the addition of 0.5 wt.% Mn. Additionally, the $Ca_2Mg_6Zn_3$ secondary phase was refined and uniformly distributed into fine precipitates after the heat treatment of the Mg-1.2Zn-0.5Ca and Mg-1.2Zn-0.5Ca-0.5Mn alloys. It has been determined that the heat treatment greatly improves the mechanical and in vitro corrosion properties of the alloys, which is attributed to the microstructural changes. The Mg-Zn-Ca alloy had a stronger age-hardening response due to the addition of 0.5 wt.% Mn that resulted in better mechanical strength and lower corrosion rate [23].

Partha Duley et al. (2021) studied the effects of annealing heat treatment on the formation of microstructure and texture on the Mg4Zn-0.5Ca-0.16Mn alloy that was annealed for 5 minutes at a temperature of (350 °C). Also, this alloy was forged at three different temperatures (250 °C, 300 °C, and 350 °C). Additionally, the sample previously subjected forging at a temperature of 300 °C followed annealing process

at a temperature of 350 °C. Annealing applied for different durations ranging from 5 to 120 minutes. They have found that during the hot forging process, dislocations build up close to the precipitates, leading to higher dislocation density. However, when recrystallization advances over time during the isothermal annealing procedure, the dislocation density decreases. While the ductility and work hardening behavior gradually increase under the combined impact of growing grain size and its heterogeneity, the yield strength value drops with the annealing time mostly due to the coarsening of the grain size. The yield strength of the specimen forged at 300 °C decreased from 142 MPa to 119 MPa as the annealing time increased from 5 to 15 min. The yield strength does, however, continue to decline from 119 MPa to 110 MPa as the annealing treatment progresses from 15 to 30 min, mostly as a result of the coarsening of the grain size. On the other hand, after 15 min of annealing, the UTS (214 MPa), ductility (12% - 13%), and work hardening behavior was reduced due to a drop in grain size heterogeneity [24].

Yuan Zhang et al. (2018) investigated the effects of microstructure modification on the mechanical properties and corrosion performance of Mg-Zn-Mn-Ca. They applied different heat treatments on the alloy (300 °C/24 h, 350 °C/24 h, 420 °C/24 h, 460 °C/24 h, and 500 °C/24 h) in order to understand the effect of the volume fraction of the secondary phase and grain size. They demonstrated that when the temperature is increased, the amount of $Ca_2Mg_6Zn_3$ and Mg_2Ca precipitates were noticeably decreased, and grain sizes progressively increased. Also, the alloy that heat treated at 420 °C/24 h had the greatest mechanical properties, the lowest rate of corrosion (5.94 mm/a) and exhibited a denser and more compact surface film than the others. The mechanical improvement could be explained by the complete dissolution of eutectic phases (Mg_2Ca and $Ca_2Mg_6Zn_3$) which causes significant lattice deformation and makes it easier for the increased Ca solute to be structurally rearranged. The fundamental cause of micro-couple corrosion is the potential difference between the phase and the matrix, which results in a greater dissolution activity and current exchange density and speeds up corrosion. Therefore, it must have a reasonable grain size and dispersive distribution of precipitates must be matched for optimal corrosion resistance in magnesium alloys [25].

Darothi Bairagi et al. (2023) investigated the mechanical properties and in-vitro corrosion behavior of Mg-4Zn-0.5Ca-0.8Mn alloy, under ideal homogenized condition. The as-cast Mg-4Zn-0.5Ca-0.8Mn alloy was subjected to a homogenization heat treatment process at 360 °C for 6-12-24 h. They found that fine Mg-Zn-based precipitates were developed during the homogenization process. The specimen homogenized for 12 h had the maximum strength (~225 MPa) due to the highest percentage of evenly scattered fine precipitates. The maximum ductility (~8%) was found in this specimen, however, due to a significant breakdown of the network of coarse precipitates and a decreased aspect ratio of fine Mg-Zn precipitates. The specimens' corrosion behavior was influenced by the interaction between coarse and fine precipitates. The homogenized sample for 24 h showed the best corrosion resistance. Localized corrosion was suppressed in this sample as a result of the latter part of the $Ca_2Mg_6Zn_3$ phase, which had the greatest amount of interfacial conductivity disturbance, and a negligible percentage of $MgZn_2$ fine equilibrium precipitates. Maximum corrosion resistance is achieved as a result of forming the most stable and compressible product layer on the sample [10].

Chunquan Liu et al. (2021) studied systematically the effects of Ca and Mn addition on the microstructure, texture, and mechanical properties of Mg-4Zn-xCa-yMn alloys (x=0.3, 0.6, 1.0; y=0.2, 0.3, 0.7 in wt.%). The as-cast alloys were homogenized for 24 hours at 350 °C then for 12 h at 420 °C before being cooled in water at 25 °C. The ingots were then hot extruded at 300 °C. They observed two primary intermetallic phases, namely MgZn and $Ca_2Mg_6Zn_3$. The Mn was solely present as pure Mn particles. When Ca and Mn were added simultaneously, the resulting dynamic recrystallization produced well-refined grains. The particle-stimulated nucleation significantly improved the fineness of the extruded sheets. The traditional texture-softening effect of Ca was reduced by the addition of Mn due to an increase in the un-dynamically recrystallized percentage. While Mn improves the texture of other alloys having 0.6 and 1.0 wt.% Ca, it degrades the texture of Mg-4Zn-0.3Ca-yMn alloys. By adding Ca and Mn, the extruded Mg-4Zn alloys' yield strength and ultimate tensile strength increased. This improvement is attributable mainly to the strengthening from grain refinement, dislocation strengthening of un-DRXed area, and nanoscale secondary phase particles. Mg-4Zn-0.6Ca-0.7Mn yields

a material with an excellent balance of ultimate tensile strength (320 MPa) and elongation (16%) [14].

T. Nakata et al. (2023) investigated reheating the Mg-Zn-Ca-Mn alloy at 350 °C and 450 °C to understand the effect of heating temperature on the deformed microstructures and static recrystallization (SRX) behavior. They found reheating at a low of 350 °C weakened texture and reheating the alloy to 450 °C produced robust basal texture. In addition, reheating at 450 °C caused a significant amount of double twinning which often causes weakening of the basal texture and refining of SRX grain structure. The presence of deformed grains with low dislocation densities at the shear bands aided in creating basal-textured SRX grains and encouraged their expansion. As a result, the high temperature reheating produced grains with a coarse grain structure and a strong basal texture [26].

H.R. Bakhsheshi Rad et al. (2014) investigated the microstructure, mechanical properties, and corrosion behavior of the Mg-Ca-Mn-Zn alloy as compared to those of the Mg-Ca alloy in order to better understand how Mn and Zn influence these parameters. After microstructure analysis, they found that the binary Mg-Ca alloy's grain diameter was greatly refined by the addition of Mn and Zn components, and several secondary phases precipitated in the grains. The grain size was further reduced to 78 mμ by the addition of 0.5 wt.% Mn and 2 wt.% Zn. Also, the Mg-2Ca-0.5Mn-4Zn alloy's grain size was decreased to 59 mμ when the Zn content was increased to 4 wt%. The yield strength, ultimate tensile strength, and elongation of the quaternary alloy increased with the addition of zinc up to 4wt.% (83.1 MPa, 189.2 MPa, 8.71 MPa) respectively and decreased with the high addition of Zn 7wt% to become (45.4 MPa, 140.7 MPa, 4.15 MPa) respectively. Thus, increasing the Zn concentration over 4 wt.%, had no positive effects on the yield strength or ultimate tensile strength. On the other hand, the addition of Mn and Zn to the binary alloy causes the corrosion potential to shift in a more noble direction, leading to lower corrosion rate. As demonstrated by immersion testing, quaternary alloys with two secondary phases have greater corrosion resistance than binary alloys with a single secondary phase. The surface of the corroded quaternary Mg-Ca-Mn-Zn alloy is smoother and has fewer pits than Mg-Ca alloys. This is mostly due to the production

of the eutectic (Mg + Mg_2Ca + $Ca_2Mg_6Zn_3$) phase. Therefore, Mg-2Ca-2Zn-0.5Mn is an intriguing contender for the development of biological applications due to its high strength and corrosion resistance [11].

V.E. Bazhenov et al. (2021) investigated the impact of high extrusion temperature and the effect addition of Mn on the Mg-Zn-Ca-Mn alloys' microstructure, mechanical properties, and rate of corrosion. The findings demonstrated that the alloys' grain size became more refined as a result of the addition of Mn and a drop in extrusion temperature, which was followed by an increase in strength and a decrease in elongation at fracture. On the other hand, the α-Mg, Mg_2Ca, and $Ca_2Mg_6Zn_3$ phases were observed in as-cast Mg-2.0Zn-0.7Ca alloy. The Mg_2Ca phase vanished when the Zn level was increased to 4 wt.%. The microstructure of this alloy did not significantly alter with the addition of 1 wt.% Mn. This is due to the fact that relatively few precipitates in the α-Mn phase were found, while the majority of the Mn was found in the α-Mg phase in the as-cast state. The Mg-Zn-Ca alloys' yield strength, ultimate strength, and compression strength were all raised by lowering the extrusion temperature and adding Mn, but their elongation at fracture was decreased. The addition of Mn greatly decreased the rate of corrosion of the alloys in Hank's solution. When compared to alloys with 4 wt.% Zn, the alloys with 2 wt.% Zn showed lower corrosion rates. According to the results, the alloy extruded at 300 °C Mg-2Zn-0.7Ca-1Mn alloy has outstanding mechanical properties, ultimate tensile strength 278MPa, yield strength 229MPa, elongation 10%, and biocorrosion rate 0.3mm/year. Therefore, it was suggested that the alloy is suitable for use in bone implants [27].

A. Gungor and A.Incesu. (2021) investigated the homogenized and hot-rolled alloys' microstructure, mechanical properties, and corrosion behavior of Mg-Zn-Ca-Mn alloys, using the gravity die-casting method. All alloys had a constant Mn content, but Zn and Ca were added in two different ratios. They found the microstructures of the alloys are made up of $Ca_2Mg_6Zn_3$ and α-Mg as the matrix phase. The tensile strength, ductility, and toughness of the homogenized alloys increased with the Zn in the alloy but decreased when the Ca is increased. Therefore, among the homogenized alloys, the ZXM500 alloy with the greatest Zn and lowest Ca concentration exhibited

the best tensile strength, ductility, and toughness. Hot rolling led to significantly increased tensile strength, but significantly decreased ductility and toughness. Hot-rolled alloys with more calcium content have lower tensile strength and elongation than alloys containing less calcium. It is believed that greater Ca-containing content alloys have a higher volume percentage of the $Ca_2Mg_6Zn_3$ phase, which increases stress concentration sites and density of microcracks, both of them have a detrimental impact on the strength and ductility of the alloys. On the other hand, the corrosion tests showed that the immersion corrosion rates of all alloys (both before and after rolling) are less than the bio-degradation rate (0.5mm/year.) needed for the support plate for a shattered bone. The hot rolled ZXM300 alloy with 146±2.5MPa yield strength, 229±3.7MPa tensile strength, % 1.6±0.1 elongation, and 0.029mm/year immersion corrosion rate demonstrated the best mechanical properties and corrosion resistance to be used as a biodegradable alloy, compared with fracture bone plate material [8].

Alper INCESU and Ali GUNGOR. (2022) studied the effect of hot rolling after homogenization heat treatment on biodegradability and mechanical properties, which were applied on two ingots of magnesium Zn, Ca, and Mn as well as pure magnesium hot-rolled. It was found that the alloy with the highest tensile strength is Mg-1.07Zn-0.21Ca-0.31Mn. Due to its increased strength and biodegradability, the Mg-1.07Zn-0.21Ca-0.31Mn alloy can be regarded as a biodegradable implant material [28].

Tao Lv et al. (2022) investigated the microstructure and corrosion behaviors of the Mg-4Zn-1Ca alloy that was cast and homogenized. They investigated the impact of homogenization treatment on the two samples' corrosion resistance in Hank's solution. They found that the majority of the phases in both the as-cast and as-homogenized samples are α-Mg and net-like $Ca_2Mg_6Zn_3$. Also, the modification in mechanical properties is minimal following a homogenization treatment at 400 °C for 12 hours. Through homogenization treatment, the corrosion resistance of the as-cast Mg-4Zn-1Ca alloy in Hank's solution at 37 °C was significantly increased. As-homogenized samples can also experience localized corrosion, although this corrosion resistance is improved by the compact $Ca_2Mg_6Zn_3$ phases' barrier effect on

the corrosion process. As-homogenized Mg-4Zn-1Ca alloy is more suitable for orthopedic applications as a result of its increased corrosion resistance and osteogenic differentiation capacity [29].

Yu Yan Han et al. (2019) studied the effect of Mn at various concentrations on the microstructure, mechanical properties, and corrosion properties of the Mg-3Zn-0.2Ca alloy to enhance the corrosion performance and mechanical properties of biomedical magnesium alloys. Mn concentration of the alloy was changed as 0.3, 0.5, 0.7, 0.9 wt.%. After that, alloy ingots were homogenized individually before being extruded at 315 °C on a hot-extrusion molding machine. The average grain size of the as-cast Mg-3Zn-0.2Ca-5Mn alloy was 40.1% smaller than that of the Mg-3Zn-0.2Ca alloy. Initially, as more manganese is added, the alloy undergoes more subcooling, resulting in smaller grains. Yet, beyond a certain threshold, the excess manganese might trigger a reversal in this effect, causing larger grains to form in the alloy. Therefore, the amount of manganese appears to impact the degree of subcooling, affecting the grain size of the as-cast alloy. On the other hand, the subcooling degree is the difference between the actual temperature of the liquid and the temperature at which it would usually solidify. On the other hand, the greatest yield tensile strength (302 MPa) and high ultimate tensile strength (327 MPa) were obtained in the alloy containing 5 wt.% Mn. However, the elongation did not dramatically decline. The Mn concentrations also inhibit dynamic recrystallization, which would have significantly decreased grain size during the extrusion process. On the other hand, the electrochemical results demonstrated that Mn-containing alloys had a higher corrosion potential than ternary Mg-3Zn-0.2Ca (wt%) alloy. The electrochemical trials with Mn added produced a denser passivation coating and a slower rate of corrosion [30].

Stanislav O. Rogachev et al. (2023) studied the influence of hot rolling on the mechanical properties and the structure of three Mg-Y-Zn-Mn alloys. After heat treatment, the original cast alloy plates were rolled at two temperatures, 400 °C and 450 °C, from an initial thickness of 7 mm to a final thickness of 0.2 mm. They found the dynamic recrystallization process took place during the hot rolling process. As well as precipitating LPSO ($Mg_{12}ZnY$) phase particles in the structure of the (Mg–

2.5Y–1.1Zn–0.8Mn) WZM211 and (Mg–3.4Y–1.7Zn–0.8Mn) WZM321 alloys. At high reductions 96–97%, the WZM111 (Mg-1.2Y-0.6Zn-0.8Mn) alloy's strength was unaffected from increasing rolling temperature from 400 °C to 450 °C, but its ductility was decreased. All alloys exhibited an increase in strength at the same rolling temperature 450 °C and at high reductions, even though ductility showed an inverse relationship. For all three alloys, rolling to total reduction of 88–97% results in the greatest desirable combination of strength and ductility [31].

PART 3

THEORETICAL BACKGROUND

3.1. OVERVIEW

This chapter discusses biomaterials and magnesium's role in bone grafting and transplantation as a biomaterial. Additionally, the classification of biomaterial materials was covered. On the other hand, we also looked at the magnesium alloys that were the subject of this study, their components, and mechanical processing techniques including hot rolling, after that heat treatment. Finally, we briefly discussed corrosion and some of its different kinds.

3.2. BIOMATERIAL

Due to the constantly increasing demands in medical and healthcare procedures, the field of biomaterials has quickly grown, science and technological advancements have made it possible to fabricate and reengineer biomaterials into useful medical implants and devices, which are utilized in medical implants or devices that come into contact with the human biological system [2].

In general, we can define biomaterials as materials that support or augment living tissues while performing specific functions. Biomaterial could be used in replacement of tissues and organs entirely or partially, to improve tissue aesthetics or functions, and to accelerate the healing process [32]. Biomaterials are a class of artificial materials. It is currently the subject of extensive research and may be used in a wide range of fields [33]. Biomaterial use has increased significantly in modern medicine due to their distinctive properties, including biocompatibility and mechanical strength [34]. The benign cohabitation of a biomaterial with a biological

system that it interfaces with is a distinguishing property that sets it apart from other materials [35]. In this regard, it is possible to describe biocompatibility as the material's ability to prevent adverse responses and correctly carry out its intended function when in touch with (or entering into) the biological environment. As a result, biocompatibility must encompass a functional assessment of the entire implantable system [36]. In other words, the capacity of the substance to conduct its functions concerning a specific remedy (while avoiding deleterious repercussions within the recipient's body or patient) may lead to an improved cellular response and optimal therapy for a specific usage [37]. In general, before using biomaterials in clinical practice, the FDA (United States Food and Drug Administration) should issue its mark of approval [38].

The advancement of biomaterials has facilitated to substitute impaired or injured bodily components with synthetic or natural materials, such as metals, ceramics, or polymers. Additionally, ongoing progress in tissue engineering holds promise for the prospective creation of new organs and tissues, offering a means to replace those adversely affected by disease or trauma [34].

Biomaterials are characterized as substances devoid of systemic and pharmacological activity and intentionally devised for placement within or integration into biological systems [39]. The European Society for Biomaterials Second Conference defined biomaterials as materials that are designed to interact with biological systems to replace, augment, or treat any tissue, organ, or the functioning of the body [40].

A biomaterial is described by Park and Lakes as a material that either replaces a tissue within the body or a function of the body [41]. In addition, any artificial substance that comes into regular or irregular contact with body fluids and is utilized to replace or repair body tissue is referred to as a biomaterial. Therefore, materials used to fabricate devices, such as surgical or dental instruments, are excluded from this categorization. Although these instruments come into contact with bodily fluids, they do not serve to replace or enhance the functionality of human tissue. [5].

3.3. APPLICATIONS OF BIOMATERIALS

Some of the application fields of biomaterials are:

Orthopedics: In this field, biomaterials can be used for the hip, knee, shoulder, ankle, and elbow.

Cardiovascular systems applications: The cardiovascular system, also known as the circulatory system, employs biomaterials for the remediation Including heart valves, vascular grafts etc. demonstrating their efficacy in therapeutic intervention.

Scaffolds: This is one of the foremost techniques employed in tissue engineering for the generation of tissues intended for reparative or substitutive purposes is the creation of customized, bioactive, three-dimensional (3D) scaffolds designed to retain their structural integrity over a predefined duration.

Ophthalmic: A diverse spectrum of ocular tissue-damaging conditions can culminate in refractive anomalies and blindness. For instance, a variety of biomaterial-based implants have been developed to enhance the quality of life for affected individuals. Notable examples of ophthalmic disorders also, age-related macular degeneration, as well as include cataracts and diabetic retinopathy.

Dental applications: Several materials can be used to repair or restore tooth crowns and roots.

Wound healing: The invention of sutures for wound closure is one of the earliest documented uses of implantable biomaterials. Fracture fixation materials constitute a crucial subset within the domain of wound-healing technologies, encompassing bone plates, rods, screws, nails, and various other instruments employed for the treatment of fractures. [41].

Interestingly, the term scaffolds refer to porous, biodegradable structures. They are supposed to disintegrate and be replaced by autologous freshly generated tissue after implantation. That can either have a randomly organized architecture resembling a

sponge or a highly complicated structure with ideal pores and channels for cell adhesion, proliferation, and growth [36].

Fig. 3.1 is an image showing the artificial hip joint and artificial knee implant [42]. Also, Fig. 3.2 is a vascular stent and an aneurysm clip [4]. Fig. 3.3 is an image showing the orthopedic devices and implants for the human body [43].

Figure 3.1. The artificial hip joint and artificial knee implant [42].

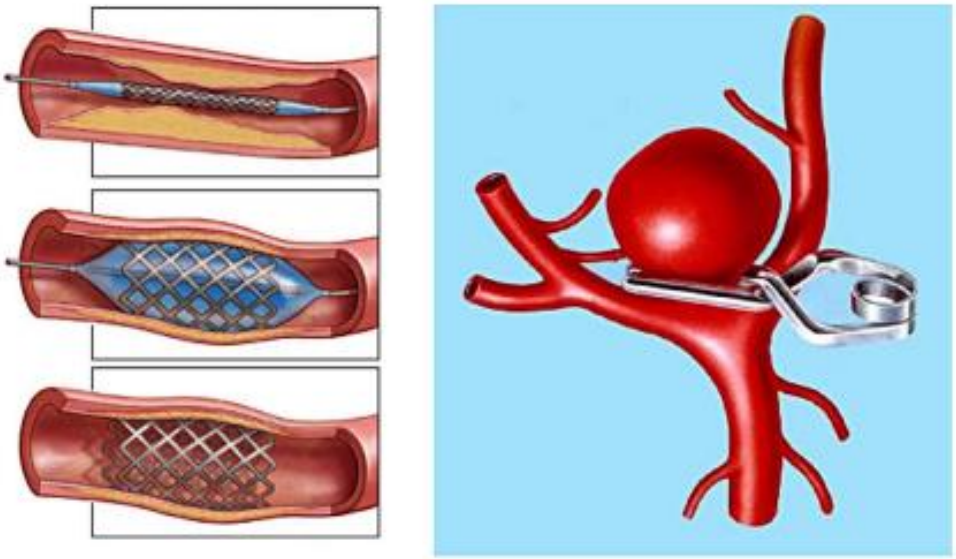

Figure 3.2. A vascular stent on the left and an aneurysm clip on the right [4].

Figure 3.3. A range of orthopedic devices and implants designed to be used in the human body [43].

3.4. BIOMATERIALS REQUIREMENTS

Biomaterials must be biocompatible because they are always in contact with body fluids. Therefore, there are very strict restrictions on the kinds of materials that can be used as biomaterials. Biomaterials must also be non-toxic and non-carcinogenic. The biomaterial should also have mechanical and physical properties to augment or replace bodily tissues [5]. Hardness, tensile strength, modulus of elasticity, and elongation are a few properties of paramount relevance. On the other hand, the stress shielding effect is a term used to describe the biomechanical incompatibility that causes bone cell death. Therefore, biomaterials should have low stress shielding value. In addition, if the implant and bone are not correctly connected, fibrous tissue will develop between them. Therefore, using materials with the right surface for the implant to bond appropriately with the nearby bone is crucial. Thus, surface chemistry substantially impacts the formation of robust, surface roughness, and surface topography [44]. Fig. 3.4 shows the requirements of implants [5]. In general, the special requirements for biomaterials can often be divided into three categories.

1. Biocompatibility: Implants used in the human body must prioritize non-toxicity and avoid triggering inflammation or allergies. Also, a substance

mustn’t elicit any unfavorable reactions from the host. Rather, it should facilitate positive tissue-implant integration and foster compatibility. Biocompatibility concerns often involve thrombosis, which involves blood clotting and platelet adhesion to the biomaterial surface, as well as the encapsulation of implanted biomaterials within fibrous tissue in soft tissues, these interactions significantly influence the compatibility of implants within our system [44].

2. Sterilizability: The substance must be sterilizable.
3. Function ability: The pliability of a material used in medical device fabrication is of paramount significance for the device's operational efficacy. It is imperative that the material can be readily and economically manipulated through engineering manufacturing processes. The manipulation of the material during the shaping process often represents the ultimate hurdle in the device's production. Engineers assume a pivotal role in surmounting this challenge [45].

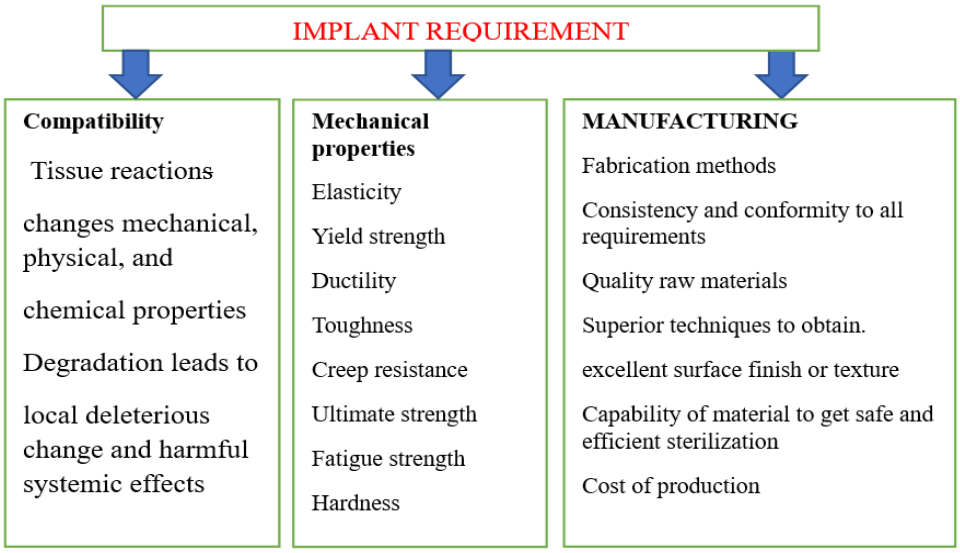

Figure 3.4. The schematic requirements of implants [5].

3.5. CLASSIFICATION OF BIOMATERIALS

The categorization of biomaterials is imperative for the selection of materials that offer greater safety and enhanced biocompatibility, given that biomaterials consistently interface closely with the physiological fluids or tissues of the recipient [2]. Before using biomaterials, it's important to keep in mind their classifications, with the focus being on biocompatibility, bio inertness, biological activity, biodegradable properties sterilizability, etc [39].

Biomaterials can be categorized in several ways, frequently based on how well they operate in the human body and how well they are made.

Firstly, biomaterials may be categorized based on the hierarchical levels of the human body. At the organ level, interventions such as artificial heart valves, complete valves, and cardiac pacemakers facilitate the mending and replacement of the human heart. Similarly, the skeletal system can undergo restoration and repair through interventions like joint replacements and bone plates [2].

Secondly, treated body parts can be used to classify biomaterials. For instance, biomaterials are frequently employed in the substitution of compromised or ailing anatomical structures with synthetic counterparts. As an illustration, artificial hip articulations and renal dialysis machinery are routinely employed as surrogates for bodily components affected by injury or disease, whereas bone plating systems, screws, and suture materials are instrumental in expediting the recuperative processes associated with wound healing [2].

Thirdly, depending on their material properties, biomaterials can be ceramics, polymeric, and metallic based materials [40].

Table 3.1 describes some of the different methods by which biomaterials can be classified [40]. On the other hand, the biomedical sector relies on the use of metals, ceramics, polymers, and composites to develop biomedical implants and devices [41]. Among the most studied and prevalently utilized categories of biodegradable

materials within this context are biodegradable polymers, biodegradable metals, and ceramics [43].

Table 3.1. Various methods for categorizing biological materials [40].

	Method	Different kinds of biomaterials
1	Chemical structure	Include polymers, ceramics, composite materials, and metals.
2	Nature of formation or origin	Comprise materials that are semi-synthetic, synthetic, natural, and hybrid.
3	Dimensional stability	Biomaterials are available in various scales, encompassing macro, micro, and nano dimensions.
4	Interaction with tissues	Bioactive, non-bioactive, resorbable, and inert
5	Biodegradability	Biostable and degradable
6	Structural side	Porous and non-porous

3.5.1. Metallic Biomaterials

Metals have been used as implants since Lane developed metal plates for treating bone fractures over a century ago [39]. Metallic biomaterials are preferred due to their inertness and structural capabilities. On the other hand, the selection of metal for biomedical applications varies according to the specific purpose of the implant [38]. Biocompatibility of metals is a major concern because metals can corrode in a vivo environment. Corrosion processes can adversely affect nearby biological tissues and organs, as well as contribute to the degradation of the implant material [39]. Metallic implants that erode have also negative effects on both the surrounding tissues and the implant itself. It degrades the implant's mechanical properties and produces toxic chemicals harmful to human inner organs. As a result, a metallic implant's ability to resist corrosion is crucial to determine its biocompatibility. Even though metals that can corrode are occasionally suggested for use as temporary implants, the biocompatibility is always necessary [37]. The development of numerous metallic biomaterials with non-toxic and allergy-free constituents is now underway. When 18-8 stainless steel was developed in the 1920s, doctors were immediately intrigued since it had a much higher level of corrosion resistance than anything else available at the time. In the years that followed, metal implants experienced substantial development and clinical usage. Temporary implants composed of a novel type of biodegradable metals have been suggested. All metal

implants often have a high density and are nonmagnetic. These are essential for X-ray visibility and compatibility with implants' magnetic resonance imaging (MRI) methods [38]. The types of metals that are often used for the various implant divisions are listed in Table 3.2 [38].

Table 3.2. The types of metals that are often used for the various implants [38].

Metals	Main alloying composition (wt%)	Mechanical properties			
		YS (MPa)	UTS (MPa)	YM (GPa)	Max elongation (%)
Stainless steel: 316L type (ASTM, 2003)	Fe; 16-18.5Cr; 10-14Ni; 2-3Mo; <2Mn; <1Si <0.003C	190	490	193	40
CoCr alloys: CoCrWNi (F90) (ASTM, 2007a) CoNiCrMo (F562) (ASTM, 2007b)	Co; 19-21Cr; 14-16W; 9-11Ni	310	860	210	20
	Co; 33-37Ni; 19-21Cr; 9-10.5Mo	241	793	232	50
Ti and its alloys: Pure Ti grade 4 (F67) (ASTM, 2006)	Ti; 0.05N; 0.1C; 0.5Fe; 0.015H; 0.4O	485	550	110	15
Ti6Al4V (F136) (ASTM, 2008)	Ti; 5.5-6.75Al; 3.5-4.5V; 0.08C; 0.2O	795	860	116	10
Degradable metals: Pure iron (Goodfellow, 2007) WE43 magnesium alloy (ASTM, 2001)	99.8Fe	150	210	200	40
	Mg; 3.7-4.3Y; 2.4-4.4Nd; 0.4-1Zr	150	250	44	4

3.5.2. Polymeric Biomaterials

Polymers are the building blocks of numerous natural and man-made materials as well as many components of biological creatures. Polymers can be classified into natural or synthetic categories, comprising extensive macromolecules. These macromolecules are constructed by repeating simpler chemical units referred to as monomers. Nylon, polyester, Teflon, polyethylene, and epoxies are some examples to the synthetic (artificial) polymers. On the other hand, silk, wool, cellulose, and proteins are some examples to the naturally occurring polymers [46]. In the field of biomedical applications, a multitude of items including medical disposables, prosthetic devices, dental materials, implants, wound dressings, extracorporeal instruments, encapsulating agents, and related components, frequently utilize synthetic polymeric materials. Synthetic polymeric biomaterials manifest a plethora of noteworthy merits when juxtaposed with metallic or ceramic counterparts. These merits encompass the capacity to customize mechanical and physical properties to precise specifications, facile transformation into an array of structures, such as films, sheets, and fibers, ease of secondary processing, and a favorable cost-acceptable ratio. Like other biomaterials, polymeric biomaterials must be biocompatible, sterile, have good mechanical properties, and physical qualities, and be easily manufactured [39].

3.5.3. Ceramic Biomaterials

Bioceramics can be classified based on their shape, behavior within the physiological environment, or distinct fields of application. Considering their utilization within the human body, a classification system founded on their performance within the biological context offers significant benefits and relevance [47]. Implants constructed from ceramic materials can be categorized into three principal groups: non-absorbable characterized by their relative inertness, bioactive or surface-reactive exhibiting semi-inert properties, and biodegradable or resorbable [39]. Bioinert ceramics remain stable and have no harmful effects or bioactivity when inserted into the human body. On the other hand, bioactive ceramics are ceramics that can directly

bond with bone tissue without any connective tissue in between. Bioceramics are the only biomaterials that exhibit this beneficial trait of directly connecting with bone. Bioactive and bioinert ceramics can endure within the human body for an extended duration without inducing unfavorable reactions. On the other hand, biodegradable or bioresorbable ceramics will be constantly but gradually absorbed by the body, as the name suggests. Its main benefit is the progressive degradation of a bioresorbable ceramic in the body [47].

3.6. BIOMATERIAL AS IMPLANTS

The implants can be divided into three categories, some are external for example surgical instruments, surgical forceps, scalpels, reconstruction prosthetics, and dental crown bridges, and some are internal permanent for example hip implants, knee implants, retinal implants, dental implants. Some are internal temporary for example biodegradable plates and screws [6].

Most artificial implants need to be extremely strong and flexible since they must bear loads that are either static or repeated. Metals have this advantage over polymers and ceramic materials [38]. The implants can be either permanently (non-degradable) or temporarily (degradable) to replace a lost body part or support a damaged one. For instance, spine screws and heart pacemakers.

In the context of biomedical implants, the implant’s surface interacts dynamically with blood, bodily fluids, tissues, proteins, and cellular components in the human body. These interactions may make the transplanted tissue or organ develop a fiber-like covering, slowing its recovery [37]. Researchers identified some efficient alternatives because of unpredictability, which may eliminate the anticipated dangers of post-surgical procedures. These were referred to one of these alternatives as name degradable implanted devices [122]. Thus, the patient may experience a decrease in anxiety in circumstances where further surgical treatment may be prevented by using degradable implant. Additionally, the utilization of these materials will result in cost savings for the patient pertaining to secondary surgical interventions [8].

Magnesium and its alloys are among the best in this series regarding outstanding degradable biomaterial because it is biocompatible, its Young's modulus ranges from 40-45 GPa, and its density is around 1.75-18.5 g/cm^3. However, the early breakdown of magnesium and its alloys, which might partially mend the damaged bone, is a frequent problem [37].

3.7. MAGNESIUM AND MAGNESIUM ALLOY

Investigations on biodegradable metallic implants have focused mostly on alloys based on magnesium, recognized as pioneering materials within the domain of biomedical applications. These alloys created by alloying magnesium with other elements are also biodegradable and show potential for use in bone healing applications [48]. Unfortunately, Mg alloy-based implants still face a lot of difficulties, Mg and its alloys lose their mechanical integrity and stop working before a bone fracture has healed completely due to the rapid breakdown of these materials in biological fluids as in the case of orthopedic implants. The predominant challenges associated with Mg alloy implants include elevated corrosion or degradation rates, compromised mechanical integrity, hydrogen gas evolution, and the potential toxicity of alloying elements. Despite these challenges, it is possible to increase the properties of biodegradable implants utilizing Mg alloys by refining implant geometry and design, precisely managing alloy composition and metallurgy, applying surface treatments, and employing mechanical working techniques. Fig 3.5 shows the key obstacles for implants made of magnesium alloy [49]. Therefore, it has been suggested that the enhancement of mechanical properties and resistance to corrosion in magnesium ingots can be achieved by carefully selecting appropriate alloying elements. However, persistent concerns remain regarding their cytotoxic properties and potential for long-term inflammatory responses [49]. Owing to their relatively low density and exceptional specific strength, magnesium alloys have garnered considerable interest, yet their expected broad applicability is constrained by their insufficient yield strength and poor deformation ability. Alloying is proposed as a practical solution to these issues. Sasaki et al. note that high-content alloying is conducive to improve mechanical properties [50]. Since magnesium solidifies more easily than other cast metals, melting and casting magnesium alloys in an inert

atmosphere with vacuum assistance are the favored manufacturing process. Furthermore, any contamination from reactive gases can be avoided in an environment that is chemically inert [51]. Numerous studies have demonstrated that alloying can improve mechanical properties in comparison to pure metallic forms. Further improvement in mechanical properties can be obtained by applying methods for post-processing methods such as, extrusion, rolling, heat treatment, and forging. Since only a small number of metal elements can be safely introduced into the human body, thus, the biocompatibility of magnesium alloys can be optimized based on the application requirements [52]. In practice, cytotoxicity can result from high concentrations of magnesium and potentially dangerous alloying elements produced during corrosion. The level of toxicity is correlated with the dissolution rate of the alloy. Several in vitro studies have explored the degradation rate and mechanisms. Furthermore, various kinds of magnesium alloys and pure magnesium have been proposed for biomedical uses. An overview of typical magnesium alloys, their compositions, and phases in Table 3.3 [53].

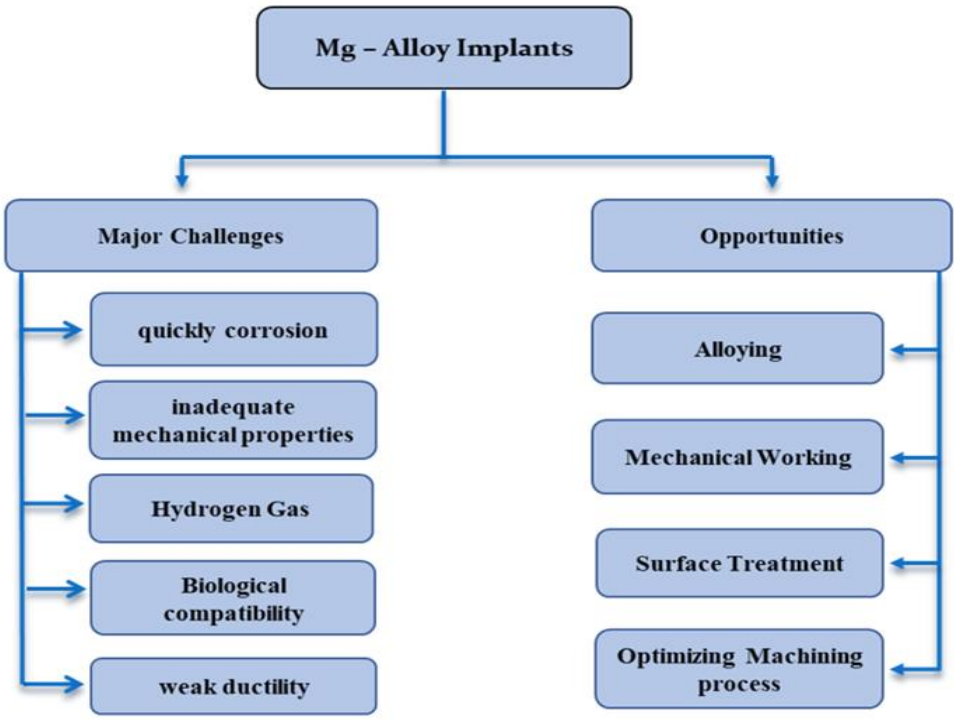

Figure 3.5. The primary challenges associated with implants fabricated from magnesium alloy [49].

Table 3.3. Examples of magnesium alloys utilized within the domain of biomedicine [53].

Family	Representative alloys	Alloying elements (wt.%)			Main phases
Pure Mg	Mg				Mg
Mg–Al–Zn	AZ31	3Al	1Zn		Mg; $Mg_{17}Al_{12}$
	AZ91	9Al	1Zn		
Mg–Ca	Mg–xCa[11,14,15] (x=1,2,3,4,5, ...)	xCa			Mg; Mg_2Ca
Mg–Zn–Ca	Mg–1Zn–1Ca	1Zn	1Ca		Mg; Mg_2Ca; $Ca_2Mg_6Zn_3$
Mg–Zn–Mn–Ca	Mg–2.0Zn–1.2Mn–1Ca	2Zn	1.2 Mn	1 Ca	Mg; Mg_2Ca; $Ca_2Mg_6Zn_3$; $Ca_2Mg_5Zn_{13}$
Mg–Si–Ca		1Si	1Ca		Mg; Mg_2Si; SiMgCa
Mg–Zn	Mg–xZn (x=1,3 10)	xZn			Mg; MgZn Mg_2Zn_3 Mg_7Zn_3
Mg–Zn–Mn	Mg–1Mn–1Zn	1Mn	1Zn		Mg; MgZn Mg_2Zn_3 Mg_7Zn_3
Mg–Mn	Mg–1Mn	1Mn			Mg; Mn
RE containing magnesium alloy	LAE442	4Li	4Al	2 RE	Mg; $Al_{11}RE_3$;
	WE43	4Y	3RE		Mg; $Mg_{12}YNd$; $Mg_{14}YNd_2$
	ZE41	4Zn	1RE		Mg; MgZn (RE)
	AE44	4Al	4RE		Mg; $Mg_{17}Al_{12}$; $Al_{11}RE_3$; $Al_{12}RE$
	Mg–xGd (x=5,10,15, ...)	xGd			Mg; Mg_5Cd
	WZ21	2Y	1Zn		Mg; $MgYZn_3$; Mg_7Zn_3; Mg_3YZn_6
	Mg–8Y	8Y			Mg; $Mg_{24}Y_5Mg_2Y$

3.7.1. Magnesium (Mg)

Magnesium is an element with the chemical formula Mg and atomic number 12, and silver-colored [54]. The melting point of pure magnesium is 650°C, and its crystal structure is HCP [55]. Pure magnesium is more ductile and castable than aluminum and steel and has a higher strength-to-weight ratio [56]. When exposed to air, magnesium oxidizes and takes on a greyer color due to forming an oxide layer (MgO) that stops further corrosion. Magnesium ignites when it is exposed to air with an ignition source present, creating a strong white flame. It is dangerous to try and douse the flame with water because magnesium reacts violently with water vapor, creating hydrogen and intensifying the flame. A magnesium fire may be extinguished

with sand [54]. New categories of biodegradable magnesium are currently being developed. Different biomaterials exhibit unique mechanical properties, biodegradation mechanisms, and biological properties. Because the corrosion product, Mg^{2+}, is quickly removed in urine, Mg and its alloys exhibit positive biological behavior in medical applications [43]. The biological reactivity of magnesium represents a noteworthy aspect, it is a lightweight metal with mechanical properties like natural bone, a natural ionic presence, important functional roles in biological systems, and in vivo corrosion in an environment of the body. As a result, magnesium-based implants have the potential to be biocompatible [57]. Higher magnesium levels might encourage the growth of new bone. According to numerous research on different Mg alloys, there has been increased bone formation surrounding the corroding Mg implant. Additionally, biochemical blood testing revealed that the liver and renal functions were unaffected by Mg implants, proving that they were not harmful [58]. Furthermore, Mg and its alloy counterparts have garnered significant scholarly interest in recent times, primarily attributable to their notably low density. Where the bone density ranges from (1.8-2.1) g/cm^3, almost identical to that of Mg and its alloys (1.7-2.0) g/cm^3 [48]. Conversely to the modulus of elasticity of iron (211.4 GPa) and zinc (90 GPa), magnesium demonstrates an elastic modulus of 41-45 GPa that aligns more closely with the range observed in natural bone 3-20 GPa. The mismatch in elastic modulus may cause the implant to bear a larger proportion of the load. This biological incongruity may contribute to significant clinical challenges, including early implant loosening, compromised healing, bone thickening, and sustained inflammation [59]. Due to weak ductility and insufficient strength at room temperature, magnesium has not been widely utilized. These constraints arise from the distinctive hexagonal close-packed crystal structure inherent to Mg, marked by a restricted number of slip systems operative at room temperature. Consequently, Mg alloys exhibit suboptimal deformation performance [60]. Therefore, it is difficult to deform magnesium plastically at ambient temperature due to the HCP crystalline structure's restriction on the slip systems, which results in a high work hardening rate and limited flexibility. Magnesium alloys are typically processed at high temperatures because different slip planes become active at these temperatures. In addition, anisotropic mechanical properties in cold rolled sheets because of their crystallographic texture is another effect of the HCP

crystal structure. Fig 3.6 shows an image of pure Magnesium [55]. Furthermore, compared to standard biodegradable materials like polymers and ceramics, magnesium-based biomaterials have superior mechanical properties [43].

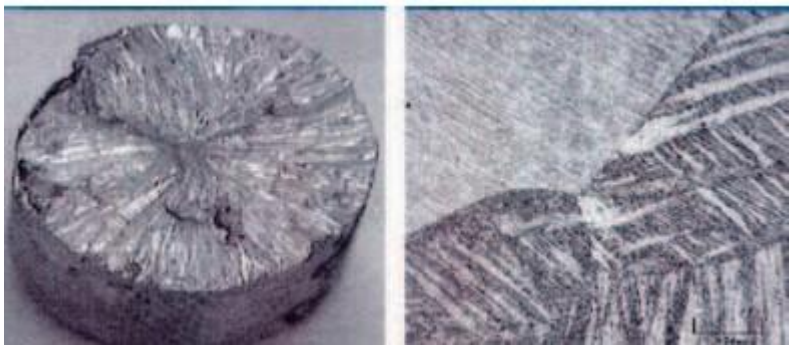

Figure 3.6. The pure Magnesium [55].

3.7.2. Zinc (Zn)

Zinc has a comparatively high boiling point (907 °C) and a low melting point (419.5 °C). When in its purest form, zinc is brittle at room temperature but becomes malleable at around 100 °C [54]. Also, pure zinc in its as-cast state has several drawbacks, including poor mechanical properties and an elongation that is typically less than 3%. It has hexagonal close-packed structure (HCP) [62].

Zn is one of the most typical alloying elements used in commercial Mg ingots. Zn additions can lower the rate of corrosion and increase the mechanical properties [63]. Zinc, a unique biodegradable metal, has more corrosion resistance than Mg, which makes it a better choice for bioresorbable implant applications [64]. In addition, zinc, being among the essential minerals in human nutrition, possesses a fundamental level of safety suitable for biomedical applications. Zn addition can also lessen the negative impacts of Fe and Ni-based metallic contaminants because Zn converts these contaminants into harmless intermetallic phases. Zinc-containing magnesium alloys have therefore received increasing attention and have been developed as potential candidates for use in biological applications [65]. Moreover, Zn is an element that is necessary for the human body and important for a variety of

biological processes, including the immune system, taste, and smell [63]. The amount of zinc that individuals should consume every day is between 8–11 mg. Patients may have concerns about pure zinc implants because daily consumption of 100–300 mg might create health issues, and a larger amount than this can be even more hazardous [59]. The upper limit of Zn solubility in Mg at 340 °C is 6.2 wt% [66]. Whereas it reduces to 0.2 wt% at room temperature [67]. The binary Mg-Zn phase diagram is given in Fig. 3.7 [67]. Zn element enhances the yield strength of magnesium through age hardening and solid solution hardening. Additionally, Zn inhibits the emission of H_2 gas from magnesium alloys [22]. As the content of zinc increases, the grain size tends to decrease. As a result, mechanical properties involving tensile strength, yield strength, and hardness are enhanced when zinc concentration is increased. Besides, increasing zinc enhanced lower rate of corrosion, which may be because of the effects of finer grain size and more evenly distributed zinc on the alloy's surface, which improved negative film formation [68]. The current applications of the Mg-Zn binary alloy are limited by certain undesirable properties, including a broad crystallization temperature range and a susceptibility to hot cracking. Thus, to enhances both the mechanical and microstructure properties of the Mg-Zn ingot, the incorporation of additional alloying elements becomes necessary [14].

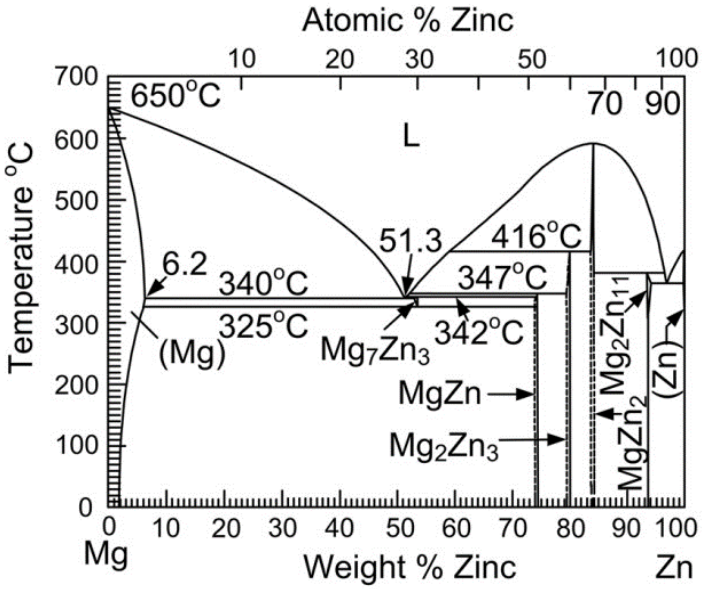

Figure 3.7. Displays the phase diagram of the (Mg-Zn) system [67].

3.7.3. Calcium (Ca)

Calcium (Ca) is the predominant mineral primarily stored in bones and teeth. The Ca ion and its derivatives have very low toxicity when compared to other metals, given the body's great natural abundance of calcium molecules, this is not surprising. Kidney stones are the most frequently observed adverse effect of calcium. Although acute calcium poisoning is uncommon, excessive calcium carbonate supplementation has the potential to harm the kidneys [69]. On the other hand, Although the amount of calcium consumed may have an impact on the formation of bone tissue, the excessive quantity of calcium ions may lead the risk of hypercalcemia, and cardiovascular problems [70].

When combined with the right thermomechanical treatments, addition of calcium can enhance the microstructure of magnesium alloys, increase their strength, reduce their flammability, and improve their heat resistance. The exceptional creep-resistant properties of Mg-Zn-Ca alloys, which are caused by thermally stable $Ca_2Mg_6Zn_3$intermetallic particles, were what initially sparked so much interest in them [71].

Calcium exhibits a limitation that is its maximal solubility in magnesium capped at 1.34 wt.%. Higher levels of calcium exceeding 1 wt.% result in the diminishing in both the strength and ductility of magnesium-based alloys. Specifically, as the calcium content surpasses 0.5 wt.%, there is a notable reduction in the ductility and ultimate tensile strength of Mg-4Zn-based alloys. [59]. Additionally, at room temperature, Ca is not soluble in magnesium [56]. By creating intermetallic phases with magnesium, the Ca element functions as a grain refiner in magnesium alloys and enhances the strength and creep properties of Mg [22]. The Mg-Ca phase diagram in Fig 3.8 [66]. The advantageous combination of affordable prices and desirable properties, such as relatively high corrosion resistance, strength, and plasticity, have increased interest in the Mg-Zn-Ca system. Ca achieves a good combination of ductility and strength by weakening the basal texture and increasing the corrosion resistance through the creation of a more corrosion-resistant oxide layer. Zn and Mg can combine to generate several different intermetallic compounds. The $Ca_2Mg_6Zn_3$ stable intermetallic combination, which is advantageous for high temperature applications. However, Mg-Zn-Ca alloys with zinc concentrations above

4.0 wt.% led to grain coarsening, which reduced the mechanical properties of the alloy. Ca levels above 1 wt.% also contribute to sticking or hot ripping during casting. Therefore, to create high-performance alloys, the researchers should determine the alloy composition carefully [14].

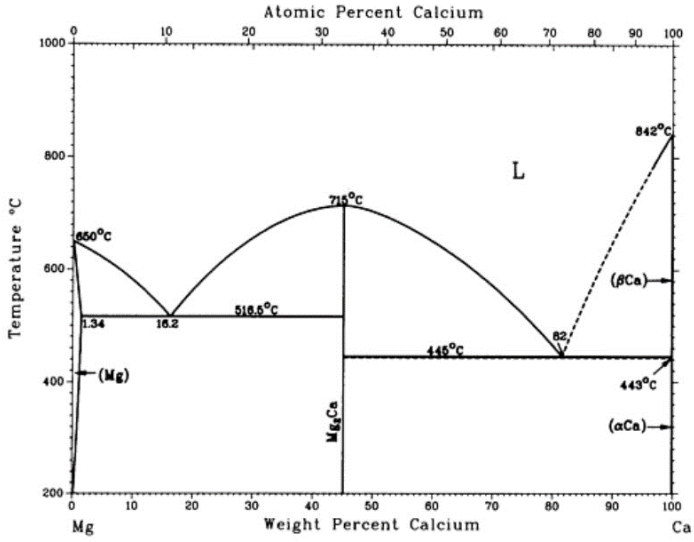

Figure 3.8. Displays the phase diagram of the (Mg-Ca) system [66].

3.7.4. Manganese (Mn)

Most organisms need manganese (Mn), a chemically active micronutrient. It is quite hard and a brittle metal that is difficult to melt, since it oxidizes quickly. When manganese is pure, it rusts like iron, when it is a powder, it combines with oxygen. The Mn melting temperature is 653 °C [54]. Manganese is an important mineral that functions as a cofactor for several metalloenzymes in biological systems [69].

The ability of Mn to improve the microstructure of extruded alloys has just been discovered, Mn contributes to high ductility because Mg atoms combine less readily with it to generate intermetallic compounds [72]. Manganese (Mn) may be mixed with magnesium alloys as an alloying element to enhance their resistance to corrosion and ameliorate the adverse consequences stemming from impurities. Furthermore, incorporating manganese into magnesium alloys has the potential to enhance both their yield strength and ductility [7]. On the other hand, Mn addition

can increase thermal conductivity, and improve formability [73]. Manganese also enhances creep behavior, increases damping capacity, and smooths out the microstructure [14]. Figure 3.9 provides the phase diagram of the magnesium-calcium (Mg-Mn) system [66].

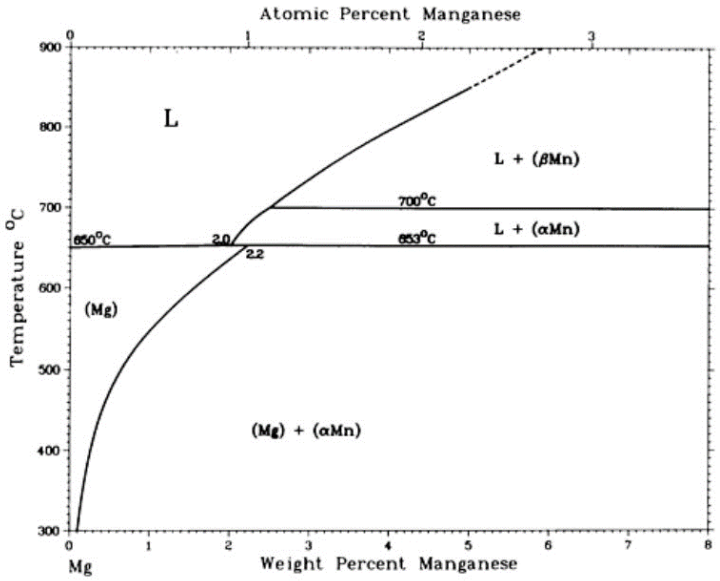

Figure 3.9. Displays the phase diagram of the (Mg-Mn) system [66].

3.8. PLASTIC DEFORMATION BEHAVIOR OF Mg ALLOYS

Plastic deformability is a measure of a material's ability to strain under applied load or stress without shattering. As with all HCP metals, magnesium alloys have two plastic deformation mechanisms: slip and twinning [74]. In Figure 3.10 a schematic representation is presented, depicting (a) the slip planes, and (b) the twinning planes within the crystal lattice of magnesium [75]. Magnesium alloys exhibit intricate deformation behavior, wherein the initiation of twinning and slip mechanisms during deformation is intricately linked to a multitude of factors, including stress-strain condition, temperature, alloy composition, strain rate, presence of secondary phases, precipitates, and the initial textural state. Consequently, enhancing the resistance to twin and slip deformation serves as a viable strategy for increasing the strength of Mg and its associated ingots. On the other hand, particularly in hcp materials with

few available suitable deformation modes, the temperature is thought to have a significant influence on the activation of deformation processes [75].

In Figure 3.11 the impact of deformation temperature on the critically resolved shear stress (CRSS) and the primary modes of deformation in magnesium is elucidated. It is evident that within this context, the basal slip system consistently exhibits the lowest CRSS value [76]. Magnesium and its alloys exhibit a c/a ratio approximately 1.62354 at a temperature of 25 °C, representing a slight deviation from the theoretically ideal c/a ratio of 1.633 for HCP structures. In comparison to other HCP metals, this c/a ratio of Mg results in a greater primitive cell volume than that of other HCP metals, which lowers stacking fault energy (SFE) levels in Mg alloys. The stacking fault energy (SFE) levels in metals play a crucial role in governing the activation energies for deformation processes, rendering SFE as a significant metric for assessing deformation mechanisms in metals. The SFE is influenced by elements such as dislocation configuration, the existence of local defects, and grain size. Low SFE raises the activation energies for a slip but promotes twinning deformation. Increasing SFE lowers the activation energies for dislocation movement, promoting slip.

Consequently, a contributing factor to the reduced ductility is the low SFE observed in magnesium and other hexagonal close-packed metals. An HCP structure encompasses approximately six distinct slip systems, with only two of them oriented favorably for slip movement. The limited symmetry of HCP lattice, which presents challenges in accommodating strain within this crystal structure, is associated with the restricted number of crystallographic planes and directions favorably aligned for slip movement. In this regard, it is significant to bear in mind that factors such as the CRSS of slip and twinning, accessible deformation modes, c/a ratio, and the imposed deformation in relation to crystallographic texture all affect the deformation processes in HCP metals [74].

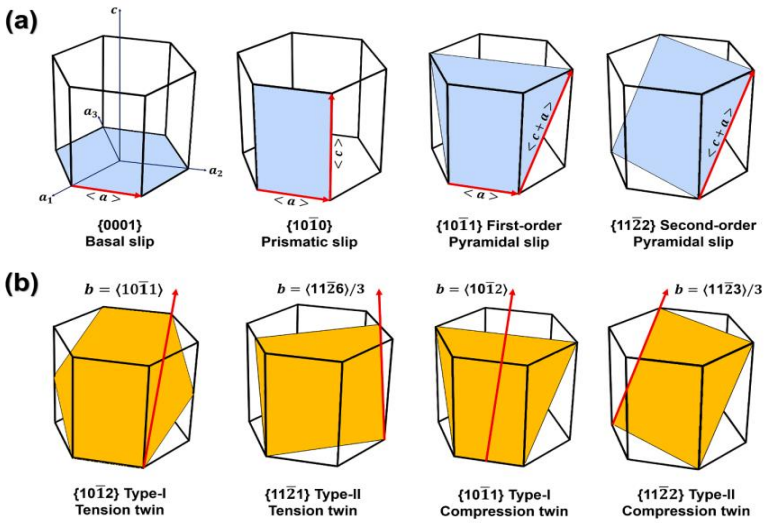

Figure 3.10. The schematic forms planes for twinning and slip crystal lattice of the magnesium [75].

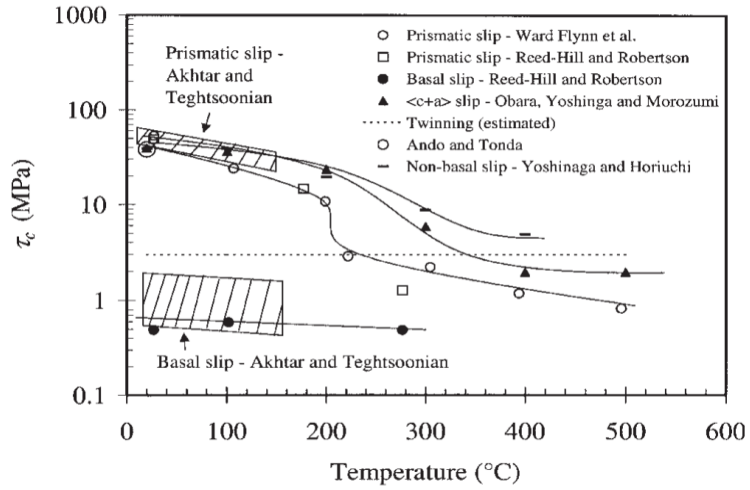

Figure 3.11. The Impact of Deformation Temperature on (CRSS) [76].

3.8.1. Slip In Magnesium Alloys

Since there are a few slip systems for magnesium at low temperatures, its deformability is severely constrained. Basal slip happens along the path of the plane. Other slide mechanisms become activated when the temperature rises. In Mg alloy systems, there are three main slip modes: pyramidal <c + a>, prismatic <a>, and basal <a>. Fig 3.9.a shows slip systems in Mg [75]. Each of these modes possesses a

critical resolved shear stress governing their respective slip motions. In magnesium alloys, the atomic planes begin to reorient, and dislocation glides occur when CRSS is accessed by a slip system. Because of crystal orientations different in a material, active slip in the various slip modes contributes to anisotropy in magnesium alloys. As a result, many slip modes in a single material are simultaneously activated, producing the directionality of properties that exhibit different properties or behaviors depending on the direction in which it's measured or observed. However, the poor symmetry of the crystal structure, which restricts formability, is principally responsible for the limited plasticity in Mg alloys [74]. Unfortunately, hcp metals have few slip systems with low CRSS values, limiting their ductility. As a result, twining mode is required, which allows for further strain accommodation [75].

3.8.2 Twinning In Mg Alloys

Studying twinning behavior is important for comprehending the deformation process of magnesium alloys and influencing their properties. The mechanical response, strength and ductility, texture development, and fracture of magnesium alloys can all be significantly impacted by twinning [77]. In magnesium alloys, a uniform distribution of shear stress along the crystallographic c-axis induces the reorganization of atomic planes within the parent grain, leading to twinning in magnesium alloys at or below room temperature [74]. In magnesium and its alloys, twinning performs two significant functions. The twinned regions of the grains are reoriented, which aids in texture development. Additionally, twinning can influence the strain-hardening behavior of magnesium alloys [78].

Twins may act as preferred locations for the nucleation of recrystallization during hot deformation, improving grain refinement, possibly modifying the texture while concurrently enhancing the strength and ductility of magnesium alloys. The major twin lamellae are divided into smaller lamellae by (LAGBs) low-angle grain boundaries, which is the basic nucleation process in twin-induced recrystallization [79]. The initial lattice reorientation and formation of twin boundaries initiate various deformation mechanisms, including texturing, dislocation glide, re-twinning, and detwinning. Mechanical twinning substantially influences the deformation conduct of

Mg alloys [75]. Deformation twinning is a crucial deformation process for magnesium alloys lacking adequate slip systems. In Mg alloys, the, {1011} <1012> compression twin, {1011}– {1012} double twin and {1012} <1011> tension twin are often seen [80]. Contraction twins, observed in Mg alloys, emerge under higher CRSS conditions compared to extension twins and accommodate compressive strains along the same axis [74]. The twinning commonly serves as a corrective mechanism to offset the absence of c-axis deformation in each crystallographic direction. In magnesium (Mg) alloys, there is mechanical (tension-compression) asymmetry during twinning because the kind of twins that form depends on the loading direction and cannot occur concurrently in the alloys. Twin boundaries in the grains operate as barriers to slip and reduce the ductility of the alloys. This is the important adverse effect of twinning in magnesium alloys. Additionally, it has been shown that twinning can rotate the material's basal poles in the direction of loading, causing the material to rapidly harden and exhibit nonlinear mechanical behavior [74].

On the other hand, at ambient temperature, plastic deformation leads to notable twinning on multiple crystallographic systems and the formation of densely packed dislocation clusters within the initial grain structures. Twin boundaries surround crystallites that form from intersecting primary and secondary twins within primary twins. This is called twin dynamic recrystallization [119]. It should be noted that the process of twin dynamic recrystallization has three steps. In the first step, nucleation happens when different twin systems cross or lattice dislocations are rearranged inside twin lamellae. Due to the production of orientation misfit dislocations, twin boundaries are transformed into random high-angle barriers. This is the second stage. The outcome is that the nuclei change into newly crystalline grains. The third stage is the beginning of border movement (migration) [81].

3.9. THE HOT FORMING

Metalworking procedures are utilized to give the metal the appropriate shape and size, and to obtain the best mechanical properties possible [82]. Many industrial alloys' microstructures and properties can be controlled by hot deformation and post-deformation heat treatments [83]. Metals can be mechanically deformed cold or hot

to obtain the desired shapes. When the tensile stress in a metallic material, induced by external forces, attains the yield point, it results in the initiation of plastic deformation within the material. Slip and twins are the two common mechanisms that control the plastic deformation of the metals. In crystalline materials, the process of metal deformation, known as slip, occurs along the plane experiencing the highest shearing stress due to externally applied forces. The second situation involves deformation along two planes that run parallel to each other and traverse diagonally through the unit cells. These parallel planes are identified as twinning planes, delineating the region between them within the grains, termed the twinned region. Twinning planes are essentially the planes along which this twinning deformation occurs [82]. Dislocations become less mobile during cold working because they accumulate at grain boundaries and tangle into lattices. This causes strain hardening, which makes it more challenging to induce further deformation. The degree of strain hardening can be lowered by working at higher. During hot working, recovery and dynamic recrystallization mechanisms can take place and transform elongated grains into smaller, dislocation free equiaxed grains [84].

3.10. ANNEALING

The process of annealing normally entails heating the material to a high temperature (above its recrystallization temperature) enough to soften it, maintaining it there for a certain amount of time, and then cooling it down. Annealing alters the physical, mechanical, and occasionally chemical properties of the materials, improves ductility, decreases hardness, makes the material more workable. For instance, cold-worked alloys are annealed to reduce strain accumulation in the cold-worked microstructure or to soften the worked alloy. Also, the homogenization annealing of casting alloys is another fundamental annealing process that allow uniform distribution of the chemical elements throughout the material. Redistributing alloying elements to promote diffusion and assisting in recovery by lowering internal stresses are two significant advantages of annealing, as well, as encouraging the growth of grain, and new recrystallized grain creation. In nonferrous alloys, annealing is largely influenced by two key factors: the temperature to which the material is heated and

the hold time at temperature. The hardness of a cold-worked alloy remains mostly consistent when annealing is carried out quickly or at low temperatures [84].

The three stages of the annealing process of a deformed material are recovery, recrystallization, and grain growth. The recovery is considered the first stage, it operates at relatively lower temperatures and aims to induce softening of the metal. This softening is achieved through the elimination of internal stresses stemming from dislocations, which are typically linear structural defects. Notably, during the recovery stage, t the shape and dimensions of the existing grains remain unaltered.

The second stage is recrystallization, in which new grains without internal stresses nucleate, grow, and replace the old ones. If annealing continues, grain growth take place that is the third step. Grain growth is followed by coarsening mechanism in which some abnormal grain growth occurs. Grain coarsening might lead the metal to lose a significant amount of its initial strength [85].

3.11. HOT ROLLING

Hot rolling is an important method to obtain magnesium alloy sheets, strips, or plates that are highly efficient and flexible [86]. Magnesium alloys can have fine grains, their impurity tolerance levels can be raised, their crystallographic orientation can be changed, etc. As a result, the hot rolling process has an impact on the alloy's mechanical properties [22]. Also, hot rolling can change several significant microstructural factors, such as grain refinement brought on by dynamic recrystallization (DRX) [87]. Deformation-induced imperfections, such as dislocations, render the microstructure of a deformed magnesium alloy inherently unstable. Consequently, additional annealing treatments are often employed to attain a stable state through processes such as static recovery (SRV), static recrystallization (SRX), and grain growth. This step is essential since the deformed alloy, in its current state, is not suitable for ultimate applications [88]. Therefore, it has always been stressed how important it is to comprehend micro factors and their effects on metallurgical phase changes via the hot-rolling process [89]. Hot rolling is mainly used to obtain uniformly thin workpiece and impart necessary and useful properties

to the workpiece through a series of plastic deformations [90]. To increase material workability and reduce deforming metal flow stress, the substance is heated in the hot deformation area in the first step of this method. The metal is then repeatedly rolled to achieve the appropriate size and shape by plastic deformation. The kinetic the process, including dynamic and static recrystallization during or after hot rolling, is greatly influenced by temperature and strain rate distributions inside the rolled metal [89]. Figure 3.12 illustrates the rolling process and grain refinement during hot rolling [82].

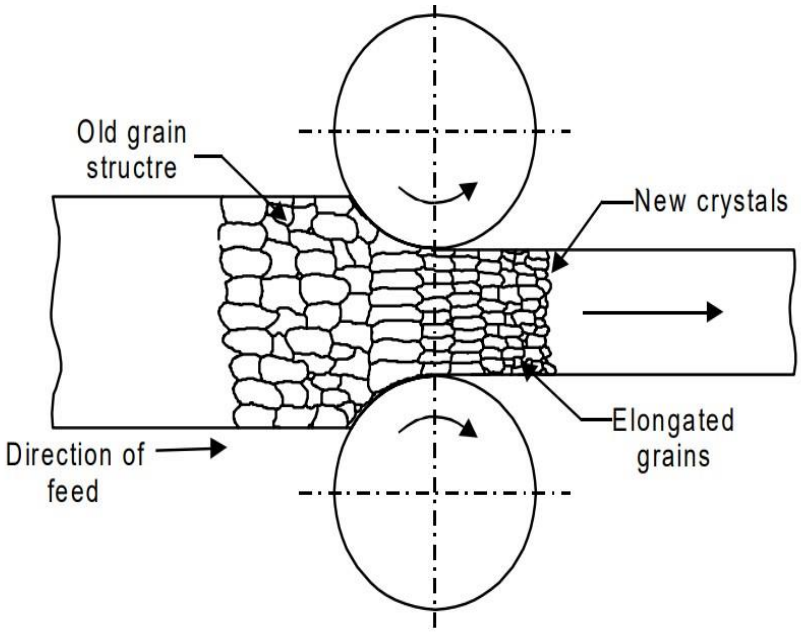

Figure 3.12. The hot rolling [82].

3.12. EFFECT OF THE TEMPERATURE

The morphology and dimensions of grains undergo alterations throughout the plastic deformation stages in metal forming. During the recrystallization process, new grains initiate growth at the locations of internal stresses induced by deformation. The recrystallization temperature of the metal is the temperature at which recrystallization is complete. Hot working temperature is crucial because any residual heat from the metalworking process promotes grain growth that depends on both time and temperature. Thus, grain growth reduces mechanical properties [82].

When the annealing temperature and time rise, the degree of recrystallization also increases progressively. Thus, it causes twins to gradually disappear and the intensity of dislocations to diminish. The driving force increases at higher annealing temperatures and annealing time also contributes to grain development [86].

Since magnesium alloys do not have many slip systems available in room-temperature, deformation behavior of magnesium is significantly influenced by temperature. Magnesium alloys exhibit increased deformability and thermal activation above 225 °C. Consequently, the majority of magnesium alloy-forming processes are conducted at temperatures exceeding 225 °C. Hot deformation causes the dislocation density to rise in the grains, which causes the materials to become more durable over time. However, if the stress concentration due to the dislocation cannot be reduced, it may result in fracture [91].

3.13. EFFECT OF THE GRAIN BOUNDARY

Grain boundary sliding plays a contributing role in high-temperature deformation, specifically these exceeding 0.5 of melting point (0.5Tm). The superplastic behavior that results from this deformation process, or a very high elongation-to-failure, is a beneficial property for shaping materials into complicated forms [92]. The most popular and effective way to improve grain boundary sliding is grain refining. The emergence of precipitates at grain boundaries while the material is in a supersaturated state serves as a mechanism to impede grain growth at elevated temperatures, such as those encountered in conventional superplastic conditions. Therefore, an increased concentration of alloying elements serves as a significant factor in impeding grain growth by creating a restrictive barrier that limits the movement of grain boundaries during recrystallization and grain growth processes. This results in the formation of a finer and more densely distributed grain structure within the material [92]. The grain size may achieve significant enhancements in the properties of the Mg alloys, as per the Hall-Petch.

As mentioned above, the few deformation modes that may be used and the robust basal texture produced by conventional deformation processes are the major causes

of the weak ductility of magnesium ingots at room temperature [93]. Most of the grain boundary may be thought of as an atomically disordered zone. Stress concentration at the grain boundary occurs when dislocation motion is inhibited by the grain boundaries that act as source of dislocations. Therefore, constrained dislocations at the grain boundaries result in increased strength [93]. The influence of grain size on the deformation mechanisms and ductility of magnesium ingots can be examined its impact on dislocation slip. Grain refining promotes grain boundary movement and rotation, triggers potential non-basal slip systems, and shortens dislocation slip in magnesium ingots. This results in a homogeneous deformation. Additionally, reducing grain size to finer levels may mitigate the undesired transition from easy-glide dislocation to immobile basal-dissociated dislocation [93]. Briefly, reduction in grain size that activates the easy-glide dislocation and prevents the unfavorable transition increase the ductility of magnesium significantly [93]. As for, the twin is impacted by grain size [94]. Therefore, in addition to limiting the development and spread of twinning, the stress concentration at grain boundaries also aids in the nucleation of twins [95]. By lowering the grain size, which would essentially restrict twinning but activate unnecessary slip processes, magnesium would go from twinning to slip. Additionally, the anisotropy of Mg may be reduced, and its strong texture can be weakened with the formation of fully fine grain structure by dynamic recrystallization process. As a result, grain refining at the micron or submicron size greatly enhances the ductility of Mg ingots [93]. Moreover, the results of various studies indicated that diminishing the grain size of magnesium alloys may lead to a reduction in the propensity for twinning [96]. However, it should be kept in mind that increasing the total grain boundary area by reducing grain size reduces the corrosion resistance of the alloy since grain boundaries are two-dimensional defects [87].

3.14. CORROSION

According to the literature, it is possible to describe corrosion in several ways, such as the disintegration of the metal owing to its interaction with the medium to which it is exposed, or it may also be referred to as the failure of the metal for reasons other than mechanical. Also, wear is the term used when metal wears out as a result of

friction. Sometimes it is referred to as it is a failure that affects the metal's surface due to chemical causes or chemical variables supported by mechanical forces present in the environment in which it operates [97]. In chemical corrosion, the substance is dissolved by a corrosive solvent (corrosion liquid). In an electrochemical corrosion, an electric circuit is created [85]. Electrochemical reactions on a metal's surface are the primary source of most corrosion processes in metals. When a metal atom is oxidized and passes into a solution as a positive ion, leaving electrons on the surface of the metal, it is called anode (where the oxidation process happens). The other components of an electrochemical corrosion are electrolyte (the immersion solution that transports ions to and from the metal surface) and cathode (which consumes the released electrons). Corrosion may show up in a variety of ways depending on various parameters such as oxidation potential of metal, the properties of the corrosive medium, the structural geometry, and other relevant factors. Appearance of the metal surface after corrosion is often used to categorize the various corrosive attacks [54]. The regions of anodic and cathodic reactions took place can vary significantly during metal corrosion and provide important information about the type of corrosion like crevice corrosion uniform attack and pitting. Fig.3.13 shows some types of corrosion [84]. Most materials come into contact with many different kinds of environments in one way or another. Such interactions frequently reduce a material's utility by degrading its mechanical properties (such as strength and ductility), other physical properties, or appearance [97].

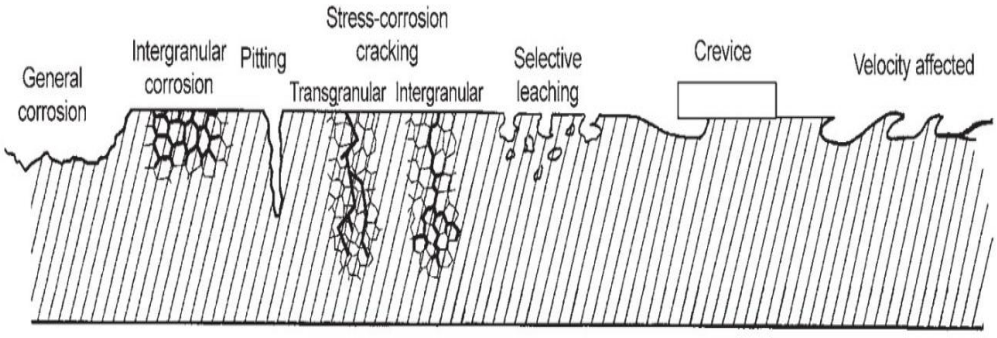

Figure 3.13. Forms of corrosion [84].

3.14.1. Implants Corrosion

The several corrosion occurrences are frequently under dispute or inquiry. For instance, one can wonder how long certain corrosive circumstances have existed or how long it will take before the product fails due to corrosion. Unfortunately, corrosion rates are notoriously unpredictable, making it difficult in some situations to make exact projections [98]. The interactions between the implants and the tissues are of utmost importance, in addition to the hostile environment and the heavy load, the implant must be durable. The dissolution of metal ions initiates corrosion, contributing to the material's brittleness and implant fracture [99]. The assessment of implant deterioration and corrosion holds paramount significance in biomaterial design. The impact of degradation in a biological setting can manifest as advantageous or adverse, contingent upon the specific application. Biodegradable implants, in particular, are engineered for a temporary role, facilitating tissue regeneration, and subsequently undergoing a gradual and deliberate degradation process [100]. A significant challenge of biodegradable implants lies in achieving a suitable degradation rate, ensuring the comprehensive regeneration of damaged tissues before complete in vivo degradation. Biodegradable magnesium alloys frequently exhibit notably high degradation rates, especially during the initial stages of implantation [101]. All implanted materials experience some level of corrosion after surgery, a protective, inert film forms on the metal surfaces, limiting corrosion. Relevant forms of corrosion in contemporary alloys include fretting, stress-corrosion cracking, intergranular, galvanic, and pitting corrosion [102]. Among them, fretting corrosion, pitting, and fatigue are three types of corrosion that are typically observed in implant applications [95].

3.14.2. Pitting Corrosion

Pitting is a serious type of localized corrosion that causes considerable amount of damage and the release of metal ions. Pitting can be observed by developing holes or small cavities on the material's surface, typically protected by a thin layer [102]. Pitting occurs because of the passive protective film on the metal surface breaks down [103]. Pitting is among the various types of corrosion that do the greatest

damage. Because it develops in small regions (pits), it is harder to detect and has a greater impact on structural integrity than overall corrosion [104]. The significance of pitting is greatly affected by the type of layer or film that develops on a material's surface due to its interaction with the environment. When the material enters a state of "passivity", the dissolving process at the surface is delayed, protecting it against general corrosion [102]. Pitting corrosion failures may be caused by the local site of the pit, metal inclusions, or a localized breakdown of the film layer. A metal's poor crystal structure may cause pitting corrosion failures, which refer to structural nonuniformity or deficiencies that render the metal more susceptible to this form of corrosion. These defects can act as initiation sites for localized corrosion, thereby accelerating pitting corrosion [103]. The initiation of these pit formations is ascribed to the interplay between certain aggressive ions and the passive film, particularly at locations where the film exhibits vulnerabilities or flaws. In certain instances, these pits might be discernible without the aid of optical instruments, however, they remain obscured and represent a substantial risk. They have the capacity to accelerate the onset of stress corrosion cracking or fatigue-induced fractures, ultimately leading to the catastrophic failure of components during operational use [102]. Pit formations can be classified into two discrete categories: trough pits (upper) and lateral pits (lower). In instances of corrosion, the pitting can lead to the accumulation of corroded material, thereby leading to the creation of caps covering the pits, and occasionally, the development of nodules or tubercles [105]. Fig.3.14 shows forms of pits [105]. At the base of pits, there is a notable elevation in corrosion current density, while their apex is shielded by a protective film that obstructs the migration of both metal ions and hydrogen ions (H^+). As pitting progresses, metal ions tend to accumulate at the pit's apex, sometimes forming a film that encloses the pit, blocking the entry of solution and oxygen [102].

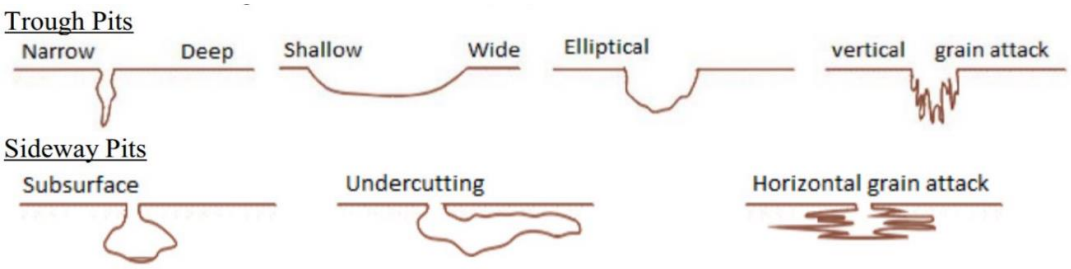

Figure 3.14. The Forms of pits [105].

3.14.3. Crevice Corrosion

Crevice corrosion type of structural degradation resulting from a localized corrosion process. It arises when a metallic substrate experiences incomplete protection against environmental factors [106]. The presence of a crack, a small, deep fracture, such as between a plate and a screw head, or flaws like fatigue cracks, are fundamental conditions for the occurrence of this process. It often appears below the screw head holding the plate or in areas comparable to these, such as the point where two parts meets, the hip nail, etc. Crevice corrosion issues may frequently be solved using the right device design and material selection [102]. A tiny volume of a stagnant solution must be present for crevice corrosion. The crack's geometrical specifications, especially its gap, must be precise to maintain an occluded environment inside the crevice while allowing the solution to pass through. The depth and the ratio of the external to the inside area have a significant role in defining the attack's severity [108].

3.14.4. Galvanic Corrosion

Galvanic corrosion manifests as an electrochemical phenomenon when two materials exhibit significantly different electrical potentials, enabling the smooth flow of electrons between them. Galvanic corrosion is an electrochemical process that takes place when two materials have enough dissimilar electrical potentials for electrons to easily flow between them [108]. Galvanic corrosion requires the presence of three things to occur. Firstly, when two metals with different electrode potentials are in

electrical contact. One metal act as the anode (more reactive, tends to corrosion), while the other serves as the cathode (less reactive, often protected from corrosion) [109]. Secondly, an electrolyte is crucial, typically present as a liquid or moisture in the environment. This electrolyte allows the movement of ions between the metals [110]. Lastly, in an electrical connection, there must be a conductive path between the two metals to enable the flow of electrons, this connection allows the transfer of electrons from the anode (where oxidation occurs) to the cathode (where reduction occurs), completing the electrochemical reaction [109]. Figure 3.15 displayed a schematic representation of corrosion galvanic in metals [110]. Two-metal corrosion, or galvanic corrosion, happens when two different metals come into direct contact in an ionic-conducting fluid medium like interstitial fluid or serum [120]. Differences in the composition or manufacturing processes of a plate and the adjacent screws cause the formation of a galvanic pair. Surgical implants may experience galvanic corrosion if the metals or alloys used to construct the bone plate and bone screw are made of different metals or alloys. The potential for corrosion is particularly pronounced at the interface between the plate and the lower regions of the screw holes [102]. The material with the lower electrical potential, which is more negatively charged, serves as the anode. While the substances with the higher electrical potential, which is more positively charged, serve as the cathode. The anode loses electrons to the cathode and releases positive ions into the electrolyte when the two materials are linked [110].

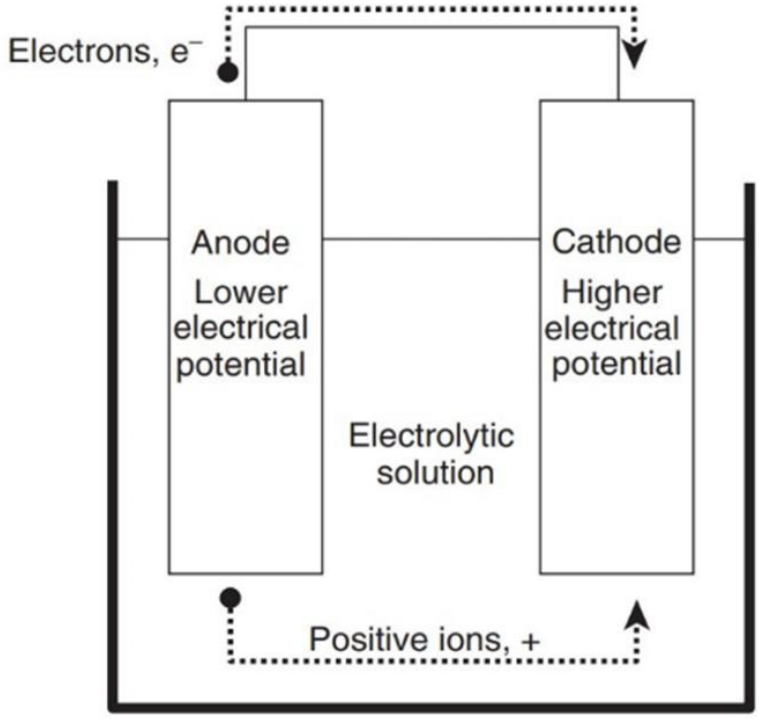

Figure 3.15. The Schematically of galvanic coupling [110].

3.14.5. Corrosion Fatigue

Corrosion fatigue is the term used to describe the early breakdown of a material caused by exposure to the combined action of corrosion and cyclic stress [109]. When electrochemical process and cyclic loads interact, corrosion fatigue, a kind of metal fracture failure, results [102]. It is a process where a metal prematurely cracks by fatigue when corrosion and repetitive cycle loading are present at lower stress levels than would normally be necessary in the absence of a corrosive environment [108]. If metals and alloys are repeatedly subjected to tremendous cyclic stress, even in the absence of corrosion, they will eventually break. As the tension is raised, the number of cycles for failure is reduced. The metal will survive forever when under a specific amount of stress. This level is called as endurance limit. However, the material's endurance limit is significantly lowered if it is exposed to a corrosive environment while under cyclic stress. The major evidence of corrosion fatigue fractures is the appearance of multiple cracks close to the fracture [109]. For metals used in cyclic motion applications or load-bearing surgical implants, corrosion

fatigue resistance is a crucial aspect to consider. In most cases, a failure won't happen, although fractures might start from latent faults, surface damage, minor irregularities, or chemical attacks. The presence of a corrosive environment may cause a localized corrosive attack that amplifies the effects of the numerous flaws [111]. The bodily fluid environment might weaken the implant's fatigue resistance. The most frequent causes of mechanical failures in orthopedic implants are fatigue or environmentally aided fatigue. For instance, it has been proposed that fretting and stress-corrosion cracking may both initiate cracks and spread them. Additionally, cracks may start as a result of corrosion phenomena and spread primarily through a fatigue process [102].

3.14.6. Fretting Corrosion

Fretting corrosion happens at the interface between two metals due to vibration or sliding. In a corrosive media, fretting corrosion originates from minute relative motion between the contacting surfaces. Notably, fretting corrosion can manifest even in the absence of a corrosive medium [98]. The clinical significance of fretting corrosion is determined by its intensity. It also significantly impacts the initiation and progression of cracks and fractures in implants [112]. Fretting corrosion, arising from small motion between implant components subjected to cyclic loads, manifests at modular junctions or connections of implant components [113]. This corrosion phenomenon is observed across various alloy types and is also prevalent in the modular connections of orthopedic implants designed for the hip and knee [121]. Bioactive corrosion products lead to localized inflammation, which in turn causes localized bone loss (osteolysis), discomfort, and eventually implant loosening. Currently, limiting fretting corrosion requires knowledge of metallurgical processing factors, reduction of modular connection tolerances, knowledge of surface chemistry and topography, and the use of the proper materials [113].

PART 4

EXPERIMENTAL PART

4.1. OVERVIEW

This section provides a comprehensive examination of the methodologies utilized for the manufacturing of the magnesium alloys under investigation in this study. It encompasses the mechanical and heat treatment processes applied to these alloys, the techniques employed for the preparation of specimens intended for microscopic and mechanical analysis, as well as the instrumentation employed in the execution of these analytical procedures.

4.2. CASTING

The gravity die-casting method was used to produce two different magnesium alloys (Mg-1Zn- 0.2Ca-0.3Mn and Mg-3Zn-0.2Ca-0.3Mn in wt.%). From here on, first alloy is called Alloy-1, and second alloy is called Alloy-2. The ingots were manufactured using an electric resistance casting furnace under controlled atmospheric conditions. The furnace comprises two primary parts. In the upper part, there is a melting unit where the molten metal is obtained according to the designed compositions. In the lower part, there is a mold-heating unit that allows us to heat the mold to a certain temperature in order to prevent solidification before the mold is completely filled with the liquid metal. In this process, the ingot was melted and held at 800 °C for 30 minutes before pouring it into the mold. Prior to molding liquid metal, the mold was heated to 400 °C. The protective atmosphere in the melting section was provided with Ar gas to prevent evaporation and oxidation. In the mold heating unit, which is the part where the casting is taken, the atmosphere control was provided using a 0.8% SF_6+CO_2 gas mixture. Melting of the ingots was carried in a stainless-steel crucible (AISI 310). In inspiration, the steel mold was coated with

boron nitride spray to prevent any reaction between the mold and liquid metal and to separate the cast easily from the mold. In addition, mold contains venting holes to remove the air in the mold and to prevent gas holes (porosities) in the solidified metal. In this manner, as the liquid metal passes through the runner, it gradually fills the mold's arms from the bottom up. The images of the melting and casting furnace are given in Fig. 4.1 and Fig. 4.2.

Figure 4.1. The casting furnaces.

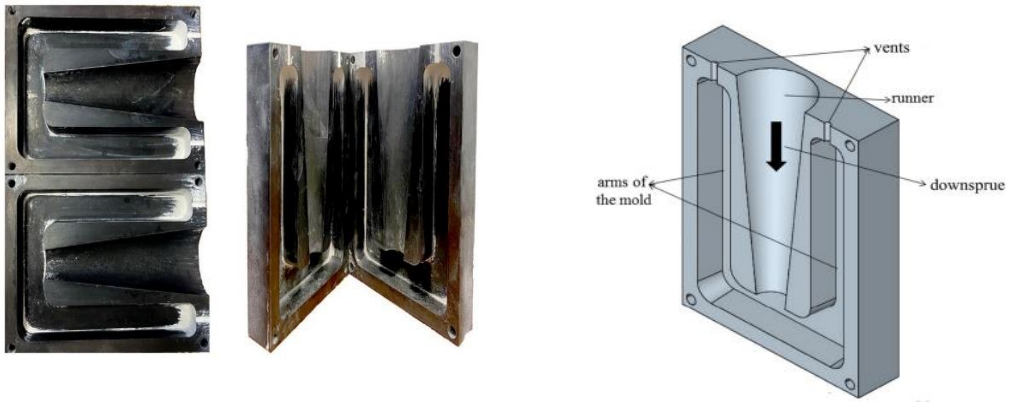

Figure 4.2. The shape of the mold.

4.3. HEAT TREATMENT FOR HOMOGENIZATION

Homogenization heat treatment was performed to obtain a uniform composition and properties. In this process, the cast alloy is heated to a specified temperature and kept at that temperature for a specific amount of time. Homogenization heat treatment ensures that the alloy has uniform chemical, mechanical and physical properties throughout the alloy. Homogenization heat treatment of the ingots studied here was carried out at 400 °C for 12 hours using a Proterm PLF 1200/45 furnace, the images of the homogenization furnace are given in Fig. 4.3. The heating rate was 5 °C/min to prevent the formation of internal stresses.

Figure 4.3. The furnace of homogenization.

4.4. CHEMICAL ANALYSIS OF ALLOYS

X-ray fluorescence is a feasible technique to examine both the major and minor elements in the materials. Here the composition of the alloys was determined using Rigaku ZSX Primus II–WD XRF spectrometer fitted with a 4 kW Rhodium tube. Table 4.1 displays the experimentally determined composition of the alloys, expressed as weight percentage (wt.%). The XRF machine is shown in Fig. 4.4.

Table 4.1. Composition of the alloys, expressed as weight percentage (wt.%)

Alloy name	Mg	Zn	Ca	Mn
Alloy 1	98.39	1.07	0.21	0.31
Alloy 2	96.57	2.91	0.21	0.29

Figure 4.4. The XRF machine.

4.5. HOT ROLLING AND HEAT TREATMENT

The rolling process was carried out in a double roller rolling device of the Şekermak brand. The roller diameter was 200 mm, and the rolling speed was 20 rpm. All samples were subjected to 10% deformation in each pass, and a total of 30% deformation was applied in 3 passes. Before the first pass, all samples were heated to 250 °C and kept at this temperature for 30 min. The samples were kept at 250 °C for 15 min between passes and then the next pass was applied. In hot rolling, the sample dimensions were 5x20x100 mm (thickness x width x length) and they were cut from the cast alloys by using the wire-erosion method. Six samples from each alloy were hot rolled. Fig 4.5 shows the rolling machine used in the process. After hot rolling, heat treatment was applied to five out of six hot rolled alloys at 325 °C for (10-20-30- 60-120) min to compare with homogenous and hot rolled samples. Proterm PLF 1200/45 furnace was used for the heat treatments. Samples were quenched after hot rolling and heat treatments.

Figure 4.5. The rolling machine used in the process.

4.6. METALLOGRAPHIC SAMPLE PREPARATION

Preparing samples for microscopic examination is the first step in the framework of research and accurate detection of the internal structure of the sample taken from the alloy to be studied, where the location of the sample must be chosen so that the mass taken from it represents the whole material so that we can come up with sound conclusions of practical value after the examination. In order to prepare a sample for testing, the following equipment and materials must be available; a cutting machine, mounting device, grinding device, polishing device, etching components, drying device, distill water, gloves, glasses, and a fume hood. For metallographic sample preparation, samples in rectangular prism shape with approximately 4x10x20 mm (thickness x width x length) were cut and mounted in a mixture of polyester resin and hardener. After curing polyester resin, samples were ground starting by using SiC grinding papers from 240 to 2500. The grinding-polishing machine used in sample preparation is given in Fig 4.6. Polishing was carried out using polishing cloth and 1 mμ alumina solution. After polishing, all samples were etched using etching

solutions. Two solutions were used here. The first one is acetic-picral solution, and the second one is nital solution. The composition of acetic-picral solution is 5 mL acetic acid, 6 g picric acid, 10 mL purified water and 100 mL ethanol. The composition of nital solution is 100 mL purified water and 4 mL nitric acid. Each specimen was dipped in acetic-picral solution about 10-20 s and then rinsed in distilled water. After that, the specimen was dipped in nital solution about 30 s and then rinsed in ethanol and purified water. After checking the surface of the specimen in optical microscope, etching was repeated until the grain and phase boundaries appear.

Figure 4.6. The cutting and machine, and the grinding-polishing machine.

4.7. PREPARING SIMULATED BODY FLUID (SBF)

Simulated bodily fluid was prepared at one of the laboratories at Karabuk University according to the description by, Kokuba et al, using substances given in Table 4.2 along with one litre of distilled water. To Prepare 1000 ml from SBF, 1000 ml beaker was filled with 700 ml of distilled water. After that, the water in the beaker was heated to 36 ±1.5 °C using an electric heater while the solution was stirred by a magnetic stirrer. To avoid precipitation and a high pH, we dissolved the components in the order shown in Table 4.2 from first to eighth, making sure that each ingredient had completely dissolved before we added the next. It is essential to monitor the pH level during the dissolution process. The pH usually rises during the dissolution

process of Tris. If the pH surpasses 7.45, the dissolution of Tris should be temporarily halted, and a small quantity of hydrochloric acid (some drops) should be added to adjust the pH to the desired range of 7.42 ± 0.01. Subsequently, the dissolution of Tris can be resumed. When all the content of the Tris had been dissolved, the temperature of the solution's is adjusted to 36 ± 1.5 °C. The pH of the solution is adjusted until it is precisely 7.4 at 36.15 °C by gradually adding HCl. We add the last of the remaining distilled water after the solution reaches a temperature of 20 °C. We also store the solution in a freezer and dark environment. Figure 4.7 shows an image of preparation equipment [114].

Figure 4.7. The preparation of SBF.

Table 4.2. The composition of SBF.

	Material	Percentage (g)
1	NaCl	8.035
2	$NaHCO_3$	0.355
3	KCl	0.225
4	K_2HPO_4. $3H_2O$ (di-potassium hydrogen phosphate trihydrate).	0.231
5	$MgCl_2.6H_2O$	0.311
6	HCl	39 (ml)
7	$CaCl_2$	0.292
8	Na_2SO_4	0.072
9	$(HOCH_2)_3CNH_2$ (Tris-hydroxymethyl aminomethane).	6.118
10	pH 4, 7 and 9 (pH standard solution).	(0 –5) (ml)

4.8. IMMERSION CORROSION

Immersion corrosion of the samples in SBF solution was conducted at 37°C for 24, 120, and 240 h. The samples were preserved in an electric resistance furnace. The images of the furnace are given in Fig. 4.8. The volume of the solution for each sample was determined using the apparent surface area that is given by the following equation.

Vs=Sa/10

Where Vs is the volume of the solution and Sa is the apparent surface area of the specimen. In immersion corrosion, the samples in rectangular prism shape were used with approximately 4x10x20 mm (thickness x width x length). The samples were ground using 1000 and 1200 grit SiC papers. The initial and final weights of the specimens were measured using a precision balance with 1/10000 sensitivity. After corrosion, samples were cleaned by pure water and dried by blowing hot air. After that, the final (dry) weight of the specimens was measured. Finally, the immersion corrosion rate of the samples in terms of mm/year and mg/cm2.h were calculated using the following equations.

Corrosion rate (mm/year) = (K*W)/(A*T*D)

Corrosion rate (mg/cm2.h) = W/(A*T)

W= weight loss (mg).

K= constant = 8,76x104

A= Surface area (cm2)

T= dipping time (hour)

D= density (g/cm3)

In these calculation, theoretical density of the alloys was used. It was calculated using mole fractions of alloying elements and their theoretical densities according to the mixture law.

D=$\sum_{i=1}^{\infty} m_i^f * D_i$, where

$m_i^f = mole\ fraction\ of\ element\ i\ and\ D_i density\ of\ element\ i.$

Calculated theoretical density of Alloy-1 and Alloy-2 are 1.77 g/cm^3 and 1.81 g/cm^3, respectively.

Figure 4.8. The furnace of samples preserved in the (SBF) solution.

4.9. MICROSTRUCTURE ANALYSIS

An optical microscope equipped with an Image Analyzer was used to examine the microstructures. The image of the device is given in Fig 4.9.

Carl Zeiss Ultra Plus FESEM, field emission scanning electron microscope (SEM) with JEOL 6060LV brand energy dispersed element analysis (EDS) apparatus was used to determine the microstructure and phase composition of the alloys. The image of the device is given in Fig 4.10.

Figure 4.9. The device Optical Microscope.

Figure 4.10. (SEM) The scanning electron microscope, and (EDS) energy dispersed element analysis.

4.10. X-RAY DIFFRACTION (XRD) ANALYSIS

To conduct phase analysis of the alloys, Rigaku Ultima IV diffractometer was employed, utilizing Cu-Kα X-ray radiation generated at an accelerating voltage of 40 kV and a current of 20 mA. The range of scanning for the measurements spanned from 20° to 90°, and the scanning rate was 3 degrees /min. The identification of phases in the X-ray diffraction pattern of the alloys was facilitated through reference to the ICDD database. Figure 4.11. displays a visual representation of the equipment.

Figure 4.11. The X-ray diffraction (XRD)

4.11. MICRO HARDNESS MEASUREMENTS

The evaluation of hardness was carried out using the microhardness tester (Q10 A+ QNESS), the image of the device is given in Fig 4.12. During the Vickers (HV) microhardness measurement, a load of 500 g was applied for 15 seconds. Measurements were taken from 5 different points of each sample. While calculating the mean value, the smallest and largest measured values were neglected and the average of the other 3 values was given as the hardness test result in HV0.5, together with the standard deviation values.

Figure 4.12. The device of microhardness.

4.12 TENSILE TEST

The tensile test was carried out to evaluate the mechanical properties of the alloys. The test samples were prepared in rectangular prism shapes with the following dimensions: the width is between 12.70 - 20.9 mm, and the length of the specimens is 120 mm. The thickness is 5 mm for homogeneous samples and 3.65 mm for hot rolled samples. Tests were done by using MTS 100 kN Dynamic Test Device and a 1 mm/s pulling rate at room temperature. The image of the device is given in Fig 4.13.

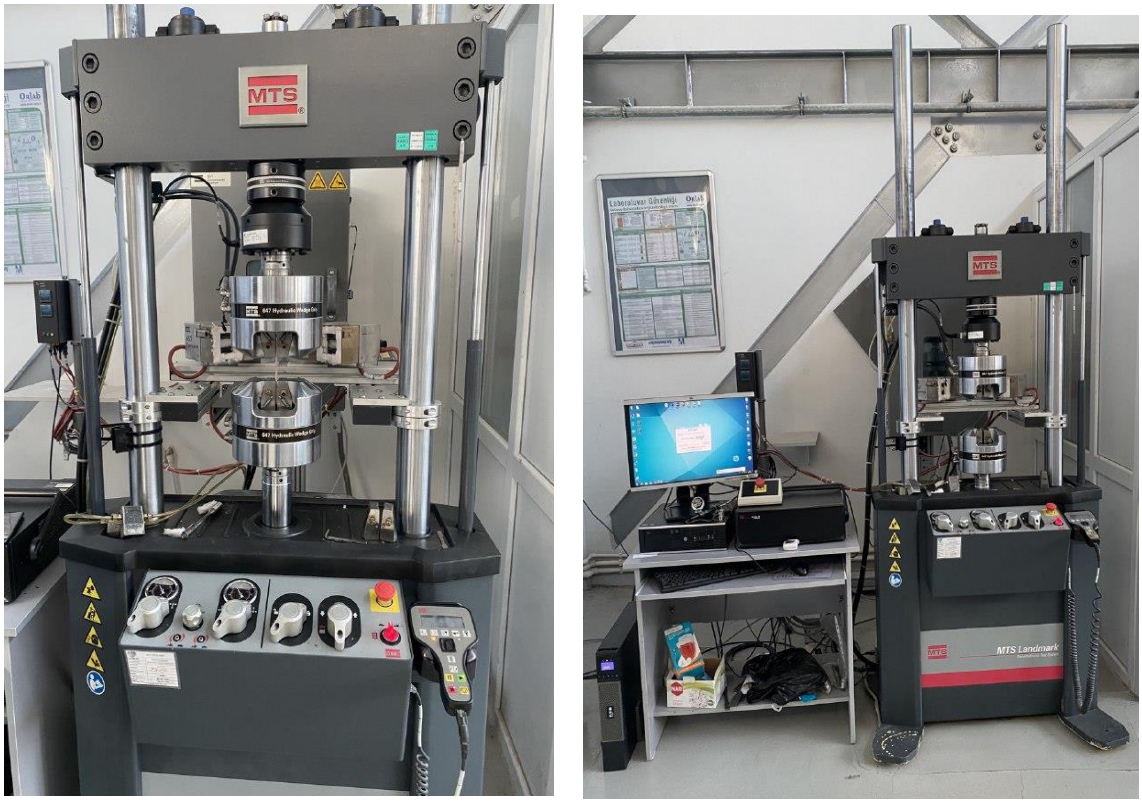

Figure 4.13. The tensile test device.

PART 5

RESULTS AND DISCUSSION

5.1. OVERVIEW

This chapter present and discuss the key results obtained from the tests and analysis conducted in this study. The experiments were designed to characterize various properties of the materials under investigation. The results are analyzed and discussed in three primary sections. The first section deals with the analysis of chemical composition and microstructure investigations. Elemental analysis using X-ray fluorescence and investigations of microstructure using optical microscopy and scanning electron microscopy are reported. This provides valuable insight into the material's baseline chemistry and microstructural features. The second section focuses on evaluating the mechanical properties of the materials. Tests such as tensile testing and hardness measurement were performed. The results from these standard tests are analyzed to understand properties like strength, ductility, and toughness as a function of alloy composition and structure. In the final section, the corrosion behaviour of the materials was investigated. Immersion corrosion tests were conducted to determine the corrosion rate of the ingots. The corrosion rate and mechanism are discussed based on the outcomes of these experiments.

5.2. CHEMICAL COMPOSITION OF THE ALLOYS

Chemical compositions of the alloys measured with X-ray fluorescence (XRF) are given in Table 5.1 which presents the nominal and actual compositions of the alloy following the homogenization process. Furthermore, the measured compositions are very close to their designated nominal compositions.

Table 5.1. XRF analysis results of the alloys following the homogenization process in wt.%

	Nominal Compositions				Measured Compositions			
	Mg	**Zn**	**Ca**	**Mn**	**Mg**	**Zn**	**Ca**	**Mn**
Alloy -1	98.5	1	0.2	0.3	98.39	1.07	0.21	0.31
Alloy -2	96.5	3	0.2	0.3	96.57	2.91	0.21	0.29

5.3. MICROSTRUCTURE EXAMINATION

5.3.1. Optical Microscope

Figure 5.1 provides optical micrographs of samples that were subjected to a homogenization process at 400 °C for a duration of 12 hours for Alloy-1 in (a), and Alloy-2 in (b).

The secondary phase, known as $Ca_2Mg_6Zn_3$, is predominantly distributed along the grain boundaries, with some instances appearing as discrete points within the grains. The $Ca_2Mg_6Zn_3$ phase is a significant component of the eutectic structure, which is formed by α-Mg and $Ca_2Mg_6Zn_3$ phases. It was also observed that the volume fraction of $Ca_2Mg_6Zn_3$ in Alloy-2 was higher than in Alloy-1. This is attributed to the higher Zn content that promoted the formation of the $Ca_2Mg_6Zn_3$ phase. This observation aligns with the findings reported in reference [8].

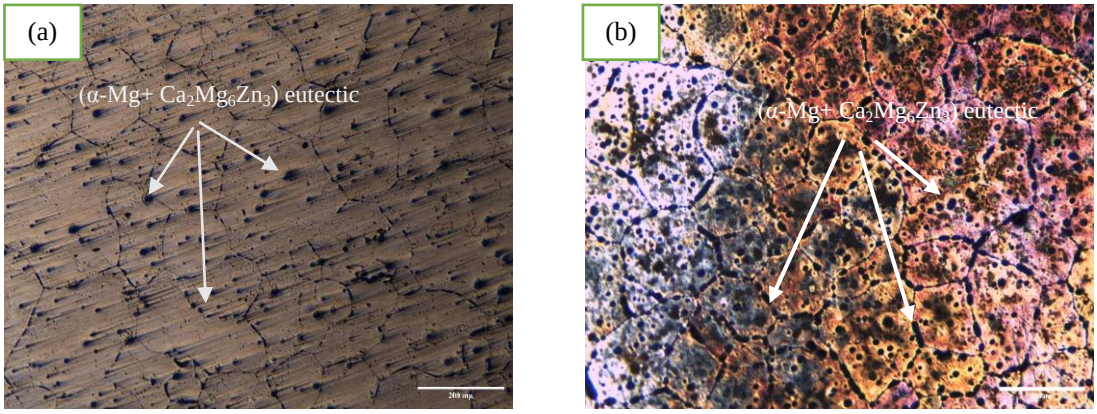

Figure 5.1. Optical micrographs of specimens subjected to the homogenization process for Alloy-1 (displayed in part a) and Alloy-2 (displayed in part b).

Figure 5.2 presents the relationship between the average grain size and the duration of the heat treatment process. The average grain size was determined utilizing image analysis software (ImageJ). The findings indicate that, for specimens homogenized at 400 °C, the average grain size was approximately 192.2 µm for Alloy-1 and 158.4 µm for Alloy-2, respectively. Notably, an increase in the zinc content in Alloy-2 in comparison to Alloy-1 led to a reduction in grain size because secondary intermetallic phases act as barrier to the grain growth. These observations align with the outcomes reported in reference [68]. On the other hand, the additional zinc forms separate phases or deposits within the microstructure. These deposits can act as extra sites for grain nucleation, thereby encouraging the formation of smaller grains [68]. In addition, it is seen that some grains have curved boundaries inwards. These boundaries are under tension force, and they will eventually shrink and disappear during annealing.

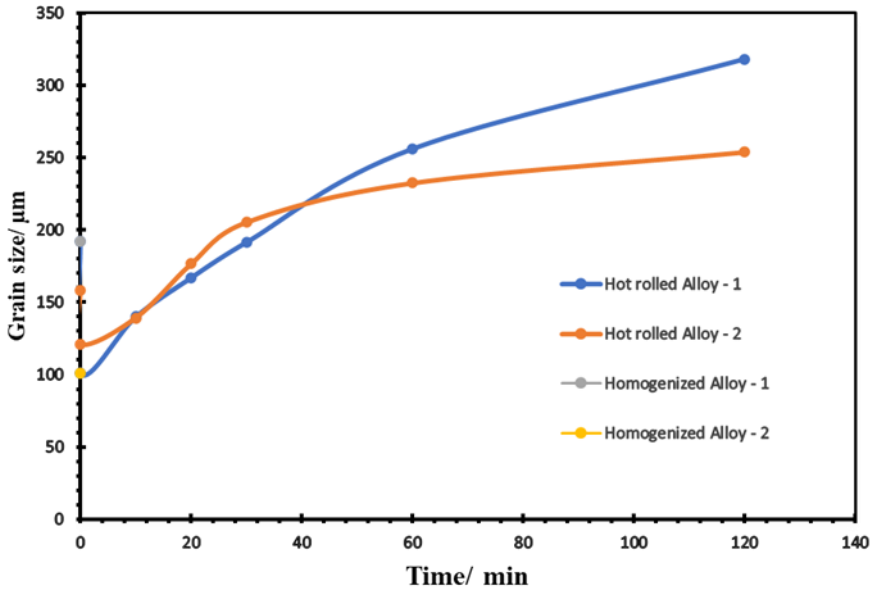

Figure 5.2. The relationship between grain size and duration of heat treatment.

As exhibited in Figure 5.2, reduction in the grain size of the alloys occurs during hot-rolling process. However, a gradual increase in grain size is observed after post heat treatment at 325 °C. Grain growth continues with the increased post heat treatment time. This is due to the fact that hot rolling results in finer grains and the formation of twin bands. Noteworthy is that the grain size decreases during rolling due to the progressive dynamic recrystallization, which is crucial for the formation of equiaxed grains [115]. Given that twinning is a significant deformation mechanism in metals with low crystal symmetry, such as those with hexagonal close-packed (hcp) and body-centered cubic (bcc) structures due to a limited number of available slip systems, twinning occurs within the hcp α-magnesium matrix during hot rolling [8]. Furthermore, heat treatment serves to reduce residual stresses over time, which typically promotes grain growth through grain boundary migration and results in larger grains with lower overall grain boundary area [84].

It was also found that the decrease in grain size for the samples subjected to hot rolling was not significant for the second alloy compared to the first alloy. For Alloy-1, the grain size decreased from 192.2 mµ to 101 mµ, while for Alloy-2 it decreased from 158.5 mµ to 121.15 mµ. This can be attributed to the higher deformation resistance of the sample due to the higher zinc content, which causes grain

refinement and improves the mechanical properties [98]. Moreover, precipitation of the ternary phase in the presence of Ca has a beneficial impact on the mechanical strength of the alloy, this phenomenon potentially leads to greater control over the rolling procedure, and lower susceptibility to plastic deformation [68]. Microstructures of the samples after homogenization heat treatment, hot rolling, and post heat treatment at 325 °C for 120 min are given in Fig. 5.3. The coarse-grained microstructure of the homogenization sample (Fig. 5.3 a and b) transforms into a relatively very fine elongated grains and deformation twins after 30% deformation (Fig. 5.3 c and d). It is expected that this may affect the material properties such as strength, ductility, and corrosion properties. In addition, twinning in the microstructure (Fig. 5.3 c and d) contributes to the grain refinement because there were more twin boundaries that restricted the movement of dislocations during the process. On the other hand, grain growth takes place when the material is heat treated at 325 °C for 120 min after hot rolling (Fig. 5.3 e and f)).

It is noticed that the grains of the homogenized samples contain a large number of secondary phase particles (black dots). Some of the secondary phases located at the grain boundaries were dissolved in the matrix due post heat treatment.

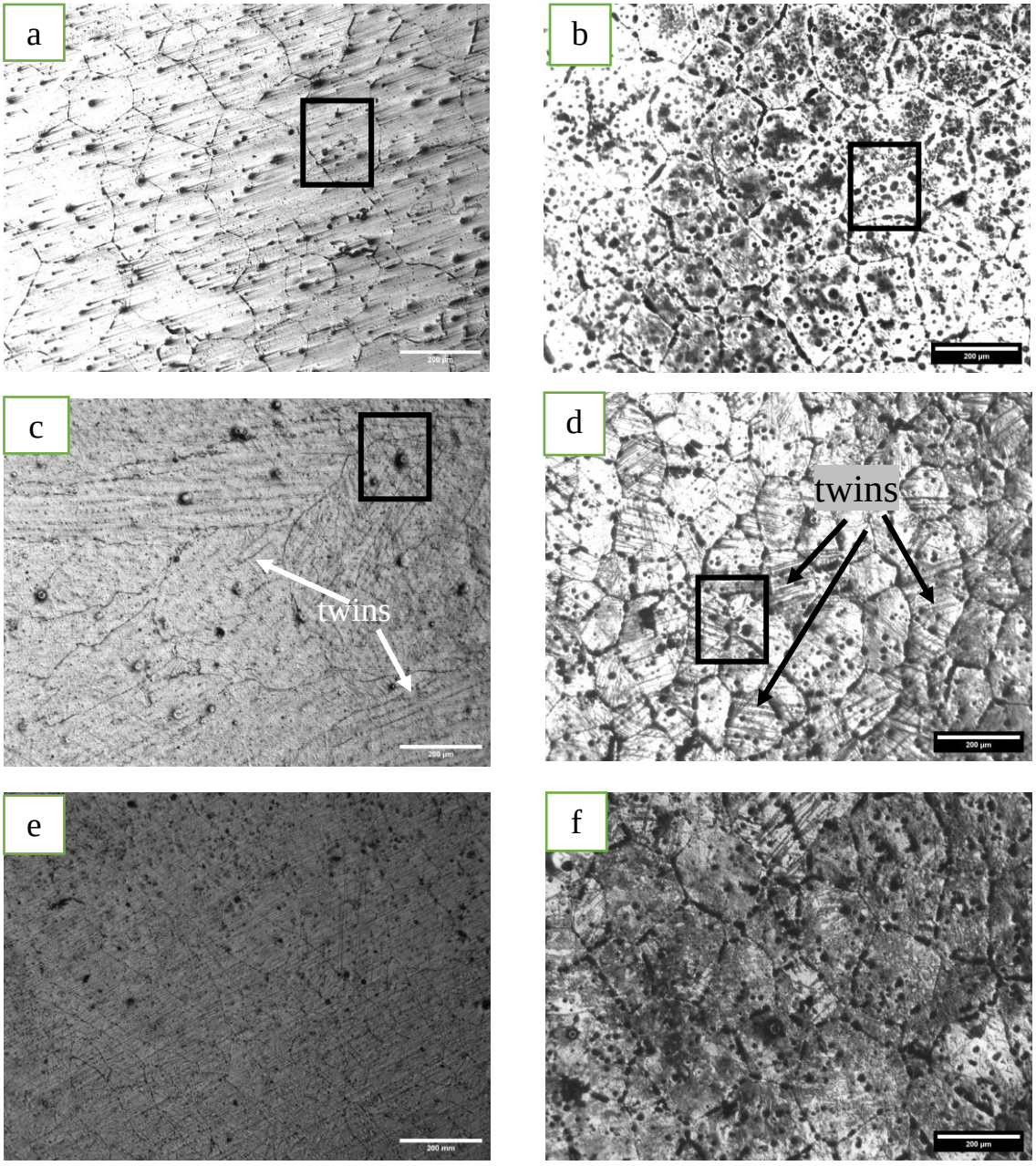

Figure 5.3. Images taken under the microscope show homogeneous specimens (a, b) of Alloys (1,2), rolled specimens (c, d), and specimens subjected to 120-minute heat treatment (e, f), respectively.

Fig. 5.4. shows the effects of hot rolling on grain size and elongation. It was found that the original grains were elongated by hot-rolled and heat treatment and that some grain boundaries were coarsely pointed. The average grain size of the elongated grains measured in these images was for Alloy-1 (length 636µm, width 110.8µm), while Alloy-2 (length 278.7µm, width 125.7µm) correspondingly.

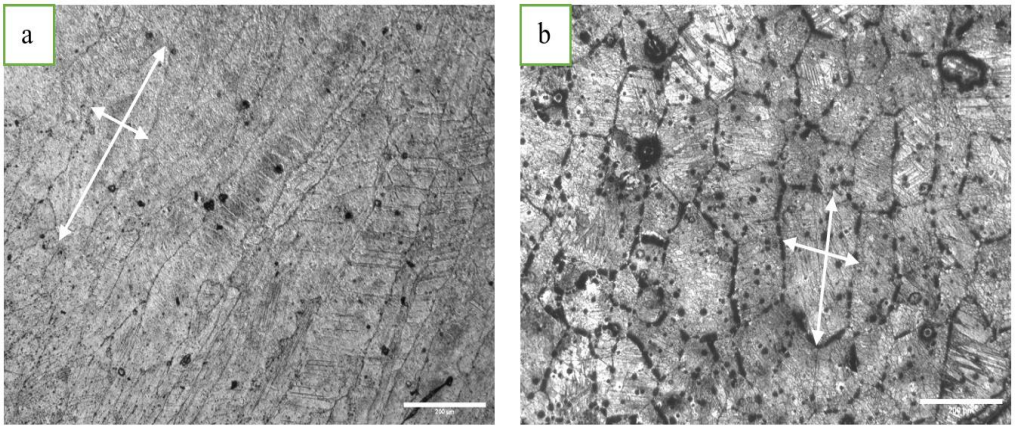

Figure 5.4. The effect of hot rolling on grain size and elongation Alloy-1 (a) and Alloy-2 (b).

5.3.2. Scanning Electron Microscope (SEM)

Examination using scanning electron microscopy (SEM) confirmed the results seen in optical micrographs. Fig. 5.5 and 5.6 display SEM images of the homogenized Alloy-1 and Alloy-2 samples, respectively. A secondary phase can be seen distributed uniformly as lamellar eutectic structures along the grain boundaries within the α-Mg matrix primary phase. Furthermore, the alloys predominantly exhibit coarse-grained microstructures containing secondary phases. The coarse-grained structure of the alloys can be attributed to grain growth and coarsening that occurred during homogenization heat treatment. While both alloys contain the same calcium ratio, Alloy-2 has a higher zinc content than Alloy-1. Thus, increasing zinc ratio of the alloys led to higher volume fraction of the $Ca_2Mg_6Zn_3$ secondary phase, as observed previously [8].

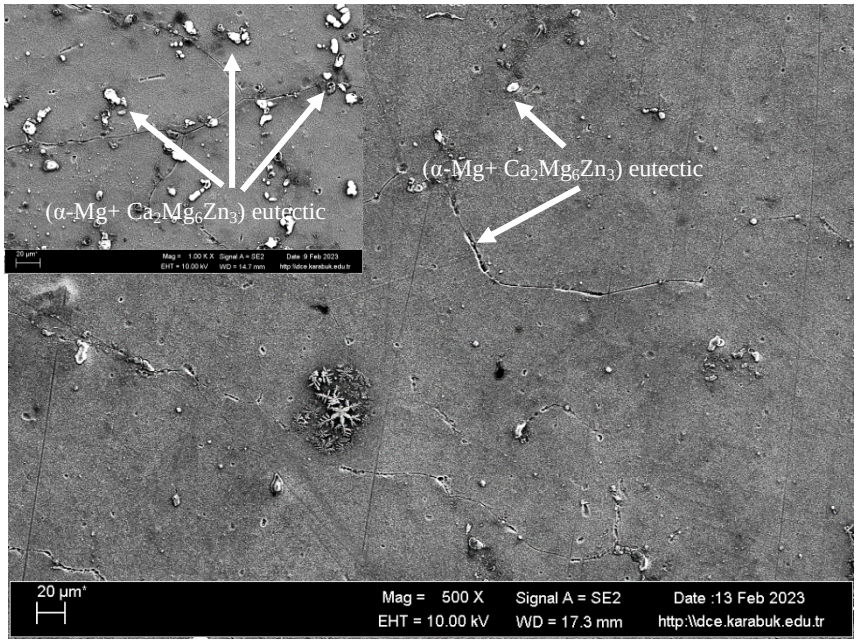

Figure 5.5. SEM micrographs of homogenized of Alloy-1.

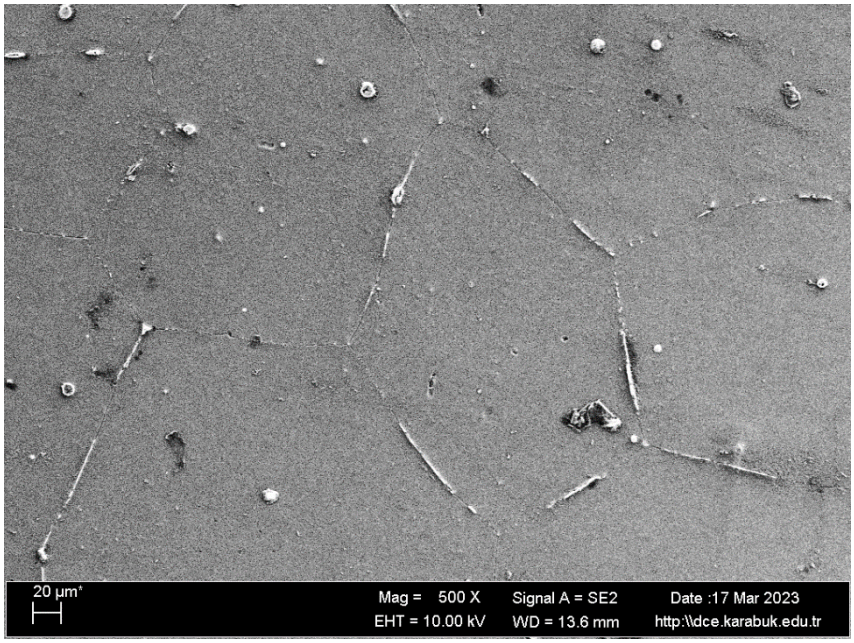

Figure 5.6. SEM micrographs of homogenized of Alloy-2.

Fig. 5.7 shows the microstructure of the alloys after hot rolling. As expected, the microstructure is characterized by twinning. Grain refinement developed as a result of a 30% deformation at 250 °C, and hot rolling transformed the coarse-grained

microstructure of the homogenized specimens into a much finer microstructure. It was found that the original grains became more elongated, and grain size decreased.

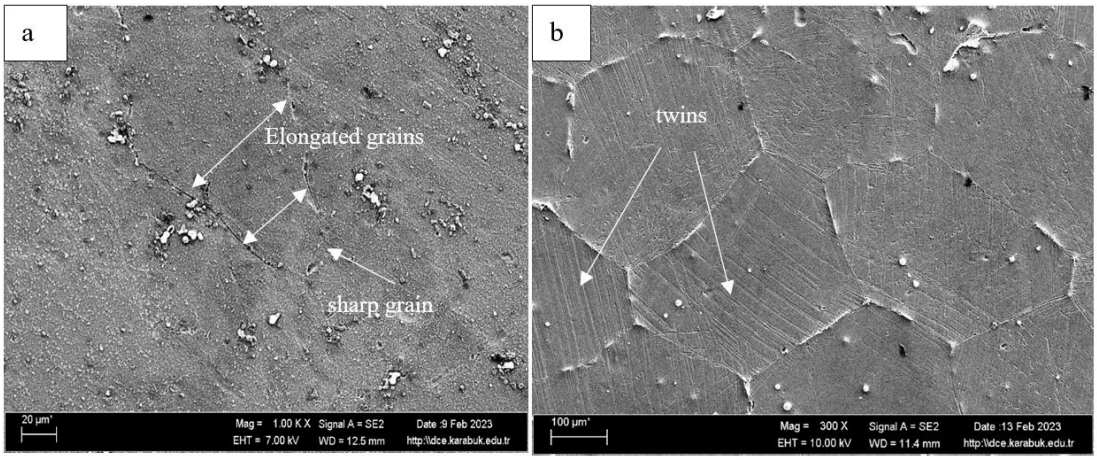

Figure 5.7. Hot-rolled specimens for alloys Alloy-1(a) and Alloy-2 (b).

The SEM images of both alloys after heat treatment for 60 and 120 minutes following hot rolling is displayed in Figure 5.8. It is seen that static recrystallization process took place and very fine grains with a few microns or less than one micron formed within the grains. In addition, presence of some coarse grains in recrystallized region indicates that grain growth process started. Therefore, the heat treatment process after hot rolling resulted in a more uniform grain size and morphology for both alloys. Additionally, most areas representative of the secondary $Ca_2Mg_6Zn_3$ phase located along grain boundaries or dispersed within grains disappeared. This confirms that the heat treatment induced a uniform redistribution of the $Ca_2Mg_6Zn_3$ secondary phase into a finely dispersed precipitated form throughout the α-Mg matrix.

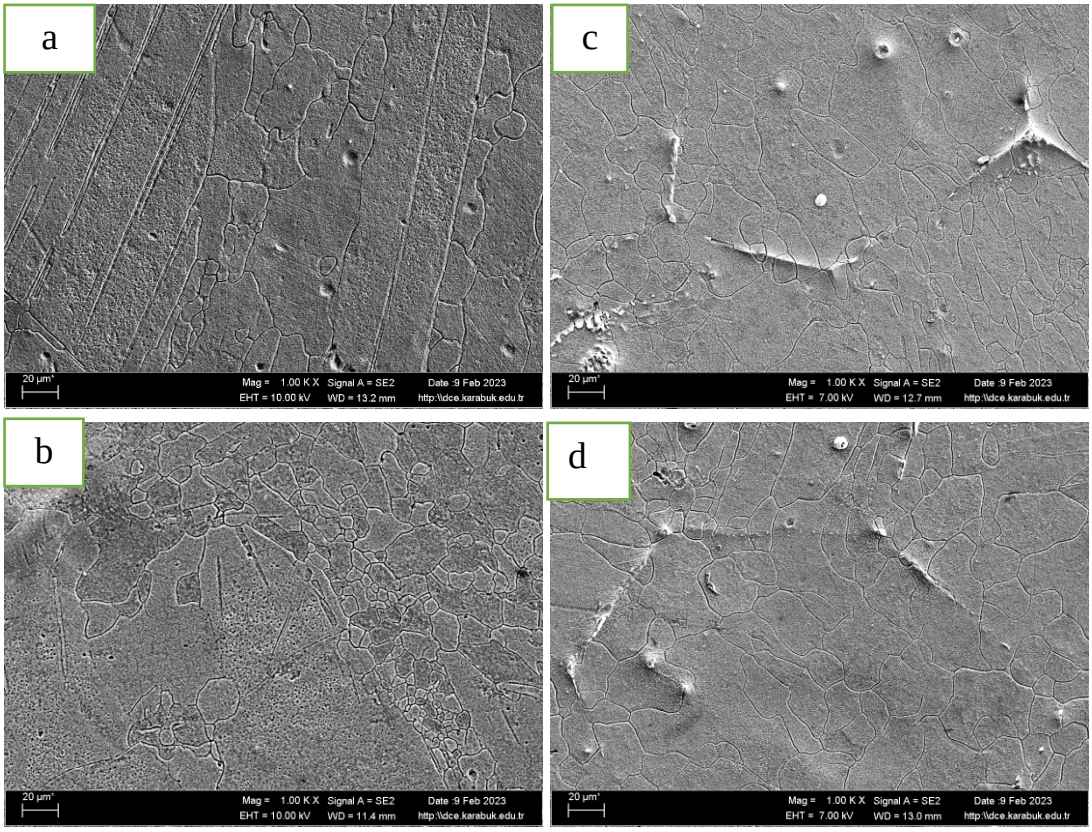

Figure 5.8. SEM images of the heat-treated alloys after hot rolling. (a) and (b) are for Alloy-1 after 60- and 120-minute heat treatment, respectively, and (c) and (d) are for Alloy-2 after 60 and 120 minute heat treatment, respectively

5.3.3. Analysis Of Energy Dispersed Element (EDS).

The EDS analysis revealed the concentration of elements at different points in the specimens and confirmed the presence of the alloy components at varying concentrations at multiple points within the samples.

Fig. 5.9 shows the EDS point analyses taken from Alloy-1 and Alloy-2. The results of the analyses are given in Table 5.2.a and b. Table 5.2.a displays the weight percent of the alloying element present in the analyzed points of Alloy-1. The point 6 may indicate the potential formation of the α-Mg, $MgZn_2$, and α-Mn phases. While the other points may indicate the potential formation of the α-Mg and $MgZn_2$ phases. Table 5.2.b shows the percentage findings for the spectrum of Alloy-2 in which

points 3, 4, 5, 6, and 7 may indicate the potential formation of the α-Mg, $Ca_2Mg_6Zn_3$, and α-Mn phases. The other points show the possibility of forming α-Mg and $MgZn_2$ at points 1 and 2, and α-Mg, $MgZn_2$, and α-Mn at points 8 and 9.

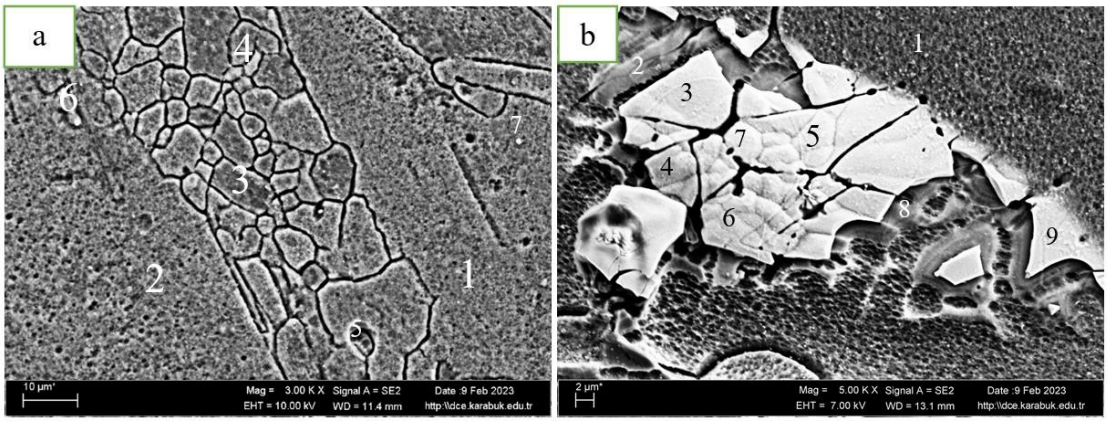

Figure 5.9. The SEM images in which EDS analysis to points of Alloy-1(a) and Alloy-2(b) alloys.

Table 5.2. The EDS point analyses of 2 hours heat treated alloys in wt.%.

(a)- Alloy-1					**(b)- Alloy-2**				
spectrum	Mg	Zn	Ca	Mn	spectrum	Mg	Zn	Ca	Mn
1	89.24	3.89	0	1.01	1	83.49	6.57	0	0.37
2	87.4	3.36	0.29	0	2	83.68	5.97	0	2.14
3	87.59	3.08	0	0	3	21.93	50.54	6.97	2.19
4	86.19	4.27	0.17	0.82	4	20.36	53.11	3.91	4.01
5	86.19	3.79	0.06	0	5	21.23	52.59	5.76	3.03
6	28.1	7.04	0.64	41.77	6	21.16	52.19	6.36	1.4
7	87.77	3.27	0	0	7	22.13	52.19	4.99	3.06
					8	82.05	5.94	0.06	3.06
					9	23.55	57.25	6.93	3.57

On the other hand, the $Ca_2Mg_6Zn_3$ phase has not been noted in the EDS analysis for the Alloy-1 since $Ca_2Mg_6Zn_3$ is expected to completely dissolve in the α-magnesium matrix during post heat treatment [116]. The fact that samples were quenched after hot rolling and heat treatments prevented formation of equilibrium ternary phase.

The higher proportions of Mg, Zn, Ca, and Mn detected in the $Ca_2Mg_6Zn_3$ phase of Alloy-2 can be explained by interference arising from signals generated by both the α-Mg phase component of the eutectic structure (i.e. α-Mg + $Ca_2Mg_6Zn_3$) and the surrounding α-Mg matrix during analysis. Previous work has shown such signal interference can obscure quantification of phase compositions when the phases are intimately distributed at a fine scale, as is the case with the eutectic microstructure observed in these alloys [8].

5.3.4. X-Ray Diffraction Analysis (XRD)

X-ray diffraction (XRD) analysis provides critical insights into the textural and microstructural evolution of Mg alloys. The XRD patterns in Figure 5.10 elucidate the microstructural changes and textural evolution of Alloys-1 and Alloy-2 during homogenization and subsequent hot rolling. The homogenized alloys exhibit nearly random textures, indicating the homogenization process effectively removed any pre-existing texture despite the different zinc contents. After hot rolling, Alloy-1 and Alloy-2 show transitions from random to preferred orientations, evidenced by intensified (002) and (103) reflections. The more pronounced (103) reflection in hot rolled Alloy-1 reveals a stronger pyramidal texture in Alloy-1 compared to Alloy-2, likely due to the higher zinc content influencing operative slip systems and texture.

The varying intensity of the (103) peak reveals zinc's potential role in modulating deformation mechanisms. Elucidating the interactive impacts of alloying, processing, and texture is critical for optimizing properties and expanding applications of these alloys. The XRD analysis provides a robust foundation for further exploration of structure-property relationships. A deeper understanding of the underlying mechanisms governing textural evolution will enable purposeful microstructural engineering of magnesium alloys for enhanced mechanical performance.

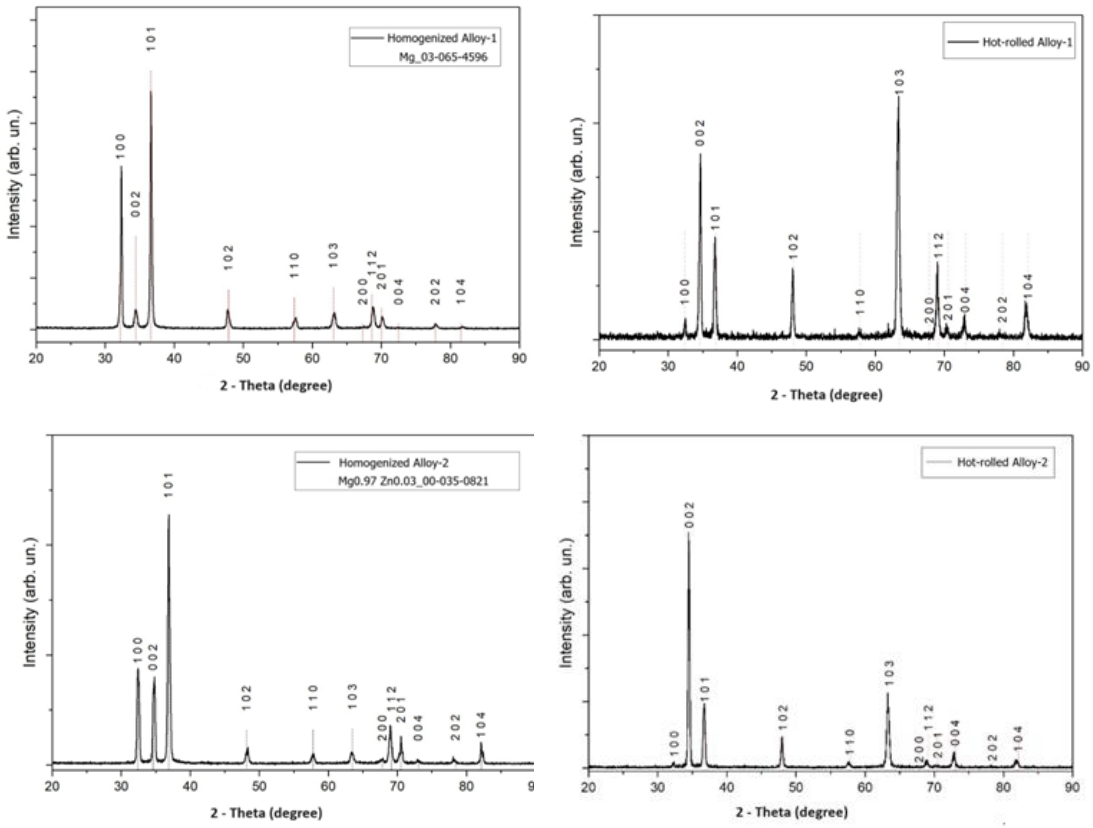

Figure 5.10. X-ray diffraction (XRD) patterns homogenized alloys and hot-rolled alloys, respectively.

As can be seen in Figure 5.10, changes in the XRD intensity of the crystallographic planes were observed in response to variations in zinc content and the application of hot plastic deformation. Variations in the intensity of the peaks in the XRD patterns are indicative of concomitant variations in the number of crystals oriented along specific axes. In particular, the intensities of crystallographic planes (100) and (101) showed a striking decrease, while some of the planes, including (002) and (102), showed an increase after hot rolling and changes in zinc content. These results indicate that a larger number of grains with random orientations are formed in the subsequent recrystallization phase [8]. This phenomenon can be explained by the role of $Ca_2Mg_6Zn_3$ precipitates, which serve as nuclei for the formation of recrystallized grains and eventually lead to the formation of finer grains with random orientations. It is worth noting that Jiang et al. observed that isolated larger particles larger than 1 μm have the potential to act as nucleation sites during the process of hot

deformation, a phenomenon commonly referred to as particle-induced nucleation [22].

Moreover, the XRD pattern of the homogenized and hot rolled alloys displayed peaks belonging to the α-Mg and $Ca_2Mg_6Zn_3$ phases. In addition, α-Mn phase was not detected because it was not within the detection range of XRD due to their low intensity. The XRD analyzes showed that the observed phases were consistent with the results of the study [8].

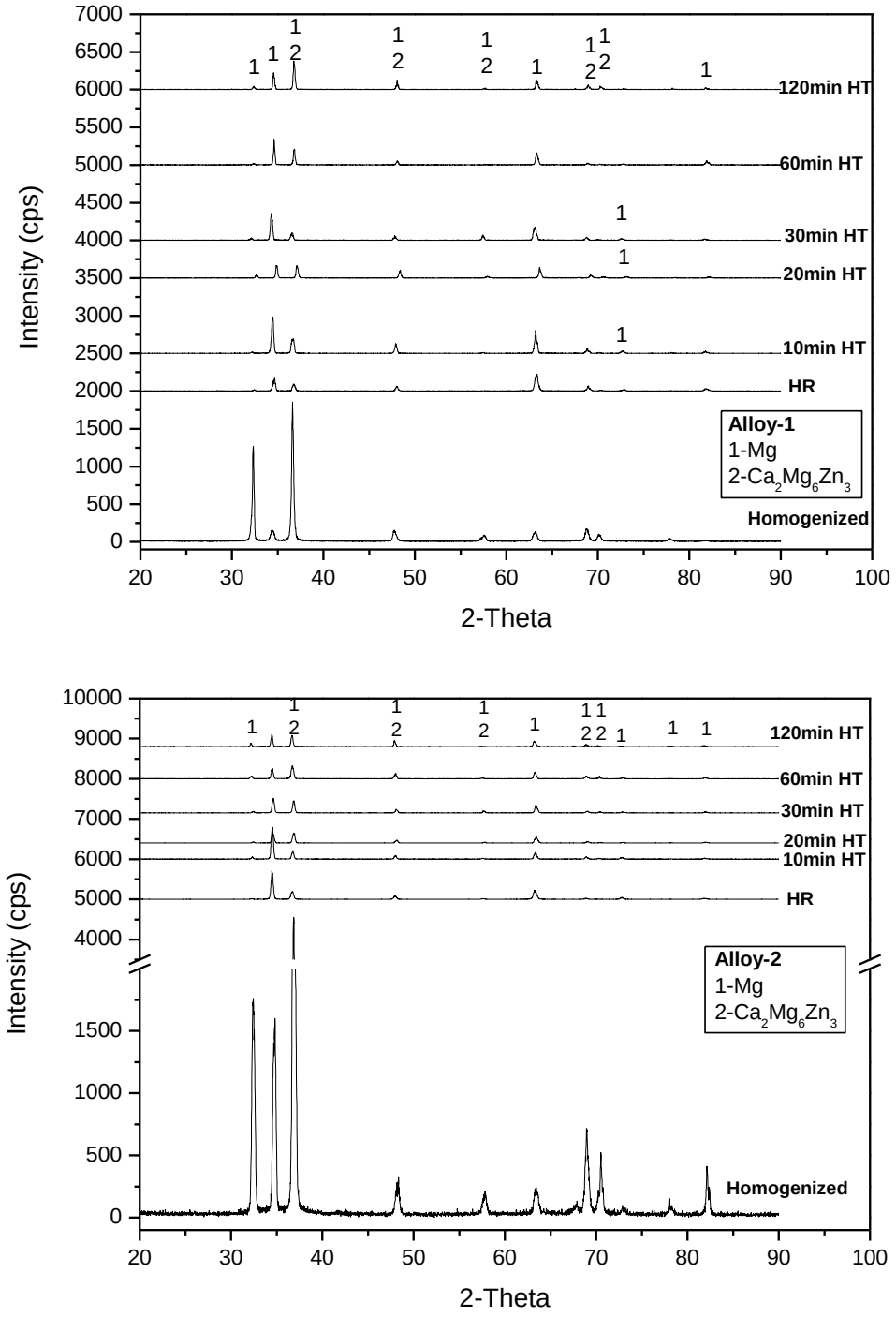

Figure 5.11. The X-ray diffraction (XRD) patterns of Alloy-1 and Alloy-2 after the stages of homogenization, hot rolling, and heat treatments.

Comparing the XRD diagrams in Fig. 5.11, the individual phases of the hot-rolled alloys and the homogenized alloy were practically identical. However, due to plastic deformation arising from hot rolling, the X-ray intensity of the planes varied according to grain size and orientation [22].

5.4. MECHANICAL PROPERTIES

5.4.1. Tensile Test

The tensile properties of the alloys were summarized in Table 5.3 and Fig. 5.12 and 5.13 after homogenization, hot rolling, and heat treatment. It can be seen that the homogenized Alloy-1 has significantly higher elongation but lower tensile strength and yield strength (5.248%, 102.4 MPa and 42.832 MPa, respectively) than the hot-rolled (1.954%, 156.4 MPa and 89.181 MPa, respectively) and heat-treated samples. Similarly, homogenized Alloy-2 has significantly higher elongation but lower tensile strength and yield strength (8.78%, 148.6 MPa and 43.955 MPa, respectively) than hot rolled (1.887%, 204.6 MPa and 133.49 MPa, respectively) and heat-treated samples. Therefore, it can be said that hot rolling and heat treatment result in lower ductility and toughness but higher yield and tensile strength. In addition, modulus of elasticity increases after hot rolling and heat treatment of the alloys (Alloy-1 and Alloy-2)

Table 5.3. The tensile test results.

	SAMPLE	Modulus of Elasticity (MPa)	Yield Strength (MPa	Tensile Strength (MPa)	Elongation (%)
Alloy- 1	Homogenous	13941	42.83	102.4	5.28
	Hot rolled	17466	89.18	156.4	1.95
	10min HT*	20873	88.19	138.0	1.39
	20min HT*	19877	87.57	171.0	3.90
	30min HT*	19274	79.39	148.1	2.52
	60 min HT*	16406	85.98	184.2	2.40
	120 min HT*	18383	77.40	174.9	7.75
Alloy- 2	Homogenous	20745	43.96	148.6	8.78
	Hot rolled	19765	133.50	204.6	1.89
	10min HT*	18876	101.13	166.0	2.01
	20min HT*	19584	93.91	166.0	2.72
	30min HT*	19171	87.75	157.2	3.04
	60 min HT*	19002	86.23	171.2	5.14
	120 min HT*	18770	84.98	170.9	5.07

* HT: Heat treatment after hot rolling.

When the effects of hot rolling on the mechanical properties of the homogenized alloys were investigated, it was found that both alloys exhibited improvement in yield strength and tensile strength, but lower elongation, as shown in Table 5.3. During hot rolling, the alloy is plastically deformed at high temperatures, which leads to a restructuring of the pre-existing grain structure, resulting in a finer and more uniform grain size. This improvement in grain size has a positive effect on mechanical strength according to the Hall-Petch relationship [68]. In addition, grain refinement and precipitation near the grain boundaries impede dislocation movement, which increases the strength of the alloy [15]. In addition, the presence of the $Ca_2Mg_6Zn_3$ phase is believed to increase the stress concentration and the density of microcracks, both of which affect the ductility and strength of the alloys [8].

When stress-strain curves of the alloys are compared, the effect of Zn ratio on the mechanical properties of the alloys is understood. It is found that the tensile strength, yield strength, and elongation of the alloys increase with increasing zinc content of the alloy. Increase in strength of the alloy can be explained with the formation of solid solution of Zn and precipitation hardening of Mg alloys [117]. It is obvious that as the Zn content of the alloy increases, the volume fraction of secondary phase

increases, and the grain size decreases. In addition, it can be said that the twin tendency increases with the increasing zinc content of the alloy as observed in SEM images [22].

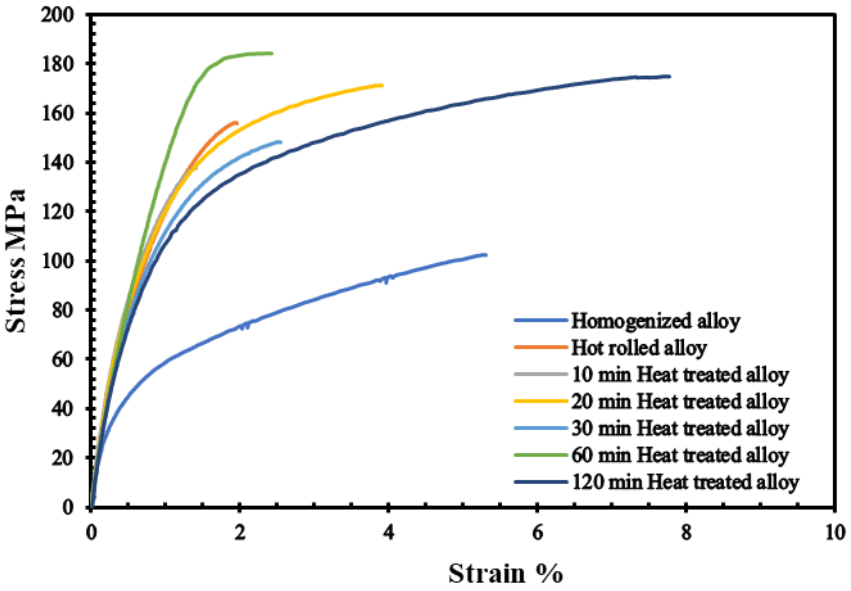

Figure 5.12. The stress-strain graphics of Alloy-1.

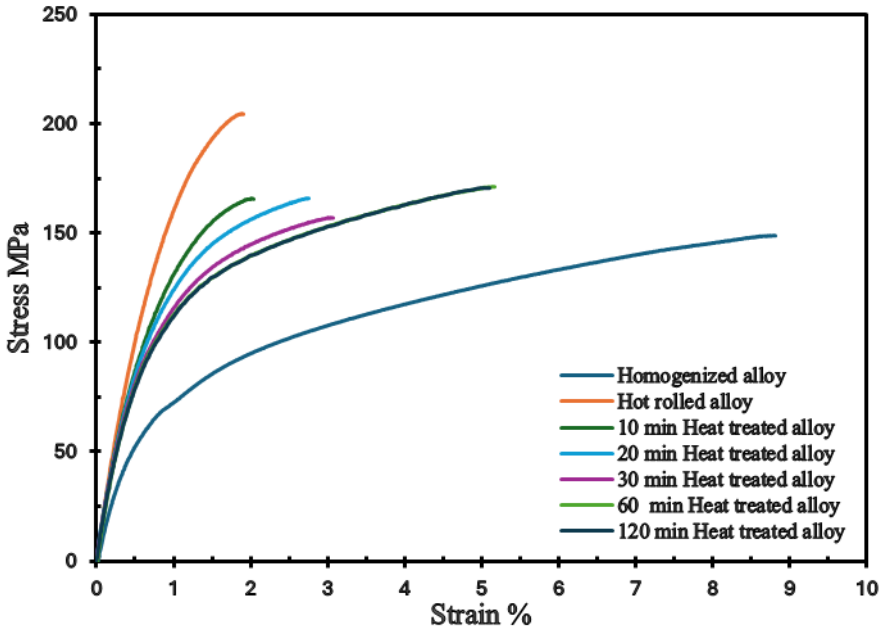

Figure 5.13. The stress-strain graphics of Alloy-2.

In general, after heat treatment at 120 min, both Alloy-1 and Alloy-2 showed decreased yield strength and increased elongation as compared to their hot rolling states as shown in Table 5.3.

Increasing heat treatment time reduces internal stresses, promotes grain growth, and decreases total grain boundary area. As a result, the dislocations can move more easily and rearrange within the crystal lattice of the material, resulting in lower stored energy within the material and lower yield strength and tensile strength, as well as increased ductility [84]. In addition, recrystallization process leads to the formation of fresh, stress-free grains that eventually replace the deformed and strained grains of the material. Compared to the deformed grains, the new grains formed during recrystallization are usually fine and equiaxed in shape. The new grains have fewer dislocations and imperfections, which contribute to the strength of the material and result in lower yield strength and hardness [85].

Generally, when the influence of heat treatment after hot rolling on the tensile strength and elastic modulus of the alloys are investigated, it was observed that tensile strength and elastic modulus do not change continuously with heat treatment time up to 30 min. However, for long heat treatment times (60 and 120 min), increase in volume fraction of secondary phases and other microstructural enhancements result in higher strength.

5.4.2. Hardness Test

The average Vickers hardness of the homogenized, hot rolled, and heat-treated alloys is given in Table 5.4 and Fig 5.14. When comparing the hardness values of homogenized, hot-rolled, and heat-treated alloys, it is found that hot-rolled alloys have the highest hardness values. In addition, the hardness of the hot rolled alloys decreases with increasing heat treatment time. It can be attributed to the relaxation of the structure and stress relief during heat treatment. The Vickers hardness of Alloy-1 in homogenized, hot rolled, and 120 min heat treated states are 52.9, 59.8, and 51.1, respectively. Similarly, The Vickers hardness of Alloy-2 in homogenized, hot rolled, and 120 min heat treated states are 52.8, 67.7, and 51.2, respectively. Therefore, it

can be said that both alloys have similar hardnesses except that hot rolled Alloy-2 has higher hardness than Alloy-1.

Table 5.4. The average Vickers Hardness of the alloys.

Alloy	Sample	Average Hardness (HV)
Alloy- 1	Homogenous	52.9
	Hot rolled	59.8
	10min HT*	59.8
	20min HT*	52.4
	30min HT*	53.3
	60 min HT*	51.9
	120 min HT*	51.1
Alloy- 2	Homogenous	52.8
	Hot rolled	67.7
	10min HT*	55.3
	20min HT*	56.6
	30min HT*	55.2
	60 min HT*	51.6
	120 min HT*	51.2

* HT: Heat treatment after hot rolling.

Notably, hardness values continue to rise with increasing Zn content in Alloy-2 specimens. Specifically, hardness increased from 59.8 HV for hot rolled Alloy-1 to 67.7 HV for Alloy-2, correlating with the higher Zn content of 2.91 wt.% compared to 1.07 wt.% in Alloy-1. This trend can be attributed to grain refinement effects induced by higher Zn levels, as previous work has demonstrated increased Zn causing finer grain structures and improved hardness [98]. Additionally, precipitation of more $Ca_2Mg_6Zn_3$ particles within the α-Mg grains occurred due to higher Zn ratio when combined with grain size reduction, explains the observed rise in hardness [118]. Therefore, both precipitation strengthening from $Ca_2Mg_6Zn_3$ and Hall-Petch strengthening from reduced grain size likely contributed to the enhanced hardness with increasing Zn content. On the other hand, compared to rolled samples, the hardness of alloy samples Alloy-1 and Alloy-2 decreases progressively with increasing heat treatment time at 325 °C. This can be due to recrystallization and grain growth processes, which result in fine and equiaxed stress free grain formation during recrystallization and grain growth in second stage reduce the material's

internal tensions and dislocation density that led to lower hardness as shown in Fig 5.14.

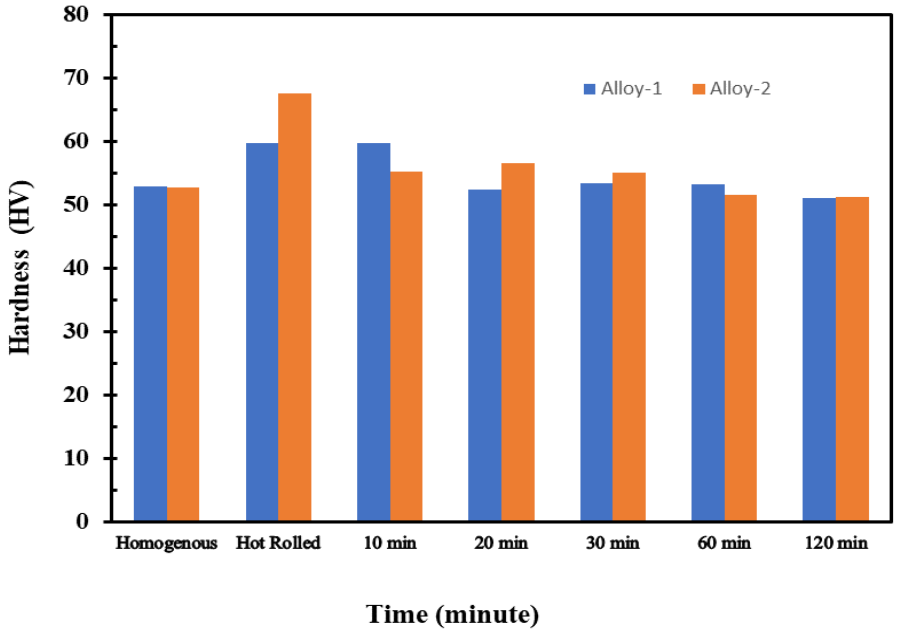

Figure 5.14. The hardness test with the time of heat treatment.

5.5. CORROSION PROPERTIES

The corrosion behaviors of homogenized, hot-rolled, and heat-treated Alloy-1 and Alloy-2 were investigated using the immersion corrosion test in the SBF solution at 37 °C for different times (1, 5, and 10 days). It was found that homogenized alloys have significantly increased resistance to corrosion compared to hot rolled alloys, as shown in Table 5.5. For 1-day corrosion, the corrosion rate of Alloy-1 in homogenized state was 3.621 mm/year and 3.731 mm/year in the hot-rolled state. In case of Alloy-2, the homogenized specimen had a corrosion rate of 3.865 mm/year while the hot-rolled specimen had a 4.086 mm/year rate. These results show that hot rolling process has negative impact on the corrosion resistance of the alloys. Similar behavior was observed for 5-day and 10-day corrosion results.

Table 5.5. The corrosion rate of Alloy-1 and Alloy-2 in the BSF solution.

	Samples	1 Day	5 Day	10 Day
Alloy -1	Homogenous	3.621	0.914	0.395
	Hot rolled	3.731	0.961	0.455
	10min HT*	3.897	0.864	0.376
	20min HT*	3.855	0.926	0.356
	30min HT*	3.455	0.83	0.335
	60 min HT*	2.371	0.913	0.312
	120 min HT*	3.226	0.9	0.262
Alloy- 2	Homogenous	3.865	1.869	0.54
	Hot rolled	4.086	1.195	0.473
	10min HT*	3.454	1.218	0.367
	20min HT*	3.193	1.204	0.487
	30min HT*	3.903	1.509	0.255
	60 min HT*	3.694	1.278	0.198
	120 min HT*	3.306	1.355	0.145

* HT: Heat treatment after hot rolling.

The results of immersion corrosion test show the corrosion rate decreases over time, as displayed in Fig 5.15 and 5.16. This is likely due to the formation of a denser and more protective layer on the surface of the samples with time, resulting in improved bio-corrosion resistance [15].

Lower corrosion resistance of the hot rolled alloys can be due to increased grain boundary area during hot rolling which is often more susceptible to corrosion compared to the grains themselves, accelerating the corrosion rate of the alloy [116]. The presence of fine grains, twin bands, and microcracks negatively affects the corrosion resistance of alloys [8].

When the effect of Zn ratio on the corrosion rate is investigated, it is seen from Table 5.5 that Alloy-1containing lower Zn has mainly lower corrosion rate than Alloy-2. This case can be explained by the fact that increasing zinc ratio of the alloy increases the volume fraction of the $Ca_2Mg_6Zn_3$ intermetallic phase that has an accelerating effect on the corrosion of α-Mg because the $Ca_2Mg_6Zn_3$ phase having higher standard electrode potential behaves as cathode compared to α-Mg [116].

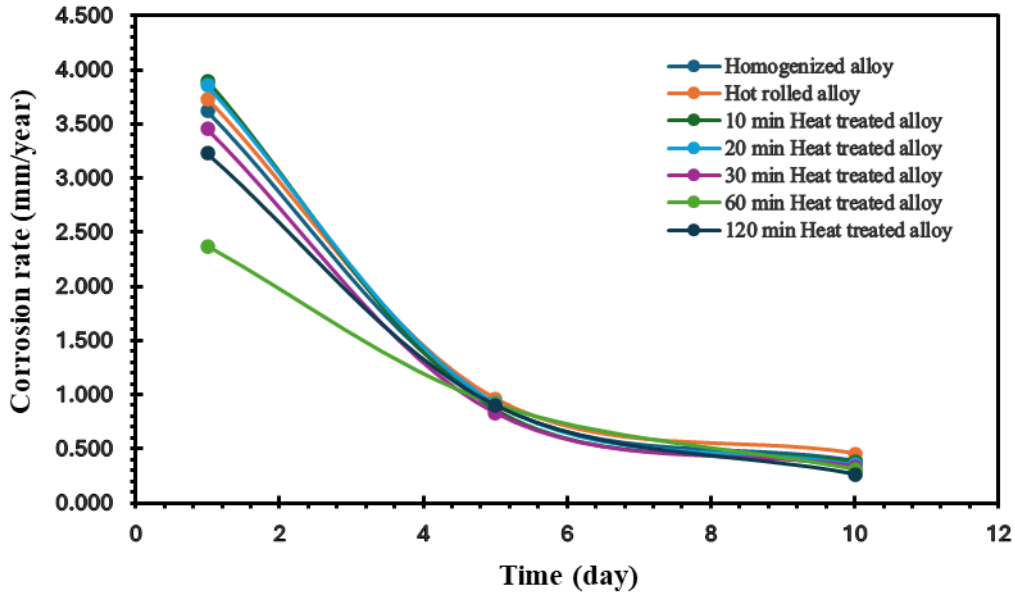

Figure 5.15. The corrosion rate of the Alloy-1

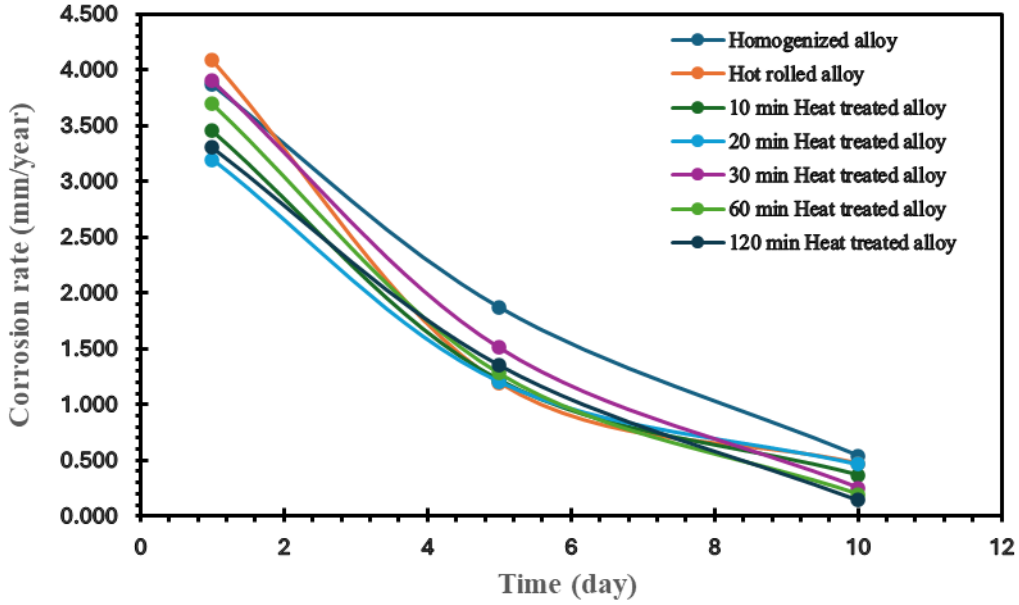

Figure 5.16. The corrosion rate of the Alloy-2.

In general, the heat-treated alloys exhibited lower corrosion rates compared to the non-heat-treated alloys, as shown in Figs. 5.15 and 5.16. The corrosion rate of Alloy-1 and Alloy-2 samples that underwent 120 minutes of heat treatment after hot rolling decreased to 0.262 mm/year and 0.145 mm/year, respectively. This indicates that corrosion resistance of the alloys increases with immersion time. The improved corrosion properties of the alloys with post heat-treatment can be explained by the

uniform distribution of secondary phases as fine precipitates induced by heat-treatment, stress relief, reduction in volume fraction of defects, etc.

PART 6

CONCLUSIONS AND RECOMMENDATIONS

6.1. CONCLUSIONS

In this study, two different magnesium alloys namely Alloy-1 (Mg-1.07wt.%Zn-0.21wt.%Ca-0.31wt.%Mn) and Alloy-2 (Mg-2.91wt.%Zn-0.21wt.%Ca-0.29wt.%Mn) were studied. The effect of Zn ratio, hot rolling and heat treatment time on the microstructure, mechanical properties, hardness, and immersion corrosion rate of Mg based alloys were investigated. The following conclusions have been obtained.

- This study demonstrated thermomechanical processing and heat treatment can significantly enhance the mechanical properties and hardness of Mg-Zn-Ca-Mn alloys for biodegradable implants.
- The alloys comprised α-Mg matrix and $Ca_2Mg_6Zn_3$ secondary phase. Increasing Zn promoted increased the volume fraction of the $Ca_2Mg_6Zn_3$ intermetallic phase.
- Hot rolling led to substantial grain refinement and improved strength and hardness.
- Dynamic recrystallization occurred during hot rolling.
- Post heat treatment induced recrystallization and grain growth that results in slightly decreasing strength but increasing ductility.
- Immersion tests showed that corrosion rate of the alloys decreased with increasing immersion time that is attributed to the formation of protective layer on the surface of the alloys.
- Immersion testing showed that hot rolling resulted in higher corrosion rate. Subsequent heat treatment reduced the corrosion rate particularly at higher heat treatment times.

- Alloy-2 (Mg-3Zn-0.2Ca-0.3Mn) displayed the lowest degradation rate of 0.145 mm/year after 120 min heat treatment.
- Alloy-2 heat treated at 325 ^{o}C for 120 min after hot rolling exhibited an excellent balance of mechanical properties (modulus of elasticity, yield and tensile strength, and hardness) and lower corrosion rate than Alloy-1 heat treated at 325 ^{o}C for 120 min after hot rolling. Therefore, Alloy-2 can be further improved, and its biocompatibility can be investigated for biodegradable orthopedic implant applications.

6.2. RECOMMENDATIONS

Following recommendations outline crucial lines of inquiry that have the potential to significantly improve our knowledge of magnesium alloys and their uses.

- Examine in depth the influence of varying proportions of manganese, zinc, and calcium on the mechanical attributes and corrosion behaviors of the alloys.
- Investigate the impact of modifying the rolling temperature and effect of altering the rolling direction such as 90 and 0 degrees on the microstructural features and grain size.

REFERENCES

1. G. Manivasagam, D. Dhinasekaran, and A. Rajamanickam, “Biomedical Implants: Corrosion and its Prevention - A Review,” *Recent Patents Corros. Sci.*, vol. 2, no. 1, pp. 40–54, 2010, [Online]. Available: http://benthamscience.com/open/openaccess.php?rptcs/articles/V002/40RPTCS.htm

2. E. T. J. Chong, J. W. Ng, and P.-C. Lee, “Classification and Medical Applications of Biomaterials- A Mini Review,” *BIO Integr.*, vol. 4, no. 2, pp. 54–61, 2022, doi: 10.15212/bioi-2022-0009.

3. F. N. Alaribe, S. L. Manoto, and S. C. K. M. Motaung, “Scaffolds from biomaterials: Advantages and limitations in bone and tissue engineering,” *Biologia (Bratisl).*, vol. 71, no. 4, pp. 353–366, 2016, doi: 10.1515/biolog-2016-0056.

4. Q. Chen and G. A. Thouas, “Metallic implant biomaterials,” *Mater. Sci. Eng. R Reports*, vol. 87, pp. 1–57, 2015, doi: 10.1016/j.mser.2014.10.001.

5. J.R. Davis, “Overview of Biomaterials and Their Use in Medical Devices,” *ASM Int.*, vol. Chapter 1, pp. 1–11, 2003, doi: 10.1361/hmmd2003p001.

6. A. A. Azeez, Y. Danyuo, and J. D. Obayemi, “Effect of particle size and sintering time on the mechanical properties of porous Ti–6Al–4V implant,” *SN Appl. Sci.*, vol. 2, no. 5, pp. 1–7, 2020, doi: 10.1007/s42452-020-2637-z.

7. V. G. Rohit1, Munish Gupta2, Puneet Katyal3, “IRJET- Mg and its Alloys , their Challenges and Opportunities for Implants : A Review,” *Int. Res. J. Eng. Technol.*, vol. 07, no. 09, p. 2763, 2020.

8. A. Gungor and A. Incesu, “Effects of alloying elements and thermomechanical process on the mechanical and corrosion properties of biodegradable Mg alloys,” *J. Magnes. Alloy.*, vol. 9, no. 1, pp. 241–253, 2021, doi: 10.1016/j.jma.2020.09.009.

9. G. K. Levy, J. Goldman, and E. Aghion, “The prospects of zinc as a structural material for biodegradable implants—a review paper,” *Metals (Basel).*, vol. 7, no. 10, pp. 1–18, 2017, doi: 10.3390/met7100402.

10. D. Bairagi, P. Duley, M. Paliwal, and S. Mandal, “Influence of second phase precipitates on mechanical and in-vitro corrosion behaviour of Mg-4Zn-0.5Ca-0.8Mn alloy in optimum homogenized conditions,” *J. Magnes. Alloy.*, vol. 11, no. 4, pp. 1343–1366, 2023, doi: 10.1016/j.jma.2022.11.011.

11. H. R. Bakhsheshi-Rad *et al.*, “Mechanical and bio-corrosion properties of quaternary Mg-Ca-Mn-Zn alloys compared with binary Mg-Ca alloys,” *Mater. Des.*, vol. 53, pp. 283–292, 2014, doi: 10.1016/j.matdes.2013.06.055.

12. J. Fu *et al.*, “Effect of the Ca2 Mg6 Zn3 Phase on the Corrosion Behavior of Biodegradable Mg-4.0Zn-0.2Mn-xCa Alloys in Hank’s Solution,” *Materials (Basel).*, vol. 15, no. 6, 2022, doi: 10.3390/ma15062079.

13. B. JIANG, Z. hua DONG, A. ZHANG, J. feng SONG, and F. sheng PAN, “Recent advances in micro-alloyed wrought magnesium alloys: Theory and design,” *Trans. Nonferrous Met. Soc. China (English Ed.*, vol. 32, no. 6, pp. 1741–1780, 2022, doi: 10.1016/S1003-6326(22)65907-7.

14. C. Liu, X. Chen, J. Chen, A. Atrens, and F. Pan, “The effects of Ca and Mn on the microstructure, texture and mechanical properties of Mg-4 Zn alloy,” *J. Magnes. Alloy.*, vol. 9, no. 3, pp. 1084–1097, 2021, doi: 10.1016/j.jma.2020.03.012.

15. M. Kavyani, G. R. Ebrahimi, H. R. Ezatpour, and M. Jahazi, “Microstructure refinement, mechanical and biocorrosion properties of Mg–Zn–Ca–Mn alloy improved by a new severe plastic deformation process,” *J. Magnes. Alloy.*, vol. 10, no. 6, pp. 1640–1662, 2022, doi: 10.1016/j.jma.2020.11.013.

16. D. H. Cho, T. Avey, K. H. Nam, D. Dean, and A. A. Luo, “In vitro and in vivo assessment of squeeze-cast Mg-Zn-Ca-Mn alloys for biomedical applications,” *Acta Biomater.*, vol. 150, pp. 442–455, 2022, doi: 10.1016/j.actbio.2022.07.040.

17. X. Chen *et al.*, “Improvement of mechanical properties of hot extruded and age treated Mg–Zn–Mn–Ca alloy through Sn addition,” *J. Alloys Compd.*, vol. 850, p. 156711, 2021, doi: 10.1016/j.jallcom.2020.156711.

18. M. Kaviani, G. R. Ebrahimi, and H. R. Ezatpour, “Improving the mechanical properties and biocorrosion resistance of extruded Mg-Zn-Ca-Mn alloy through hot deformation,” *Mater. Chem. Phys.*, vol. 234, no. May, pp. 245–258, 2019, doi: 10.1016/j.matchemphys.2019.06.010.

19. N. Pulido-González, P. Hidalgo-Manrique, S. García-Rodríguez, B. Torres, and J. Rams, “Effect of heat treatment on the mechanical and biocorrosion behaviour of two Mg-Zn-Ca alloys,” *J. Magnes. Alloy.*, vol. 10, no. 2, pp. 540–554, 2022, doi: 10.1016/j.jma.2021.06.022.

20. J. Fua, Z. W. , Ke Liub,*, Wenbo Duc,*, and Shubo Lie and Xian Duf, “Microstructure and mechanical properties of the as-cast Mg-Zn-Mn-Ca alloys,” *J. Phys. Conf. Ser.*, vol. 182, no. 1, pp. 0–5, 2017, doi: 10.1088/1742-6596/755/1/011001.

21. K. Nie, Z. Zhu, P. Munroe, K. Deng, and J. Han, “The effect of Zn/Ca ratio

on the microstructure, texture and mechanical properties of dilute Mg–Zn–Ca–Mn alloys that exhibit superior strength," *J. Mater. Sci.*, vol. 55, no. 8, pp. 3588–3604, 2020, doi: 10.1007/s10853-019-04174-4.

22. A. Incesu and A. Gungor, "Mechanical properties and biodegradability of Mg–Zn–Ca alloys: homogenization heat treatment and hot rolling," *J. Mater. Sci. Mater. Med.*, vol. 31, no. 12, 2020, doi: 10.1007/s10856-020-06468-5.

23. I. Hamdy, M. N Shayesteh, and E. Mohammad, "'Mechanical and In Vitro Corrosion Properties of a Heat-Treated Mg-Zn-Ca-Mn Alloy as a Potential Bioresorbable Material,'" *Adv. Metall. Mater. Eng.*, vol. 1, no. 1, pp. 1–7, 2017, doi: 10.36959/508/392.

24. P. Duley, S. Sanyal, T. K. Bandyopadhyay, and S. Mandal, "Implications of annealing treatments on microstructure, texture, and tensile properties of hard plate hot forged Mg-Zn-Ca-Mn alloy," *Mater. Charact.*, vol. 172, no. September 2020, p. 110885, 2021, doi: 10.1016/j.matchar.2021.110885.

25. Y. Zhang, J. Li, and J. Li, "Effects of microstructure transformation on mechanical properties, corrosion behaviors of Mg-Zn-Mn-Ca alloys in simulated body fluid," *J. Mech. Behav. Biomed. Mater.*, vol. 80, no. February, pp. 246–257, 2018, doi: 10.1016/j.jmbbm.2018.01.028.

26. T. Nakata, C. Xu, R. Abe, L. Geng, and S. Kamado, "Unexpectedly formed strong basal texture in a rolled Mg-Zn-Ca-Mn alloy sheet," *Mater. Charact.*, vol. 203, no. April, p. 113101, 2023, doi: 10.1016/j.matchar.2023.113101.

27. [27] V. E. Bazhenov *et al.*, "Microstructure and mechanical and corrosion properties of hot-extruded Mg–Zn–Ca–(Mn) biodegradable alloys," *J. Magnes. Alloy.*, vol. 9, no. 4, pp. 1428–1442, 2021, doi: 10.1016/j.jma.2020.11.008.

28. A. Incesu and A. Gungor, "Comparison of Hot-rolled Unalloyed Magnesium and Magnesium Alloys in terms of Biodegradability and Mechanical Properties," *Gazi Univ. J. Sci.*, vol. 35, no. 3, pp. 1022–1029, 2022, doi: 10.35378/gujs.825071.

29. T. Lv *et al.*, "Effect of homogenization on the microstructure, biocorrosion resistance, and biological performance of as-cast Mg–4Zn–1Ca alloy," *Mater. Today Commun.*, vol. 33, no. July, p. 104135, 2022, doi: 10.1016/j.mtcomm.2022.104135.

30. Y. Y. Han, C. You, Y. Zhao, M. F. Chen, and L. Wang, "Effect of Mn Element Addition on the Microstructure, Mechanical Properties, and Corrosion Properties of Mg-3Zn-0.2Ca Alloy," *Front. Mater.*, vol. 6, no. December, pp. 1–10, 2019, doi: 10.3389/fmats.2019.00324.

31. S. O. Rogachev *et al.*, "Effect of Hot Rolling on Structure and Mechanical Properties of Mg–Y–Zn–Mn Alloys," *Metals (Basel).*, vol. 13, no. 2, 2023, doi: 10.3390/met13020223.

32. A. Arjunan, A. Baroutaji, A. S. Praveen, J. Robinson, and C. Wang, “Classification of Biomaterial Functionality,” *Encycl. Smart Mater.*, no. January, pp. 86–102, 2021, doi: 10.1016/B978-0-12-815732-9.00027-9.

33. M. Rubežić, A. Krstić, H. Stanković, R. Ljupković, M. Ranđelović, and A. Zarubica, “Different types of biomaterials: Structure and application: A short review,” *Adv. Technol.*, vol. 9, no. 1, pp. 69–79, 2020, doi: 10.5937/savteh2001069r.

34. C. M. Agrawal, “Reconstructing the human body using biomaterials,” *Jom*, vol. 50, no. 1, pp. 31–35, 1998, doi: 10.1007/s11837-998-0064-5.

35. L. L. Hench, “Bioceramics: from concept to clinic. J Am Ceram Soc. 1993;72:93-98.,” *J. Am. Ceram. Soc.*, vol. 74, pp. 1487–1510, 1991.

36. S. Todros, M. Todesco, and A. Bagno, “Biomaterials and their biomedical applications: From replacement to regeneration,” *Processes*, vol. 9, no. 11, 2021, doi: 10.3390/pr9111949.

37. R. Davis *et al.*, *A comprehensive review on metallic implant biomaterials and their subtractive manufacturing*, vol. 120, no. 3–4. Springer London, 2022. doi: 10.1007/s00170-022-08770-8.

38. H. Hermawan, D. Ramdan, and J. R. P. Djuansjah, “Metals for Biomedical Applications,” *Biomed. Eng. - From Theory to Appl.*, vol. 1, pp. 411–430, 2011, doi: 10.5772/19033.

39. P. Parida, A. Behera, and S. C. Mishra, “Classification of Biomaterials used in Medicine,” *Int. J. Adv. Appl. Sci.*, vol. 1, no. 3, pp. 31–35, 2012.

40. T. Biswal, S. K. BadJena, and D. Pradhan, “Sustainable biomaterials and their applications: A short review,” *Mater. Today Proc.*, vol. 30, pp. 274–282, 2020, doi: 10.1016/j.matpr.2020.01.437.

41. P. Balakrishnan, S. M. S, and S. Thomas, *Fundamental Biomaterials: Metals.*, no. July. 2018.

42. P. Bartolo *et al.*, “Biomedical production of implants by additive electro-chemical and physical processes,” *CIRP Ann. - Manuf. Technol.*, vol. 61, no. 2, pp. 635–655, 2012, doi: 10.1016/j.cirp.2012.05.005.

43. Z. Sheikh, S. Najeeb, Z. Khurshid, V. Verma, H. Rashid, and M. Glogauer, “Biodegradable materials for bone repair and tissue engineering applications,” *Materials (Basel).*, vol. 8, no. 9, pp. 5744–5794, 2015, doi: 10.3390/ma8095273.

44. M. Geetha, A. K. Singh, R. Asokamani, and A. K. Gogia, “Ti based biomaterials, the ultimate choice for orthopaedic implants - A review,” *Prog. Mater. Sci.*, vol. 54, no. 3, pp. 397–425, 2009, doi: 10.1016/j.pmatsci.2008.06.004.

45. K. C. Dee, D. Puleo, and R. Bizios, *Engineering of materials for biomedical applications*, vol. 3, no. 1. 2000. doi: 10.1016/s1369-7021(00)80003-6.

46. M. Rosales, "Classifications and behavior of different types of biomaterials," vol. 6, no. 2, p. 2021, 2021.

47. K. Ishikawa, S. Matsuya, Y. Miyamoto, and K. Kawate, "9.05 - Bioceramics," *Compr. Struct. Integr. Nine Vol. Set*, vol. 1–9, pp. 169–214, 2003, doi: 10.1016/B0-08-043749-4/09146-1.

48. [48] H. Zhou, B. Liang, H. Jiang, Z. Deng, and K. Yu, "Magnesium-based biomaterials as emerging agents for bone repair and regeneration: from mechanism to application," *J. Magnes. Alloy.*, vol. 9, no. 3, pp. 779–804, 2021, doi: 10.1016/j.jma.2021.03.004.

49. K. Kumar, R. S. Gill, and U. Batra, "Challenges and opportunities for biodegradable magnesium alloy implants," *Mater. Technol.*, vol. 33, no. 2, pp. 153–172, 2018, doi: 10.1080/10667857.2017.1377973.

50. Z. M. Hua *et al.*, "Development of low-alloyed Mg–Zn–Ca–Sn–Mn alloy with high strength-ductility synergy by sub-rapid solidification and hot rolling," *J. Alloys Compd.*, vol. 855, p. 157317, 2021, doi: 10.1016/j.jallcom.2020.157317.

51. J. Tan and S. Ramakrishna, "Applications of magnesium and its alloys: A review," *Appl. Sci.*, vol. 11, no. 15, 2021, doi: 10.3390/app11156861.

52. J. Yang, G. L. Koons, G. Cheng, L. Zhao, A. G. Mikos, and F. Cui, "A review on the exploitation of biodegradable magnesium-based composites for medical applications," *Biomed. Mater.*, vol. 13, no. 2, pp. 0–25, 2018, doi: 10.1088/1748-605X/aa8fa0.

53. Y. Xin, T. Hu, and P. K. Chu, "In vitro studies of biomedical magnesium alloys in a simulated physiological environment: A review," *Acta Biomater.*, vol. 7, no. 4, pp. 1452–1459, 2011, doi: 10.1016/j.actbio.2010.12.004.

54. A. S. N. AL-GBURI, "THE INVESTIGATION OF BIODEGRADABLE AT31 MG ALLOYS," Karabuk, 2022.

55. F. C. Campbell Jr, *Manufacturing technology for aerospace structural materials.* 2011.

56. L. A. Villegas-Armenta, R. A. L. Drew, and M. O. Pekguleryuz, "The Ignition Behavior of Mg–Ca Binary Alloys: The Role of Heating Rate," *Oxid. Met.*, vol. 93, no. 5–6, pp. 545–558, 2020, doi: 10.1007/s11085-020-09970-x.

57. M. P. Staiger, A. M. Pietak, J. Huadmai, and G. Dias, "Magnesium and its alloys as orthopedic biomaterials: A review," *Biomaterials*, vol. 27, no. 9, pp. 1728–1734, 2006, doi: 10.1016/j.biomaterials.2005.10.003.

58. Y. F. Zheng, X. N. Gu, and F. Witte, “Biodegradable metals,” *Mater. Sci. Eng. R Reports*, vol. 77, pp. 1–34, 2014, doi: 10.1016/j.mser.2014.01.001.

59. Y. Chen, Z. Xu, C. Smith, and J. Sankar, “Recent advances on the development of magnesium alloys for biodegradable implants,” *Acta Biomater.*, vol. 10, no. 11, pp. 4561–4573, 2014, doi: 10.1016/j.actbio.2014.07.005.

60. Z. Yu *et al.*, “Effect of high content of manganese on microstructure, texture and mechanical properties of magnesium alloy,” *Mater. Charact.*, vol. 136, no. July 2017, pp. 310–317, 2018, doi: 10.1016/j.matchar.2017.12.029.

61. Y. Lu, “Microstructure and degradation behaviour of Mg-Zn(-Ca) alloys,” 2014.

62. L. Yang *et al.*, “Effect of Mg Contents on the Microstructure, Mechanical Properties and Cytocompatibility of Degradable Zn-0.5Mn-xMg Alloy,” *J. Funct. Biomater.*, vol. 14, no. 4, 2023, doi: 10.3390/jfb14040195.

63. P. Jiang, C. Blawert, and M. L. Zheludkevich, “The Corrosion Performance and Mechanical Properties of Mg-Zn Based Alloys—A Review,” *Corros. Mater. Degrad.*, vol. 1, no. 2, p. 7, 2020, doi: 10.3390/cmd1020007.

64. X. Liu *et al.*, “Micro-alloying with Mn in Zn-Mg alloy for future biodegradable metals application,” *Mater. Des.*, vol. 94, pp. 95–104, 2016, doi: 10.1016/j.matdes.2015.12.128.

65. S. Cai, T. Lei, N. Li, and F. Feng, “Effects of Zn on microstructure, mechanical properties and corrosion behavior of Mg-Zn alloys,” *Mater. Sci. Eng. C*, vol. 32, no. 8, pp. 2570–2577, 2012, doi: 10.1016/j.msec.2012.07.042.

66. R. Steiner, *ASM handbook volume 3: Alloy phase diagrams*. 1998.

67. D. C. Wagner, X. Chai, X. Tang, and S. Kou, “Liquation Cracking in Arc and Friction-Stir Welding of Mg-Zn Alloys,” *Metall. Mater. Trans. A Phys. Metall. Mater. Sci.*, vol. 46, no. 1, pp. 315–327, 2015, doi: 10.1007/s11661-014-2606-5.

68. E. Koç, M. B. Kannan, M. Ünal, and E. Candan, “Influence of zinc on the microstructure, mechanical properties and in vitro corrosion behavior of magnesium-zinc binary alloys,” *J. Alloys Compd.*, vol. 648, pp. 291–296, 2015, doi: 10.1016/j.jallcom.2015.06.227.

69. Q. Chen and G. A. Thouas, “Metallic implant biomaterials,” *Mater. Sci. Eng. R Reports*, vol. 87, pp. 1–57, 2015, doi: 10.1016/j.mser.2014.10.001.

70. H. Lan, M. Zhang, X. Chen, Z. Huang, and G. Yin, “Designing a novel CaO–MgO–SiO2-based multiphase bioceramic with adjustable ion dissolution behavior for enhancing osteogenesis,” *Smart Mater. Med.*, vol. 3, no. July 2021, pp. 94–103, 2022, doi: 10.1016/j.smaim.2021.09.002.

71. Y. Z. Du, X. G. Qiao, M. Y. Zheng, D. B. Wang, K. Wu, and I. S. Golovin, “Effect of microalloying with Ca on the microstructure and mechanical properties of Mg-6 mass%Zn alloys,” *Mater. Des.*, vol. 98, pp. 285–293, 2016, doi: 10.1016/j.matdes.2016.03.025.

72. T. Zhao, Y. Hu, B. He, C. Zhang, T. Zheng, and F. Pan, “Effect of manganese on microstructure and properties of Mg-2Gd magnesium alloy,” *Mater. Sci. Eng. A*, vol. 765, no. May, p. 138292, 2019, doi: 10.1016/j.msea.2019.138292.

73. C. Xu, T. Nakata, G. H. Fan, X. W. Li, G. Z. Tang, and S. Kamado, “Enhancing strength and creep resistance of Mg–Gd–Y–Zn–Zr alloy by substituting Mn for Zr,” *J. Magnes. Alloy.*, vol. 7, no. 3, pp. 388–399, 2019, doi: 10.1016/j.jma.2019.04.007.

74. K. K. Alaneme and E. A. Okotete, “Enhancing plastic deformability of Mg and its alloys—A review of traditional and nascent developments,” *J. Magnes. Alloy.*, vol. 5, no. 4, pp. 460–475, 2017, doi: 10.1016/j.jma.2017.11.001.

75. M. Ebrahimi, Q. Wang, and S. Attarilar, “A comprehensive review of magnesium-based alloys and composites processed by cyclic extrusion compression and the related techniques,” *Prog. Mater. Sci.*, vol. 131, no. September 2022, p. 101016, 2023, doi: 10.1016/j.pmatsci.2022.101016.

76. M. R. Barnett, “A Taylor model based description of the proof stress of magnesium AZ31 during hot working,” *Metall. Mater. Trans. A Phys. Metall. Mater. Sci.*, vol. 34 A, no. 9, pp. 1799–1806, 2003, doi: 10.1007/s11661-003-0146-5.

77. Y. qin CHAI *et al.*, “Role of yttrium content in twinning behavior of extruded Mg—Y sheets under tension/compression,” *Trans. Nonferrous Met. Soc. China (English Ed.*, vol. 32, no. 11, pp. 3534–3549, 2022, doi: 10.1016/S1003-6326(22)66037-0.

78. L. Jiang, J. J. Jonas, A. A. Luo, A. K. Sachdev, and S. Godet, “Influence of {10-12} extension twinning on the flow behavior of AZ31 Mg alloy,” *Mater. Sci. Eng. A*, vol. 445–446, pp. 302–309, 2007, doi: 10.1016/j.msea.2006.09.069.

79. S. H. Lu, D. Wu, R. S. Chen, and E. hou Han, “The effect of twinning on dynamic recrystallization behavior of Mg-Gd-Y alloy during hot compression,” *J. Alloys Compd.*, vol. 803, pp. 277–290, 2019, doi: 10.1016/j.jallcom.2019.06.279.

80. B. J. Lv, S. Wang, N. Cui, and F. Guo, “Twinning and dynamic recrystallization of Mg–7Sn–3Zn alloy under high strain rate hot compression,” *Mater. Sci. Eng. A*, vol. 809, no. February, p. 140986, 2021, doi: 10.1016/j.msea.2021.140986.

81. J. S. Lee, M. S. Joun, and J. K. Lee, *Hot Deformation Behavior*, vol. 129, no. July. 2007.

82. R. Singh, *Introduction to basic manufacturing processes and workshop technology*. 2006.

83. S. M. Abbasi and A. Momeni, "Effect of hot working and post-deformation heat treatment on microstructure and tensile properties of Ti-6Al-4V alloy," *Trans. Nonferrous Met. Soc. China (English Ed.*, vol. 21, no. 8, pp. 1728–1734, 2011, doi: 10.1016/S1003-6326(11)60922-9.

84. E. Reardon, Arthur C., *Metallurgy for the Non-metallurgist*. 2011.

85. D. R. Askeland, "The Science and Engineering of Materials," *book*, vol. Sixth Edit, pp. 0–495, 2011.

86. H. Chen, J. Tang, W. Gong, Y. Gao, F. Tian, and L. Chen, "Effects of annealing treatment on the microstructure and corrosion behavior of hot rolled AZ31 Mg alloy," *J. Mater. Res. Technol.*, vol. 15, pp. 4800–4812, 2021, doi: 10.1016/j.jmrt.2021.10.099.

87. G. L. Song and Z. Q. Xu, "The surface, microstructure and corrosion of magnesium alloy AZ31 sheet," *Electrochim. Acta*, vol. 55, no. 13, pp. 4148–4161, 2010, doi: 10.1016/j.electacta.2010.02.068.

88. S. Tighiouaret *et al.*, "On the evolution of microstructure, texture and corrosion behavior of a hot-rolled and annealed AZ31 alloy," *Mater. Chem. Phys.*, vol. 267, no. January, p. 124598, 2021, doi: 10.1016/j.matchemphys.2021.124598.

89. O. Daaland and E. Nes, "Origin of cube texture during hot rolling of commercial Al-Mn-Mg alloys," *Acta Mater.*, vol. 44, no. 4, pp. 1389–1411, 1996, doi: 10.1016/1359-6454(95)00289-8.

90. R. Omar Chavez-Garcia *et al.*, "Learning to Predict Metal Deformations in Hot-Rolling Processes," *IEEE Robot. Autom. Lett.*, vol. 5, no. 4, pp. 6270–6277, 2020, doi: 10.1109/LRA.2020.3013833.

91. M. Sanjari, "High strain rate deformation of Magnesium alloys," McGill, 2013.

92. H. Somekawa, D. A. Basha, and A. Singh, "Room temperature grain boundary sliding behavior of fine-grained Mg-Mn alloys," *Mater. Sci. Eng. A*, vol. 730, no. May, pp. 355–362, 2018, doi: 10.1016/j.msea.2018.06.015.

93. Z. Zhang *et al.*, "Toward the development of Mg alloys with simultaneously improved strength and ductility by refining grain size via the deformation process," *Int. J. Miner. Metall. Mater.*, vol. 28, no. 1, pp. 30–45, 2021, doi: 10.1007/s12613-020-2190-1.

94. M. R. Barnett, "A rationale for the strong dependence of mechanical twinning on grain size," *Scr. Mater.*, vol. 59, no. 7, pp. 696–698, 2008, doi:

10.1016/j.scriptamat.2008.05.027.

95. M. Vivek and S. Narnaware, “Metallic Biomaterials for Human Body Implant: a Review Study,” *Int. J. Sci. Dev. Res.*, vol. 2, no. 6, pp. 220–229, 2017, [Online]. Available: www.ijsdr.org

96. M. A. Meyers, O. Vöhringer, and V. A. Lubarda, “The onset of twinning in metals: A constitutive description,” *Acta Mater.*, vol. 49, no. 19, pp. 4025–4039, 2001, doi: 10.1016/S1359-6454(01)00300-7.

97. W. D. Callister Jr and D. G. Rethwisch, *Materials Science and Engineering an Introduction*. 2018.

98. R. W. Revie, *Uhlig ’ S Corrosion Handbook the Electrochemical Society Series*. 2011.

99. G. Manivasagam, D. Dhinasekaran, and A. Rajamanickam, “Biomedical Implants: Corrosion and its Prevention - A Review,” *Recent Patents Corros. Sci.*, vol. 2, no. 1, pp. 40–54, 2010.

100. H. Hermawan, D. Dubé, and D. Mantovani, “Developments in metallic biodegradable stents,” *Acta Biomater.*, vol. 6, no. 5, pp. 1693–1697, 2010, doi: 10.1016/j.actbio.2009.10.006.

101. K. Moghadasi *et al.*, “A review on biomedical implant materials and the effect of friction stir based techniques on their mechanical and tribological properties,” *J. Mater. Res. Technol.*, vol. 17, pp. 1054–1121, 2022, doi: 10.1016/j.jmrt.2022.01.050.

102. U. Kamachi Mudali, T. M. Sridhar, and R. A. J. Baldev, “Corrosion of bio implants,” *Sadhana - Acad. Proc. Eng. Sci.*, vol. 28, no. 3–4, pp. 601–637, 2003, doi: 10.1007/BF02706450.

103. . U. Obeyesekere, *Pitting corrosion*. Elsevier Ltd, 2017. doi: 10.1016/B978-0-08-101105-8.00009-7.

104. K. V. Akpanyung and R. T. Loto, “Pitting corrosion evaluation: A review,” *J. Phys. Conf. Ser.*, vol. 1378, no. 2, 2019, doi: 10.1088/1742-6596/1378/2/022088.

105. J. Bhandari, F. Khan, R. Abbassi, V. Garaniya, and R. Ojeda, “Modelling of pitting corrosion in marine and offshore steel structures - A technical review,” *J. Loss Prev. Process Ind.*, vol. 37, pp. 39–62, 2015, doi: 10.1016/j.jlp.2015.06.008.

106. S. F. Wika, “Pitting and Crevice Corrosion of Stainless Steel under Offshore Conditions,” *Inst. Mater.*, no. July, p. 79, 2012.

107. A. S. H. Makhlouf and M. A. Botello, *Failure of the metallic structures due to microbiologically induced corrosion and the techniques for protection*. Elsevier Ltd, 2018. doi: 10.1016/b978-0-08-101928-3.00001-x.

108. G. A. Cragnolino, “Corrosion fundamentals and characterization techniques,” *Tech. Corros. Monit.*, pp. 6–45, 2008, doi: 10.1533/9781845694050.6.

109. Z. Ahmad, *Principles of corrosion engineering and corrosion control*. 2006.

110. M. Dawood, *Durability of steel components strengthened with fiber-reinforced polymer (FRP) composites*. Woodhead Publishing Limited, 2014. doi: 10.1533/9780857096654.1.96.

111. J. T. Scales, G. D. Winter, and H. T. Shirley, “Corrosion of orthopaedic implants,” *Br. Med. J.*, vol. 2, no. 5250, pp. 478–482, 1961, doi: 10.1136/bmj.2.5250.478.

112. V. Swaminathan and J. L. Gilbert, “Fretting corrosion of CoCrMo and Ti6Al4V interfaces,” *Biomaterials*, vol. 33, no. 22, pp. 5487–5503, 2012, doi: 10.1016/j.biomaterials.2012.04.015.

113. N. J. Hallab, *Fretting corrosion of orthopedic implants*, vol. 6. Elsevier Ltd., 2011. doi: 10.1016/b978-0-08-055294-1.00205-1.

114.

115. T. Kokubo and H. Takadama, “How useful is SBF in predicting in vivo bone bioactivity?,” *Biomaterials*, vol. 27, no. 15, pp. 2907–2915, 2006, doi: 10.1016/j.biomaterials.2006.01.017.

116. S. Koleini, M. H. Idris, and H. Jafari, “Influence of hot rolling parameters on microstructure and biodegradability of Mg-1Ca alloy in simulated body fluid,” *Mater. Des.*, vol. 33, no. 1, pp. 20–25, 2012, doi: 10.1016/j.matdes.2011.06.063.

117. A. Incesu and A. Gungor, “Biocorrosion and Mechanical Properties of ZXM100 and ZXM120 Magnesium Alloys,” *Int. J. Met.*, vol. 13, no. 4, pp. 905–914, 2019, doi: 10.1007/s40962-019-00308-1.

118. H. Li, J. Wen, Y. Liu, J. He, H. Shi, and P. Tian, “Progress in Research on Biodegradable Magnesium Alloys: A Review,” *Adv. Eng. Mater.*, vol. 22, no. 7, 2020, doi: 10.1002/adem.202000213.

119. H. R. B. Rad, M. H. Idris, M. R. A. Kadir, S. Farahany, A. Fereidouni, and M. Y. Yahya, “Characterization and corrosion behavior of biodegradable Mg-Ca and Mg-Ca-Zn implant alloys,” *Appl. Mech. Mater.*, vol. 121–126, pp. 568–572, 2012, doi: 10.4028/www.scientific.net/AMM.121-126.568.

120. O. Sitdikov, R. Kaibyshev, and T. Sakai, “Dynami

121. c recrystallization based on twinning in coarse-grained Mg,” *Mater. Sci. Forum*, vol. 419–422, no. I, pp. 521–526, 2003, doi: 10.4028/www.scientific.net/msf.419-422.521.

122. D. R. Unune, G. R. Brown, and G. C. Reilly, “Thermal based surface modification techniques for enhancing the corrosion and wear resistance of

metallic implants: A review," *Vacuum*, vol. 203, no. January, p. 111298, 2022, doi: 10.1016/j.vacuum.2022.111298.

123. J. L. Gilbert, M. Mehta, and B. Pinder, "Fretting crevice corrosion of stainless steel stem-CoCr femoral head connections: Comparisons of materials, initial moisture, and offset length," *J. Biomed. Mater. Res. - Part B Appl. Biomater.*, vol. 88, no. 1, pp. 162–173, 2009, doi: 10.1002/jbm.b.31164.

124. P. Maier and N. Hort, "Magnesium alloys for biomedical applications," *Metals (Basel).*, vol. 10, no. 10, pp. 1–3, 2020, doi: 10.3390/met10101328.

RESUME

Laith Mohammed Abdullah AL MASHHADANI, a metallurgical engineer, completed his undergraduate studies B.Sc. in Production Engineering and Metallurgy/Metallurgical Engineering at the University of Technology, Iraq, in 1997–1998. Presently, he is pursuing a Master's degree in the Metallurgical and Materials Engineering Department at Karabük University in Turkey.